Benchmark on Thermomechanical Fuel Rod Behaviour

Phase I Report

GRS - 671

Gesellschaft für Anlagen-
und Reaktorsicherheit
(GRS) gGmbH

Benchmark on Thermomechanical Fuel Rod Behaviour

Phase I Report

Felix Boldt
Maik Stuke
Marc Péridis

April 2022

Remark:

This report refers to the research project RS1588 which has been funded by the German Federal Ministry for Economic Affairs and Climate Action (BMWK).

The work was conducted by the Gesellschaft für Anlagen- und Reaktorsicherheit (GRS) gGmbH.

The authors are responsible for the content of the report.

GRS - 671
ISBN 978-3-949088-62-9

Keywords:
Benchmark, Dry storage, Fuel rod, Spent nuclear fuel

Abstract

One of the key aspects for the safety of extended dry storage of used nuclear fuel in casks is the prediction of the fuel rod behaviour. A detailed and reliable prediction must consider the entire life span of the fuel rod: service in reactor with the associated radiation history, wet storage in the fuel pool, loading and drying of the cask, and finally the in-cask dry storage itself. Enhancing existing fuel performance codes to include all these steps and their associated phenomena is an ongoing task tackled by several groups. To foster the communication between these groups a benchmark was proposed at the 2019 *Safety of Extended Dry Storage* (SEDS) workshop. The report at hand summarizes the results of the Phase I.

Acknowledgements

This benchmark is based on the contributions of many colleagues from research centres, technical safety organisations, regulators, and industry. Many thanks to all benchmark participants giving valuable input to this work.

- Carlos AGUADO BASABE, CIEMAT, Spain
- Felix BOLDT, GRS gGmbH, Germany
- Francisco FERIA MARQUEZ, CIEMAT, Spain
- Luis E. HERRANZ PUEBLA, CIEMAT, Spain
- Piotr KONARSKI, PSI, Switzerland
- Vítězslav MATOCHA, ÚJV Řež, a. s., Czech Republic
- Marc PÉRIDIS, GRS gGmbH, Germany
- Roberto PLAZA MULAS, CNAT, Spain
- Radan SEDLÁČEK, Framatome GmbH, Germany
- Gerold SPYKMAN, TÜV NORD EnSys GmbH & Co. KG, Germany
- Maik STUKE, GRS gGmbH, Germany

Content

1 Introduction

The prediction of the fuel rod behaviour during dry storage using fuel performance codes is a non-trivial task and subject to various international efforts. A variety of assumptions and models must be considered and the knowledge especially for some effects during the long-term dry storage is still incomplete. After service in operation spent nuclear fuel is stored in cooling ponds for several years and, dependent on the fuel storage concept, subsequently dry stored in casks for several decades. During the entire storage period the state of the spent nuclear fuel is subject to changes e.g., due to heat generation or Helium production. While the physical and chemical processes during reactor operation are well known or at least analysed with a broad data base, the specific phenomena occurring during the drying process and the following storage period are not described to the same level of detail, yet. For example, the evolution and behaviour of the hydrogen within the fuel rod cladding remains a not entirely solved question. It is e.g., still under discussion how radial hydrides form and to which degree the fuel rod's ductility is influenced by them.

Since various fuel performance codes simulate several effects in different ways using different modelling approaches (e.g., cladding creep, pellet-cladding-gap closure, etc.) a first step was to study and compare the basic fuel rod characteristic during the long-term dry storage. This is the major aim of the SEDS Benchmark.

At the 2019 *Safety of Extended Dry Storage* (SEDS) workshop, a benchmark to investigate the fuel rod behaviour during dry storage has been proposed /STU 19/, /BOL 19/. The subsequent discussions between the participants lead to a final version of the specifications distributed in December 2019. Preliminary results were presented and discussed at the 2020 SEDS workshop and were published /BOL 20/. This report discusses results received from six participants.

This benchmark is open to everyone and relies solely on publicly available data and generic models. It includes precalculated typical values for the decay heat prediction and the cask thermo-hydraulics. The mechanical fuel rod behaviour during long-term storage is to be calculated by each participant. The task is to simulate the thermo-mechanical behaviour starting from the end of reactor operation. This article summarizes the received results.

2 Benchmark description

In the following a brief overview of some cornerstones of the benchmark description will be given. The complete specifications can be obtained from the authors of this article.

In general, simplified boundary conditions are assumed covering all important stages of the fuel. It consists of an arbitrary, realistic power history covering five cycles with stretch-out operation at the end of each cycle. After operation in the reactor the fuel rod is assumed to be stored for a period of five years in wet storage. During this time the fuel rod is stored forced-cooled and at low coolant pressure, facing comparably small changes. The wet storage ends with the loading of the fuel into the cask. The cask is dewatered after loading, vacuum dried and filled with helium gas. During this stage the cladding temperature rises to its maximum post-operation temperature. The subsequent dry storage results in a slow cool-down during the assumed (extended) storage period of 95 years, resulting in a full storage period of 100 years.

The modelling range of the benchmark includes the simulation of five years of operation, five years of wet storage, and 95 years of dry cask storage. The operational behaviour is optional, whereas the task focusses on the storage behaviour. Wet and dry storage of the spent nuclear fuel (SNF) necessitate comparably large calculational time steps with rather slow changes in parameter behaviour. However, precise boundary or initial conditions are needed since small changes in the beginning may lead to large deviations during dry storage period. For example, the peak cladding temperature and its distribution during the drying process might have a significant impact on the hydrogen behaviour in the cladding and thus finally on the mechanical properties of the cladding after the 95 years of dry storage. The general computational chain and the input and output data are shown in Fig. 2.1. The input data are given in the benchmark description and are based on a typical fuel rod design for a Pressurized Water Reactor (PWR) as well as the irradiation characteristics and power history. The burn-up code OREST96 (/HES 86/, /NEA 06/) was used to calculate the resulting burnup and decay heat of the fuel after end of operation. The axial distribution of the decay heat and its evolution is a central input parameter for the simulation of the cladding behaviour during wet and dry storage.

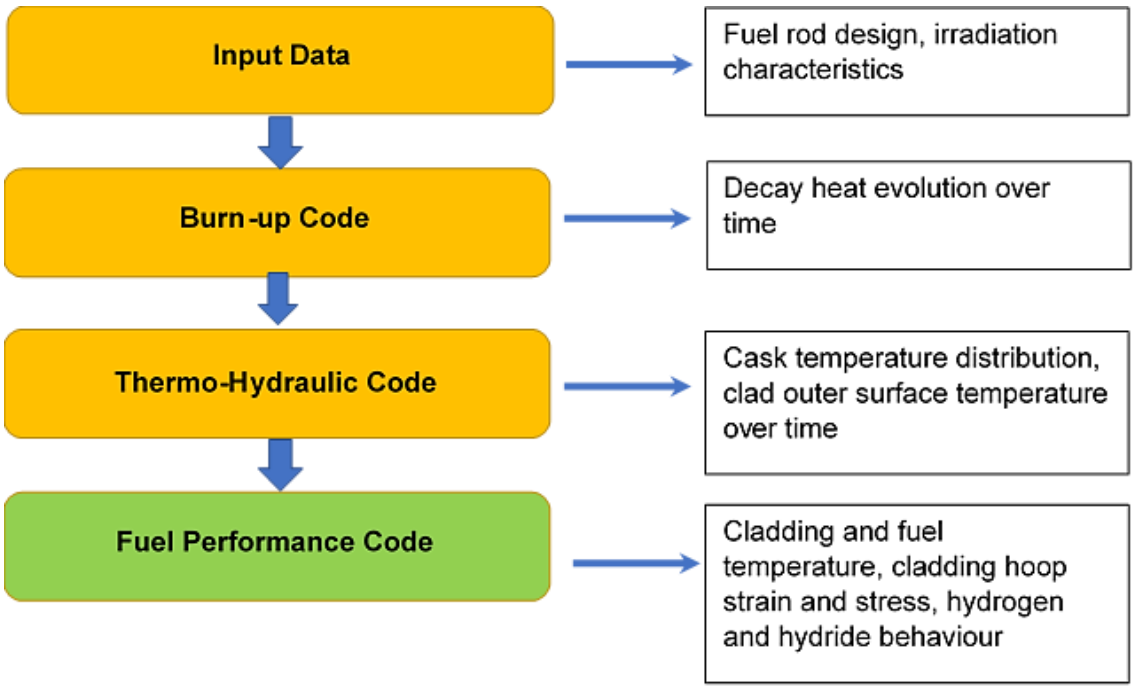

Fig. 2.1 Simulation chain for dry storage benchmark

The code COBRA-SFS /MIC 17/ was used to calculate the thermo-hydraulic boundary conditions of a generic storage cask during the drying process and the subsequent dry storage period. The resulting rod surface temperatures are further input parameters evolving over the whole simulation time.

The results of these steps were provided as input parameters for the thermo-mechanical fuel rod codes. The output parameters were chosen as fundamental parameters used for safety evaluation e.g., cladding temperature and cladding hoop strain, or of specific research interest e.g., hydrogen distribution inside the cladding.

2.1 Fuel rod specifications

The fuel rod is part of a *Kraftwerk Union* (KWU) design based 18x18-type PWR fuel assembly. The main design parameters are given in Tab. 2.1. The fuel rod's active length describes the length of the fissile fuel column, which is used as the axial length in this benchmark. The fuel rod operational history for the corner rod and the central rod are assumed to be equal.

Tab. 2.1 Fuel rod design parameters

Design Parameter	Value [mm]
Pitch	12.7
Rod length, total	4405
Rod length, active	3900
Cladding outer diameter	9.5
Pellet outer diameter	8.05
Cladding thickness	0.64

The power history of this benchmark is simplified with periodic changes in the axial power history. The power history is given in Fig. 2.2 for five cycles. The linear heat generation rate is assumed identical for all the rods of the fuel assembly, i.e., equal for a central or corner rod during operation.

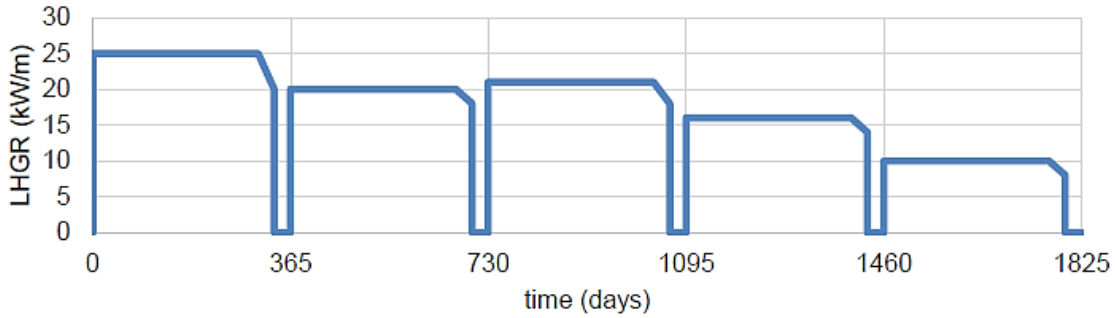

Fig. 2.2 Operational history over 5 cycles including 30 days of stretch-out at the end of each cycle

The burnup code OREST was used to calculate the resulting decay heat. After the fifth cycle an accumulated burnup of the fuel assembly of 67 GWd/t HM is reached. Results were asked for specific rods: the central and a corner rod. Also results for the assumption of two different fuel rod materials were asked: M5® and Zircaloy-4.

2.2 Boundary conditions

Fig. 2.3 shows the key stages for the fuel assembly after the in-reactor operation during the benchmark according to Tab. 2.2. After reactor operation, temperature decreases. During wet storage, the coolant pressure is defined by the atmospheric pressure plus the water level in the spent fuel pool. After the wet storage period the drying process leads to an increasing cladding temperature. The cask is dewatered and dried and the coolant is replaced by a low-pressure helium atmosphere.

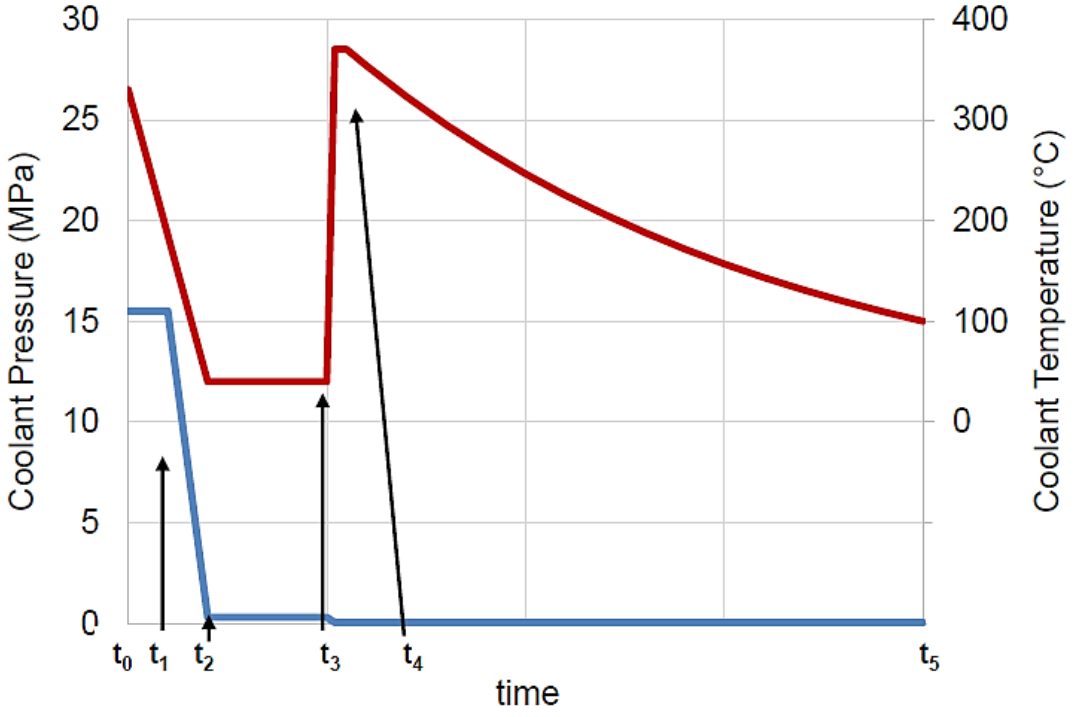

Fig. 2.3 Schematic fuel rod life during simulation period with marked key stages

Tab. 2.2 Key stages of boundary conditions during the fuel rod life after discharge

Time step	Event
t 0	Onset of temperature decrease
t 1	Onset of pressure decrease
t 2	Begin wet storage (storage for 5 years)
t 3	Begin drying process, temperature increase, dewatering
t 4	Begin dry storage (storage for 95 years)
t 5	End of simulation

The fuel assembly with the benchmark rods is loaded into the central position of a generic, CASTOR® V/19-like model with heat load of 2.21 kW (Fig. 2.4). To meet the cask maximum heat load of 39 kW, the other 18 fuel assemblies are modelled with 2.04 kW decay heat each. The active fuel rod column is divided into 32 axial zones and for each zone the benchmark results were requested.

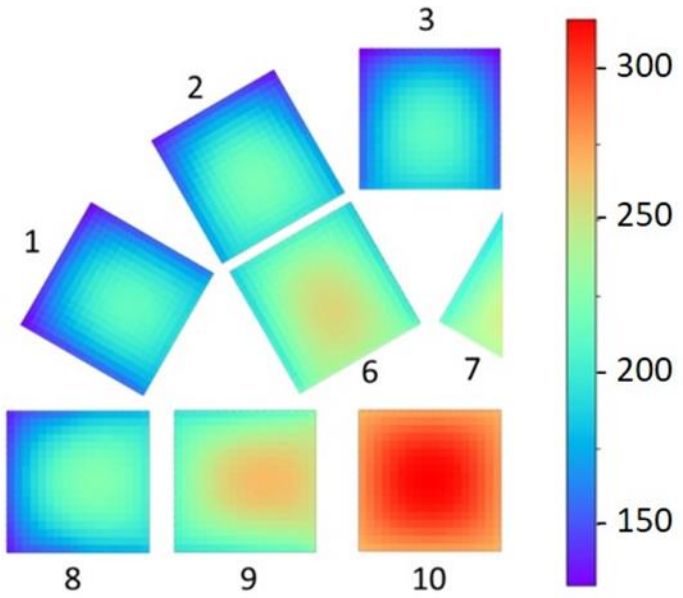

Fig. 2.4 Temperature distribution of a cask with 19 fuel assemblies and homgenious loading

3 Benchmark Results

A total of six different solutions for long-term storage were received. The solutions originate from seven different codes. Not all participants provided solutions for both rods (corner and central rod), both materials (M5® and Zircaloy-4) and all requested parameters. In the following the results are presented anonymized as *Participant (Part) 1* to *7*, referring to the groups below. All results are presented for the axial level 22 only, which is the hottest level at the beginning of the dry storage, with exception of Part 5 presenting level 7 of 10. It is noteworthy, that the following results exhibit an overview on the received data and may include different assumptions for each participant based on the benchmark description. Further information on the participants' results can be found in the appendix A. Besides a time-shift, no manipulation to the original data was applied. During the five years of operation, changes in the parameters are frequent whereas the storage period shows large changes only during the transition from wet to dry storage. To enable a better overview, the operational and storage periods are presented separately in the following. The operational behaviour is presented in chap. 3.1 and includes the five years of operation as well as the following five years of wet storage, which is also included in the storage period. Then chap. 3.2 presents the results for the storage period, including wet storage, drying process, and dry storage.

The group of participants and codes (Part 1 to Part 7) is given with following key

- Part 1 – CIEMAT using FRAPCON-xt
- Part 2 – CNAT using FALCON
- Part 3 – PSI using FALCON
- Part 4 – ÚJV Řež using TRANSURANUS
- Part 5 – GRS using TESPA-ROD
- Part 6 – Framatome GmbH using CARO-E and CSAS
- Part 7 – TÜV NORD using TRANSURANUS

3.1 Operational behaviour Zircaloy-4

To study the dry storage behaviour, it is necessary to include operational key parameters which directly influence the fuel rod state. Most notably the fission gas release, the fuel densification and swelling, the pellet-cladding gap evolution as well as the cladding oxidation and the hydrogen pick-up. The operational behaviour was calculated by five participants. During operation the boundary conditions for central and corner rods are assumed to be equal therefore both storage scenarios in chap. 3.2 are based on this calculation.

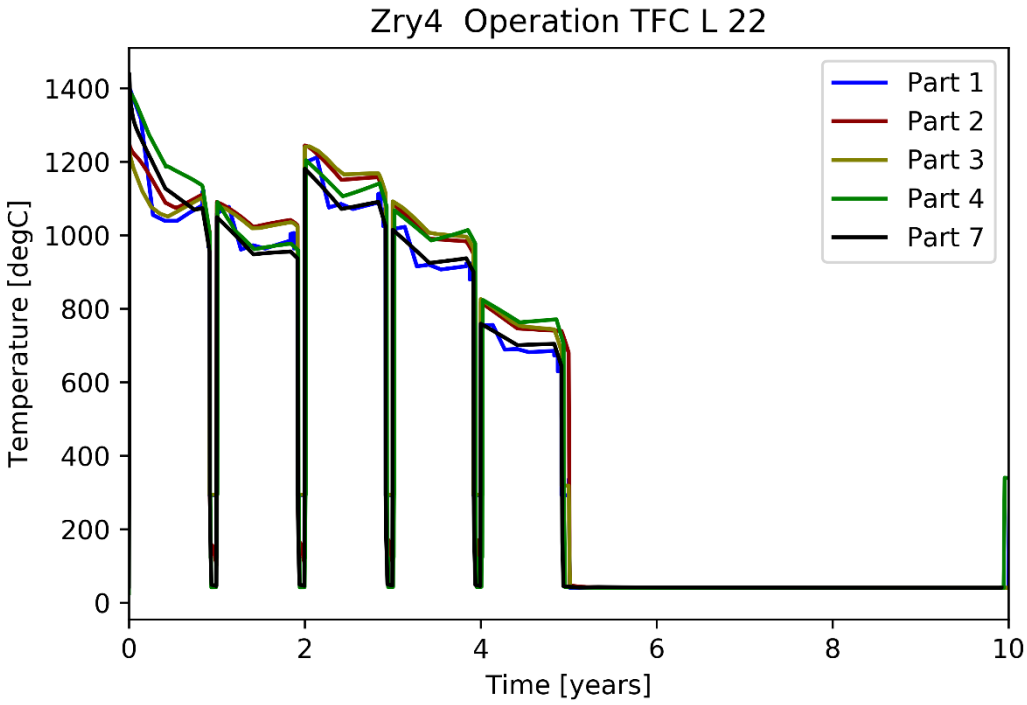

Fig. 3.1 Fuel central temperature (TFC) of Zry-4 rod during operation

The fuel central temperature (TFC) is shown in Fig. 3.1 for Part 1 to 4 and 7. In the first cycle, the temperature initially amounts to 1200 °C and 1400 °C and decreases within the cycle. Between the cycles the temperature decreases significantly (reloading operation). Some codes predict low temperatures of approximately 40 °C (Part 4 and 7) and some provide higher temperatures, such as Part 2 with ca. 150 °C continuously decreasing as well as Part 2 and 3 with 300 °C. During the reactor outages a reduction of the coolant temperature to 40 °C was assumed. Other codes may assume constant coolant temperatures during cycles and between them. With decreasing heat generation rate, the TFC reduces to approximately 700 °C at the end of operation.

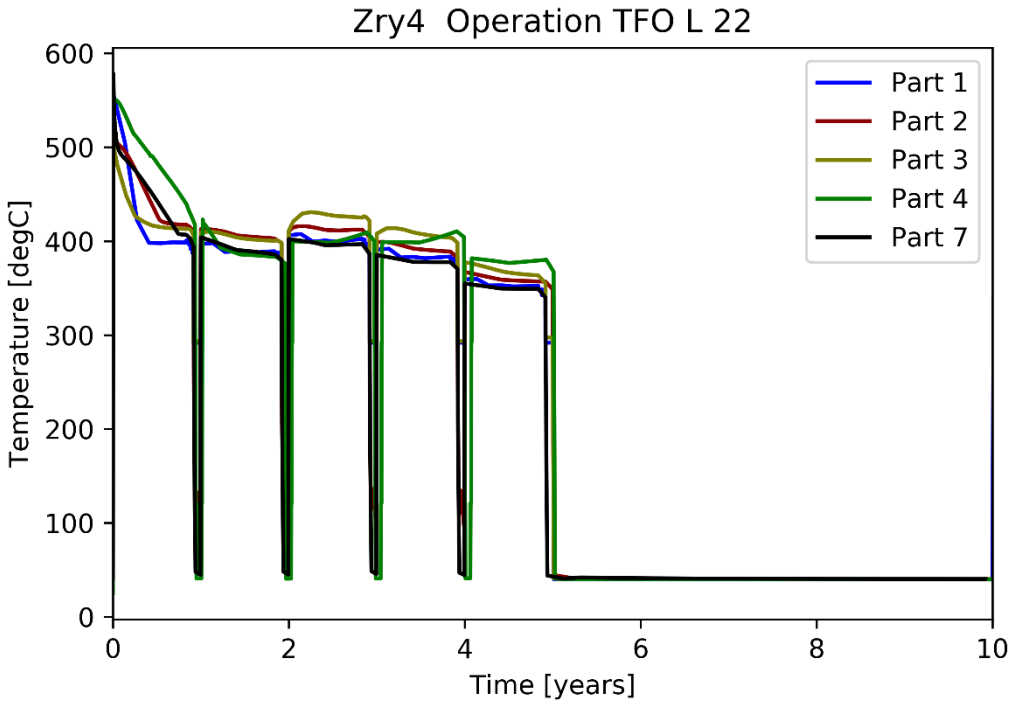

Fig. 3.2 Fuel outer temperature (TFO) of Zry-4 rod during operation

The fuel outer temperature in Fig. 3.2 shows a similar result as Fig. 3.1. The first cycle starts with high fuel outer temperatures of 500 °C to 580 °C, which decrease to the end of the cycle. Beginning with the second cycle all codes behave similar due to a closed pellet-cladding gap and constant coolant temperatures.

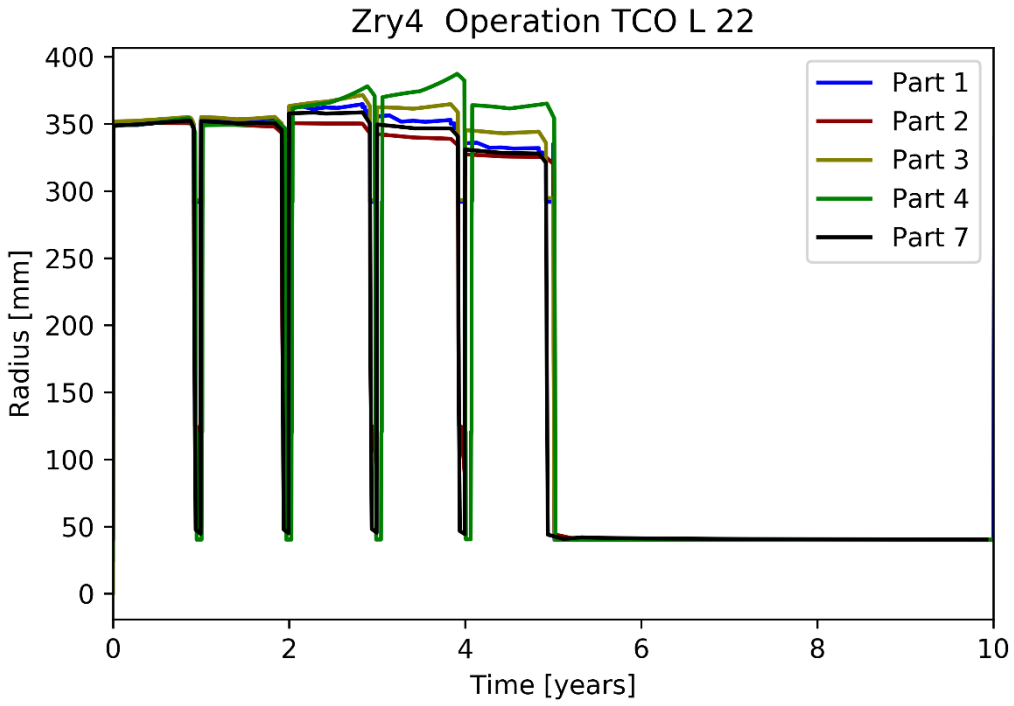

Fig. 3.3 Cladding outer temperature (TCO) of Zry-4 rod during operation

In Fig. 3.3 the cladding outer temperature is presented. The temperature remains close to coolant temperature. With increasing operating duration Part 4 results show an increased TCO reaching higher temperatures. This bifurcation of the results may be affected by the oxide thickness on the cladding outer surface. Two approaches are possible: TCO may address the metallic outer surface of the cladding which may be covered by a growing oxide thickness. Otherwise TCO describes the temperature on the outside of the zirconia layer which leads to temperatures very close the coolant temperature.

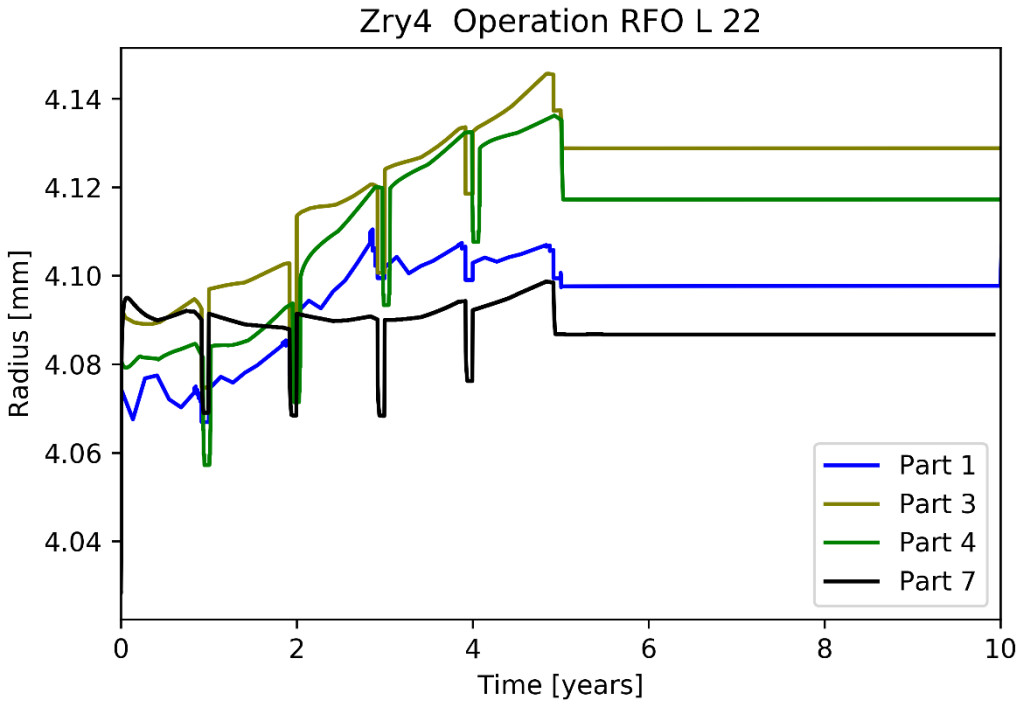

Fig. 3.4 Fuel outer radius (RFO) of Zry-4 rod during operation

The fuel outer radius for 4 codes is shown in Fig. 3.4. The codes show different behaviour resulting in slow reduction or continuous increase of the fuel radius over the different cycles. The changes in radii are dominated by fuel densification in the beginning and an ongoing swelling of the fuel. Part 3 and Part 4 show the highest values with ca. 4.12 mm and 4.13 mm during wet storage. The effect of swelling seems smaller for Part 1 and Part 7 with radii equal to 4.10 mm and 4.085 mm respectively.

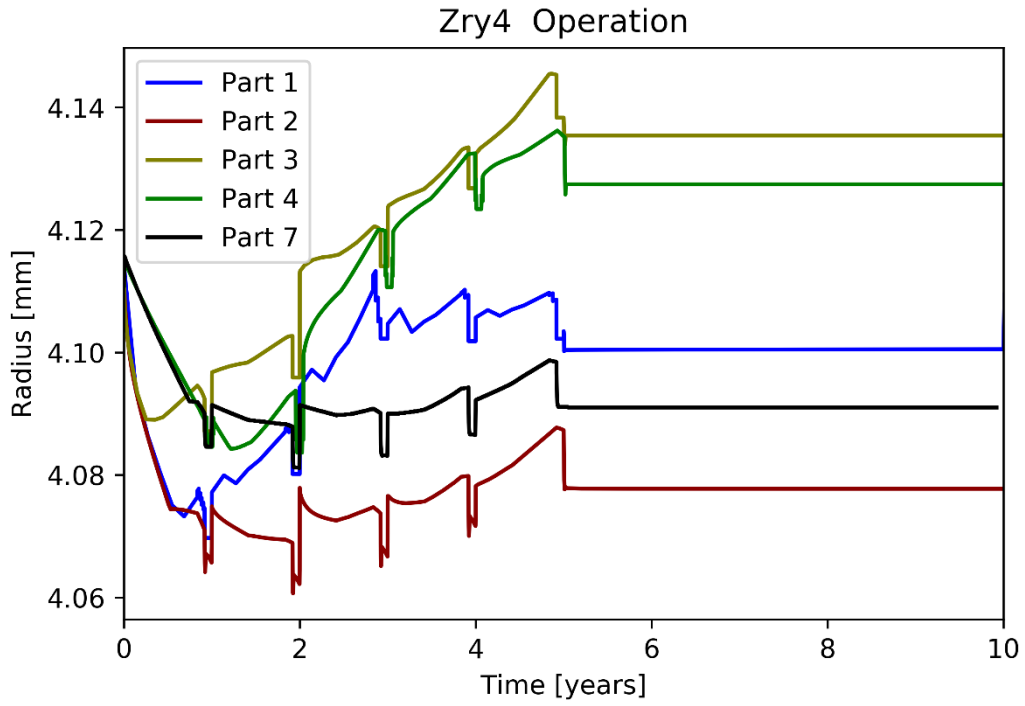

Fig. 3.5 Cladding inner radius (RCI) of Zry-4 rod during operation

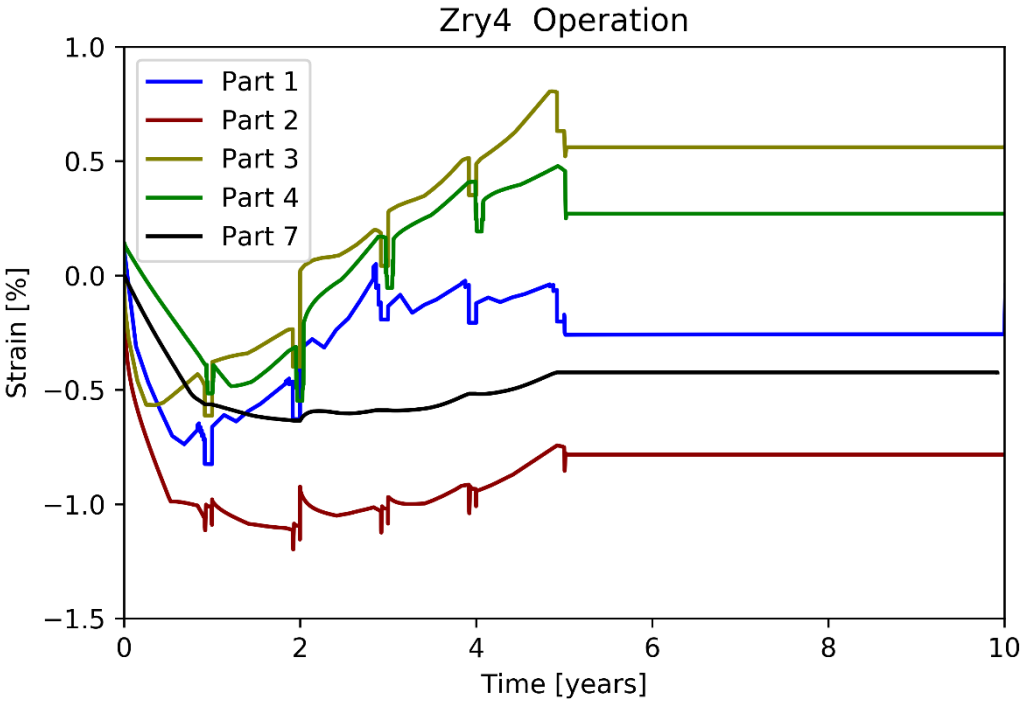

Fig. 3.6 Total cladding strain (ECTH) of Zry-4 rod during operation

The cladding geometry is given in Fig. 3.5 as cladding inner radius and in Fig. 3.6 with cladding hoop strain. In the beginning all codes show a similar trend with the decreasing cladding strain. This happens due to an open pellet-cladding gap and a positive pressure difference between the outer and the inner side of the fuel rod. Thermal creep leads to the reduction of the cladding diameter. Due to different processes (densification, swelling, creep) the pellet diameter is affected, which may lead to different gap sizes in the beginning. Part 1, 3 and 4 show a visible effect between the operational cycles. In this period thermal strain is reduced due to low temperatures. Part 7 does not show this effect in the total strain. All codes show a general trend of an increasing strain beginning between the first half cycle (Part 3) and the third half cycle (Part 7). All results remain constant after the fifth cycle, leading to a variation in strain between -80 % for Part 2 and +60 % for Part 3.

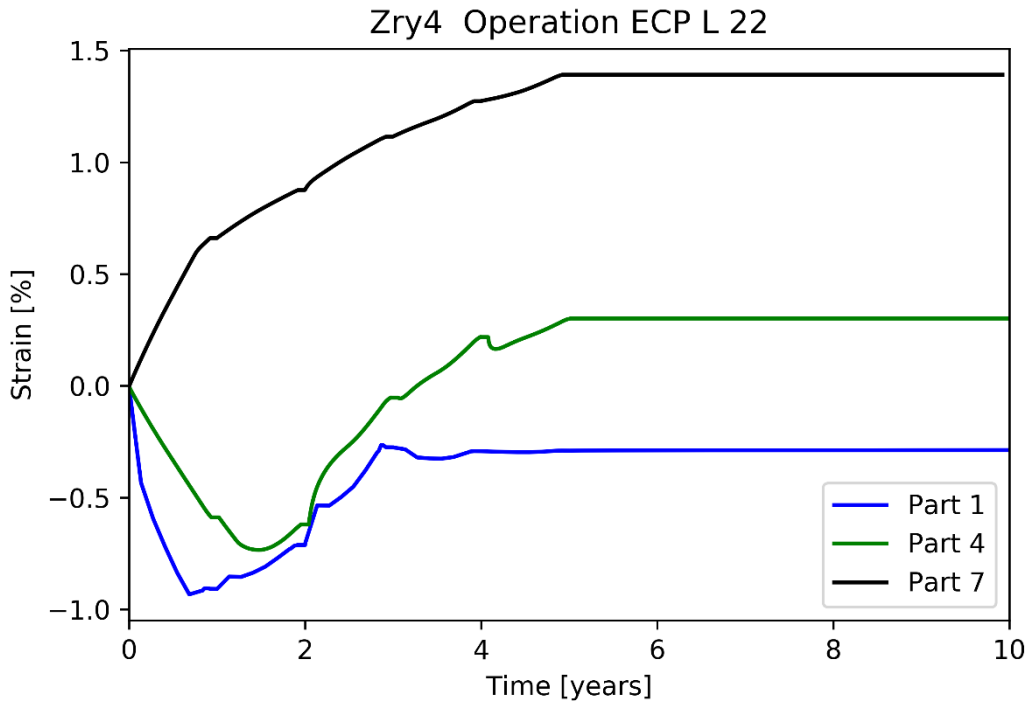

Fig. 3.7 Cladding plastic deformation (ECP) of Zry-4 rod during operation

Fig. 3.7 includes the cladding plastic deformation for Part 1, 4 and 7. Due to the creep-down of the cladding during the first operation cycle the plastic deformation is directed inward, which would be negative. Part 7 predicts a positive plastic deformation, which may be caused by a different definition of plastic deformation. Part 1 and 4 show a qualitatively similar behaviour with a local minimum during operation but shifted to different times.

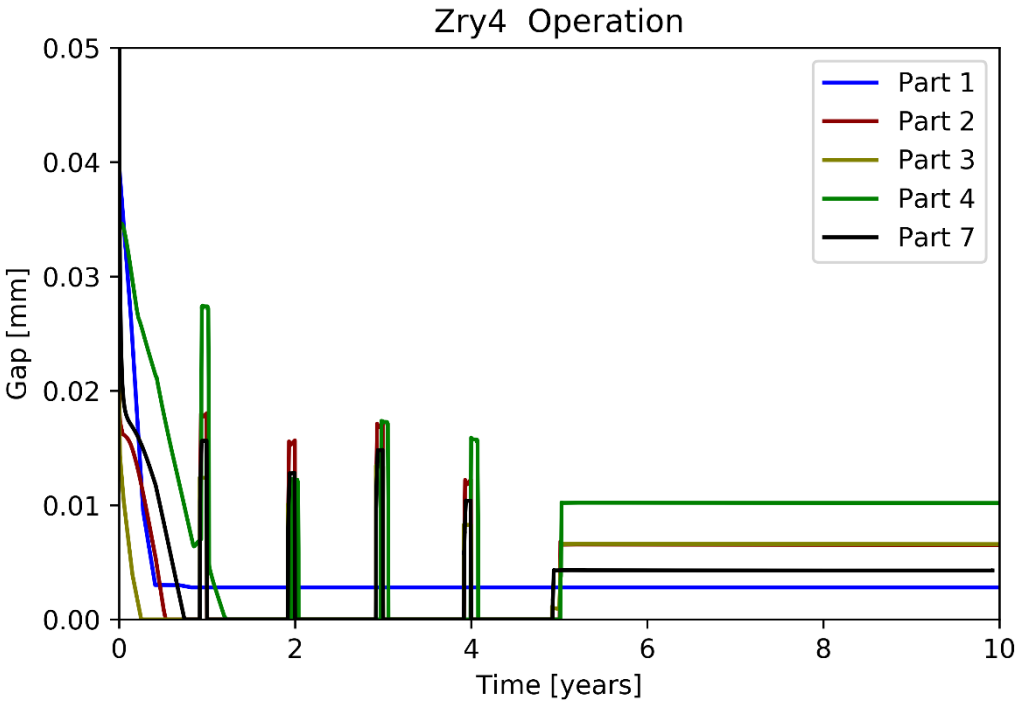

Fig. 3.8 Pellet-cladding gap (GAP) of Zry-4 rod during operation

The pellet-cladding gap is shown in Fig. 3.8 with decreasing gap sizes from the beginning of the simulation. Part 1 shows a decrease during the first cycle to a minimum of 2.8 µm, which resembles the roughness of the fuel-cladding interface, which means gap closure. The other reach gap closure during the first cycle with exception of Part 4 with gap closure in the second cycle. All codes with exception of Part 1 exhibit a reopening of the gap between the cycles with different sizes.

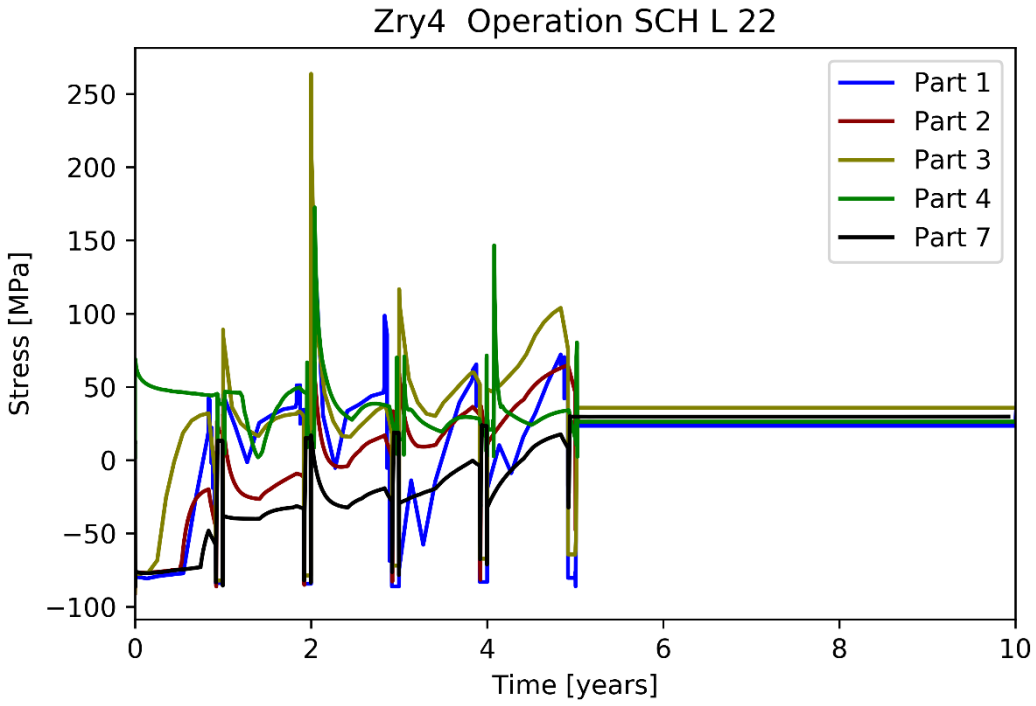

Fig. 3.9 Cladding hoop stress (SCH) of Zry-4 rod during operation

Fig. 3.9 shows the cladding hoop stress starting from different positions. Usually, tensile stress of the cladding is defined negative, which corresponds to a lower rod inner pressure compared to the coolant pressure. Part 4 shows a positive hoop stress up to 67 MPa in the beginning of the operation in opposition to the other codes showing negative values around -75 MPa. All codes start with an open pellet-cladding gap (see Fig. 3.8), thus the pressure difference between the coolant and the rod's gas filling determines the stress state in the cladding. After gap closure the pellet applies an additional body-contact pressure on the cladding contributing to high tensional stresses as seen in the beginning of cycle 2 and all subsequent cycles for each code. Part 3 and 4 show huge stresses above 260 MPa and 170 MPa, respectively. Part 2 shows a strong variation in the gradient leading to a zig-zag curve between BOC and MOC, which may be the result of the changing axial power profile over each cycle. With end of operation all codes show a similar result a positive hoop stress of around 30 MPa which is determined by the inner fuel rod pressure and the coolant pressure during wet storage.

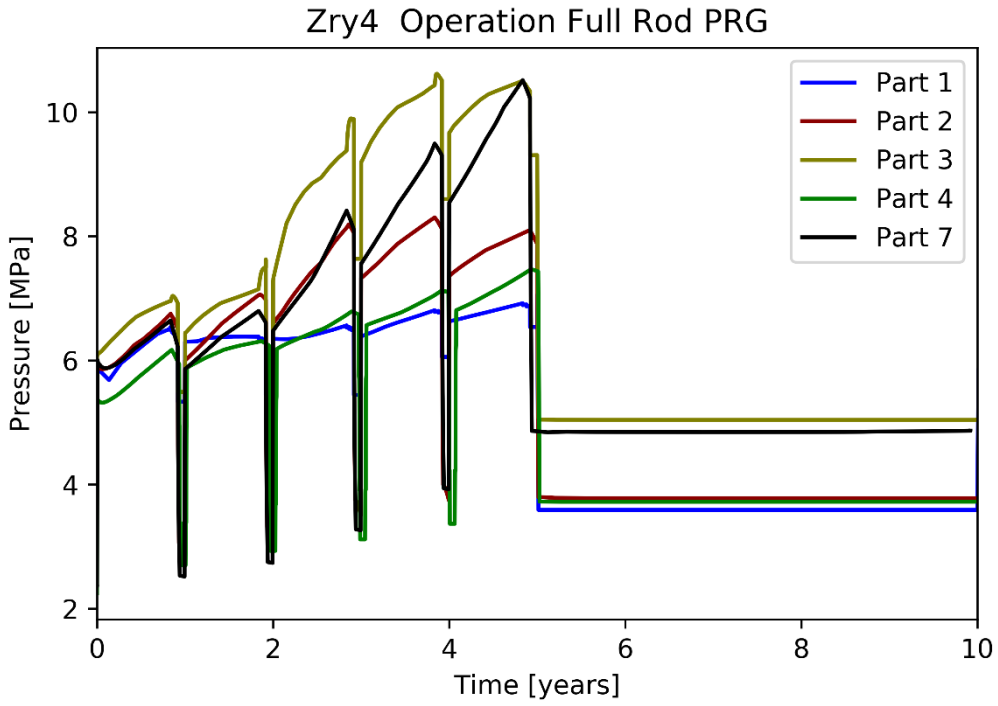

Fig. 3.10 Rod internal gas pressure (PRG) of Zry-4 rod during operation

The fuel rod gas pressure, shown in Fig. 3.10, is given for the full fuel rod since axial gas communication is assumed. All codes predict a certain increase of the rod inner pressure. Only small increases are predicted by Part 1 and 4, whereas Part 3 and 7 show large increases of above 10 MPa at the end of cycle 5. Between the operational cycles the fuel rod pressure decreases for all codes, due to the reduction of the fuel rod power. Since not all codes assume a cool-down of the coolant, the local pressure minima are different from each other. The results for the inner fuel rod pressure during wet storage is bifurcated for the codes leading to a pressure of approximately 5 MPa for Part 3 and 7 and pressures of 3.8 MPa for the remaining codes.

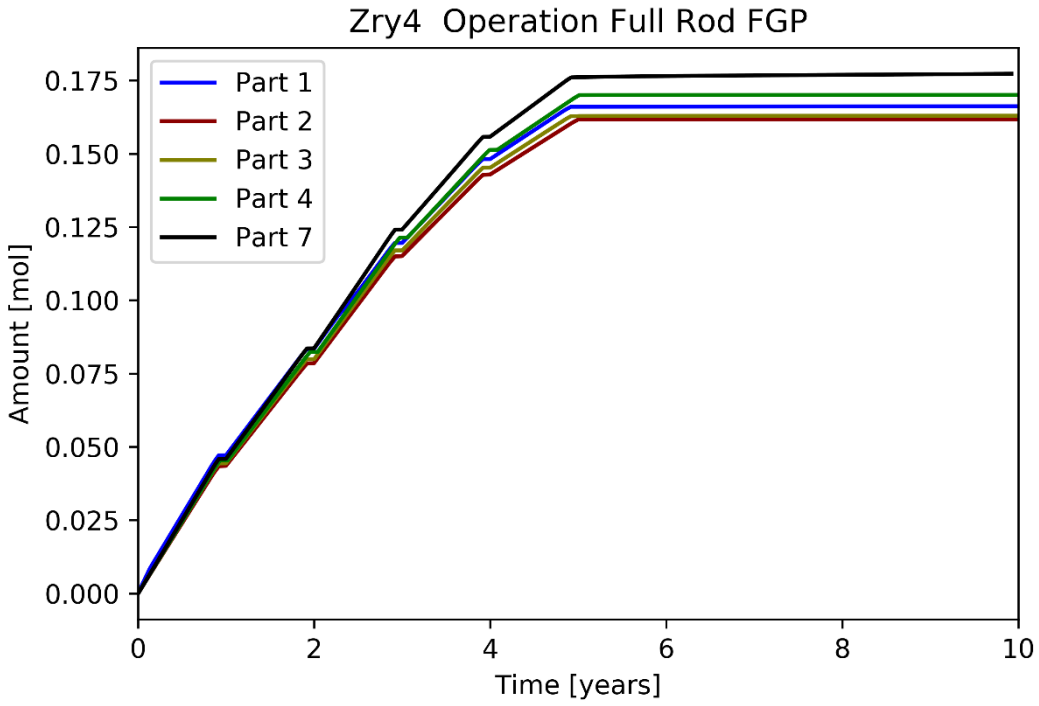

Fig. 3.11 Fission gas production (FGP) of Zry-4 rod during operation

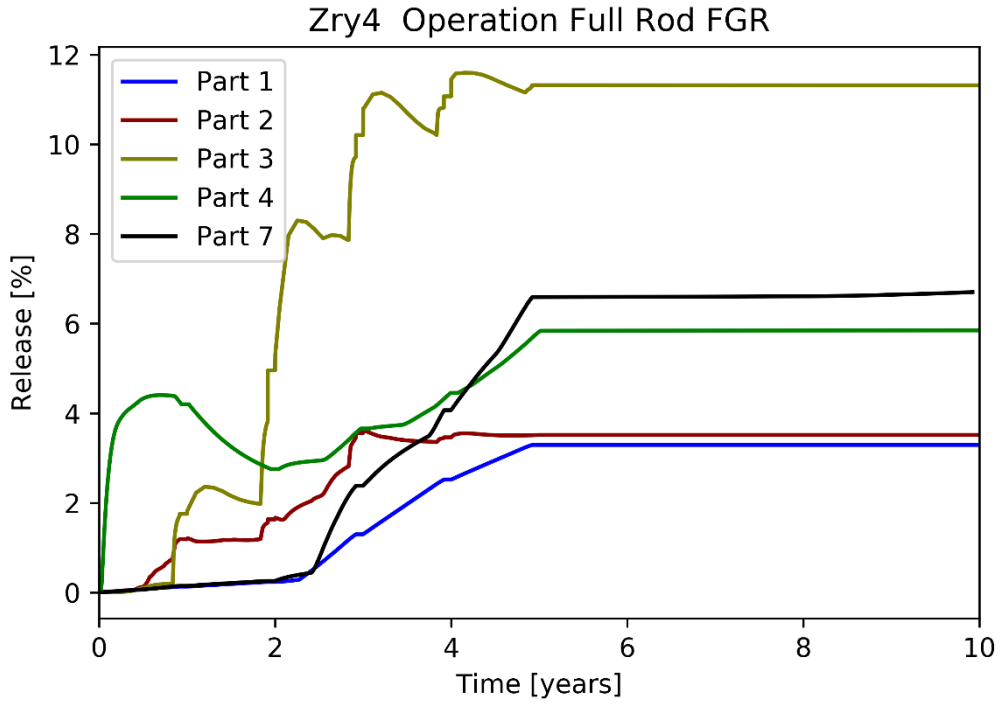

Fig. 3.12 Fission gas release (FGR) of Zry-4 rod during operation

The fission gas behaviour is shown in Fig. 3.11 as production and Fig. 3.12 as relative release. The production of fission gases is very similar for all codes, but the release differs both in total and as relative value. Part 1 and 7 show a monotonic increase of the fission gas release, while Part 2, 3 and 4 show local minima. For the first group it can be concluded that a continuous release of fission gases increases this value. For the second group the release occurs in steps, which increases the value of FGR. After one step the release stagnates while fission gas is produced and retained within the fuel resulting in a decreasing share of FGR as seen for Part 4 between year 1 and 2 as well as for Part 3 in every cycle after the first cycle. There could be a strong user effect for FGR since Part 2 and 3 as well as Part 4 and 7 use the same type of code.

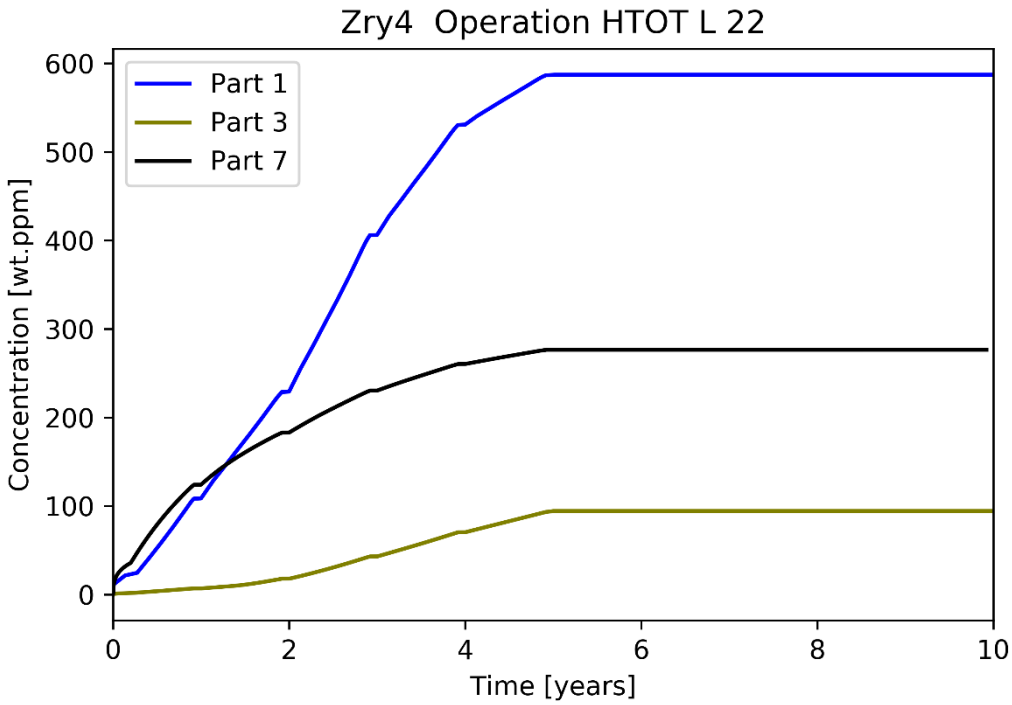

Fig. 3.13 Total cladding hydrogen concentration (HTOT) of Zry-4 rod during operation

The hydrogen concentration in the cladding given in wt.ppm is shown in Fig. 3.13. Part 1, 3 and 7 show an increasing amount hydrogen due to the operational corrosion of the cladding. The final levels for the hydrogen concentration ranging from approximately 100 wt.ppm for Part 3 to 280 wt.ppm for Part 7 and 590 wt.ppm for Part 1. These variations may result from the different pick-up fraction of each corrosion models and additional factors, which are usually based on engineering judgement and the experience of specific NPPs.

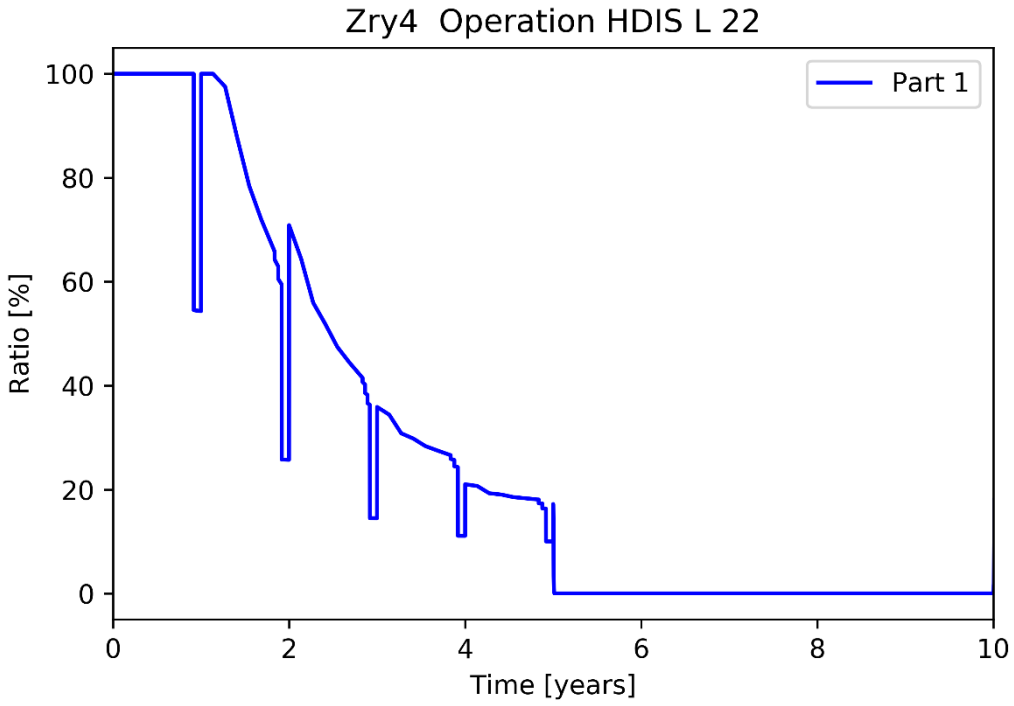

Fig. 3.14 Dissolved hydrogen in the cladding (HDIS) of Zry-4 rod during operation

Fig. 3.14 shows the share of dissolved hydrogen in the cladding for Part 1. During operation the temperature in the cladding is sufficiently high to increase the hydrogen solubility to accommodate 100 % of the hydrogen in a dissolved state. With increasing oxidation of the cladding more hydrogen is available, leading to the precipitation of hydrides. During the last cycle only approximately 10 % of the hydrogen is dissolved in the cladding. The opposite effect can be seen in Fig. 3.15, which describes the circumferentially precipitated hydrides during in the cladding. All hydrogen which is not dissolved is precipitated in circumferential orientation. In addition, it should be noted that Part 1 does not predict any radially oriented hydrides during operation and wet storage, as it can be shown in Fig. 3.16.

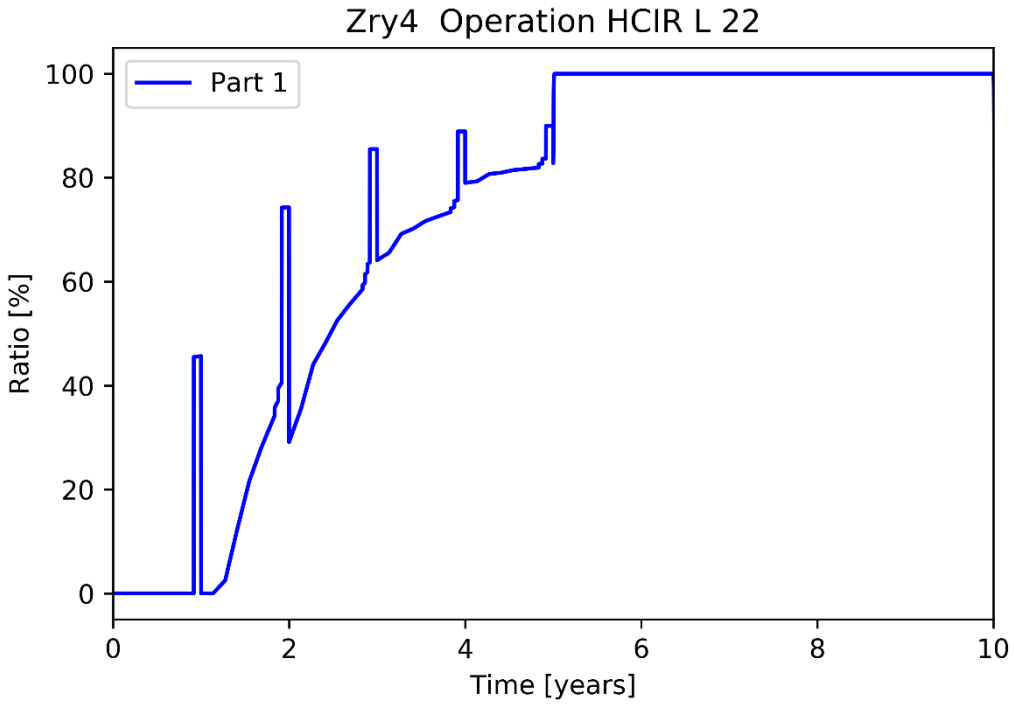

Fig. 3.15 Circumferentially precipitated hydrides in the cladding (HCIR) of Zry-4 rod during operation

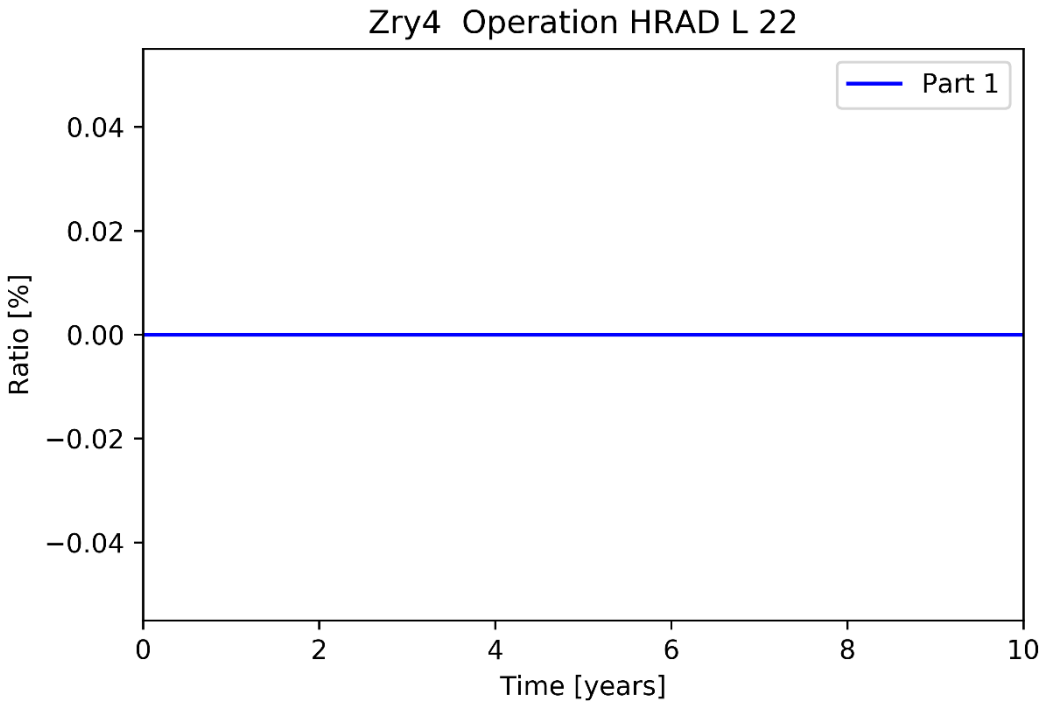

Fig. 3.16 Share of radial precipitated hydrides (HRAD) Zry-4 rod during operation

3.2 Storage behaviour for Zircaloy-4 central rod

The results for the storage behaviour show results of six participants in total.

In Fig. 3.17 the results for the fuel centreline temperature (TFC) is shown, which are nearly identical for all results. The calculated temperature follows the temperature calculated by COBRA-SFS. Most codes show only small variations to each other, depending on different model assumptions or time steps. These differences might result also from the different number of time steps provided by the output ranging from few hundred to few thousand entries. Participant two shows constantly lower temperature compared to all other participants.

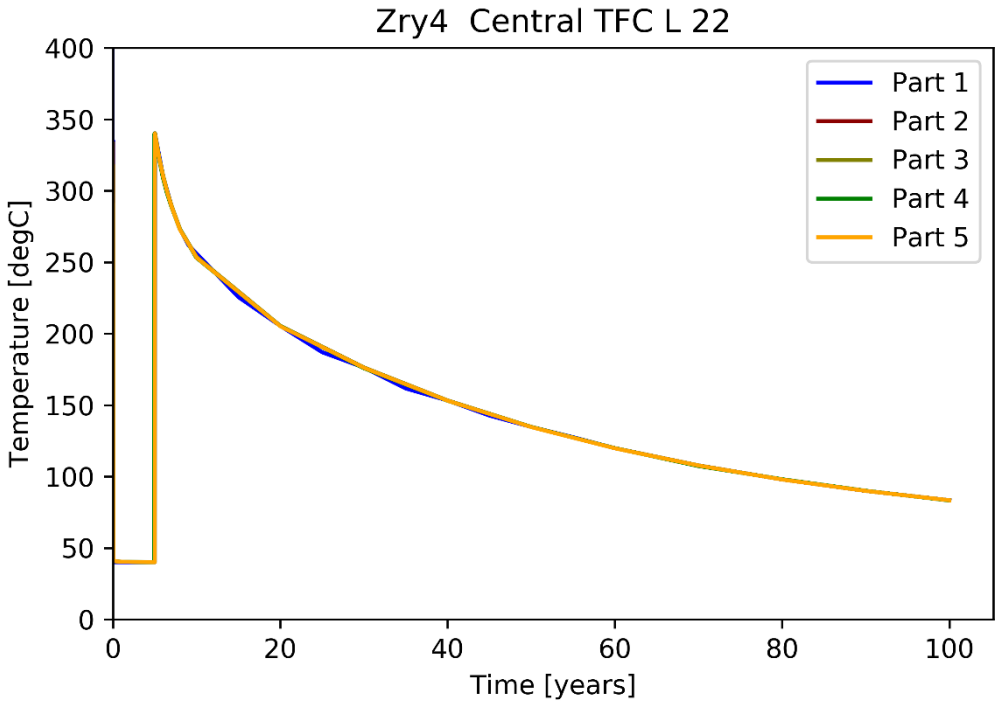

Fig. 3.17 Fuel centreline temperature (TFC) of Zry-4 central rod during storage

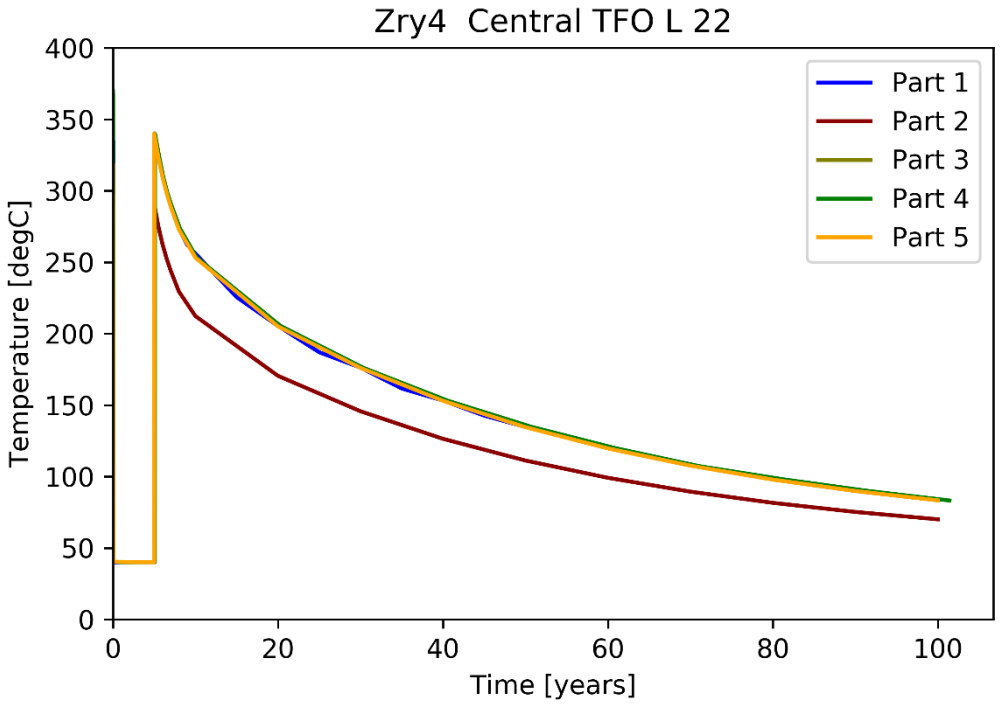

Fig. 3.18 Fuel outer temperature (TFO) of Zry-4 central rod during storage

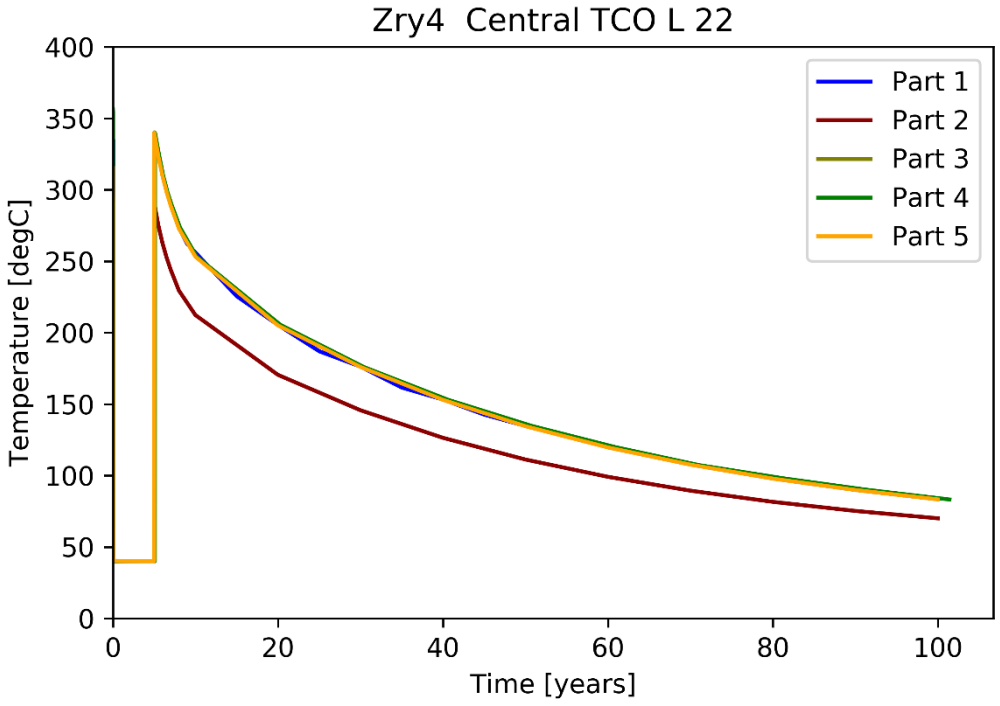

Fig. 3.19 Cladding outer temperature (TCO) of Zry-4 central rod during storage

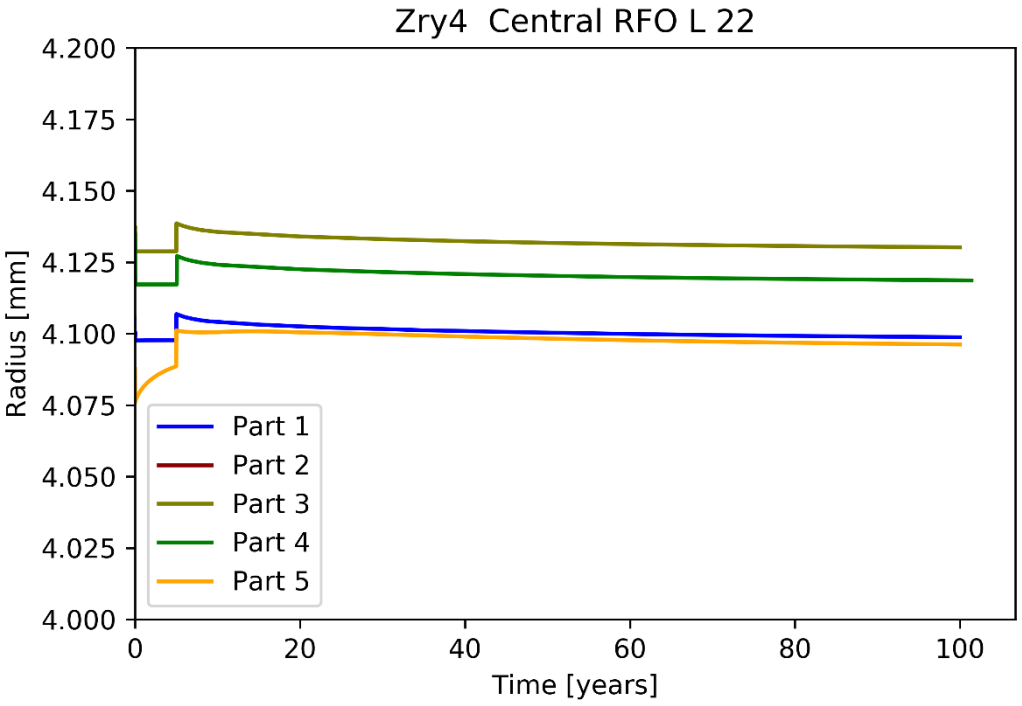

Fig. 3.20 Fuel outer radius (RFO) of Zry-4 central rod during storage

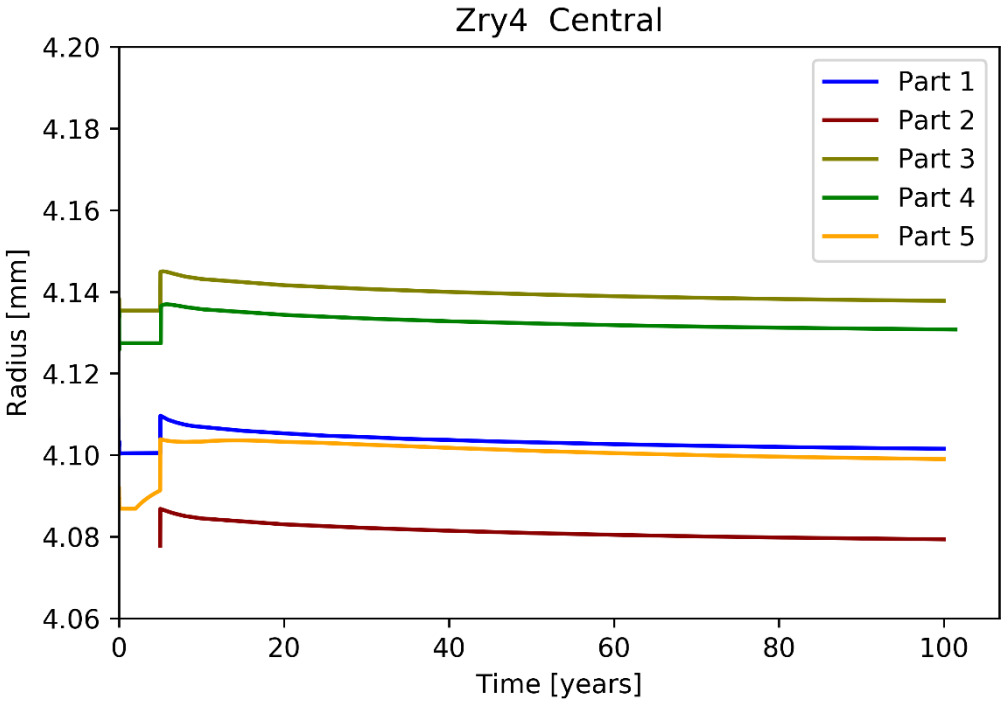

Fig. 3.21 Cladding inner radius (RCI) of Zry-4 central rod during storage

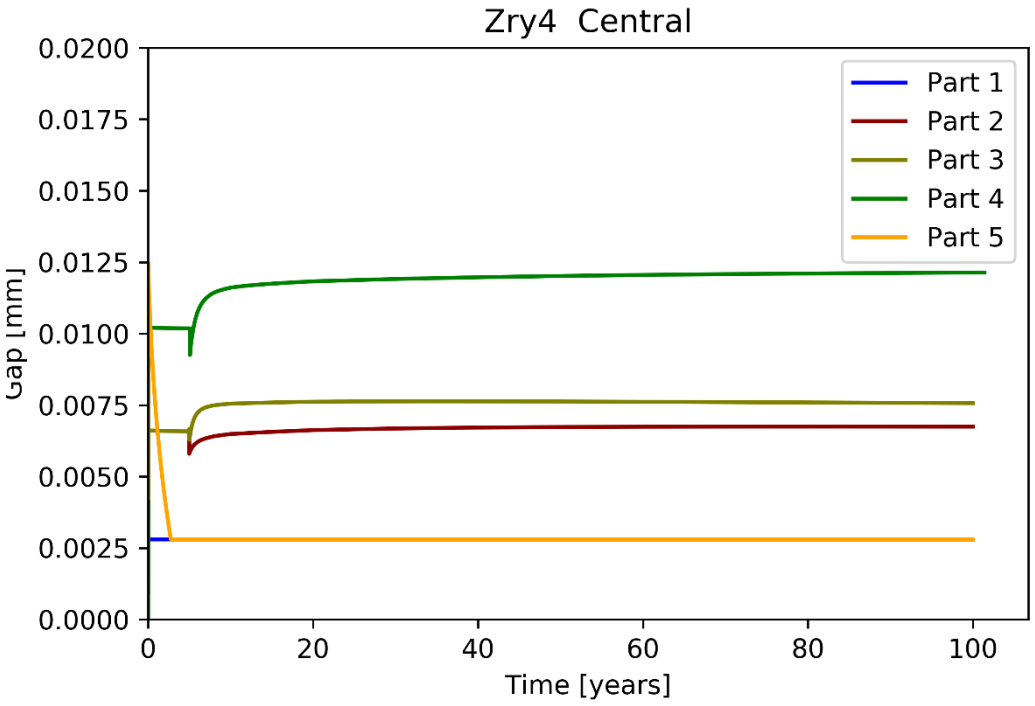

Fig. 3.22 Pellet-cladding gap (GAP) of Zry-4 central rod during storage

The calculated results for the pellet-cladding gap vary between the different codes, shown in Fig. 3.22. Some codes predict a gap closure, which is given by the gap width equal to the pellet roughness (0.0028 mm for Part 1 and 5). Some codes predict a permanent gap closure which occurs before dry storage (Part 1 and 5). The codes from Part 2, 3 and 4 predict an open gap and a shrinking of the gap width during drying procedure at t = 5 years with an increased gap afterwards.

The results received for the cladding inner radius (RCI) are presented in Fig. 3.21. All participants show a similar behaviour: After five years of wet storage the cladding inner radius increases due to the heat up of the cladding during drying procedure. Afterwards, the slow cool down leads to a decreasing radius. Part 5 shows a different behaviour, where the radius already increases during wet storage. This effect is given due to a fuel swelling induced increasing fuel radius.

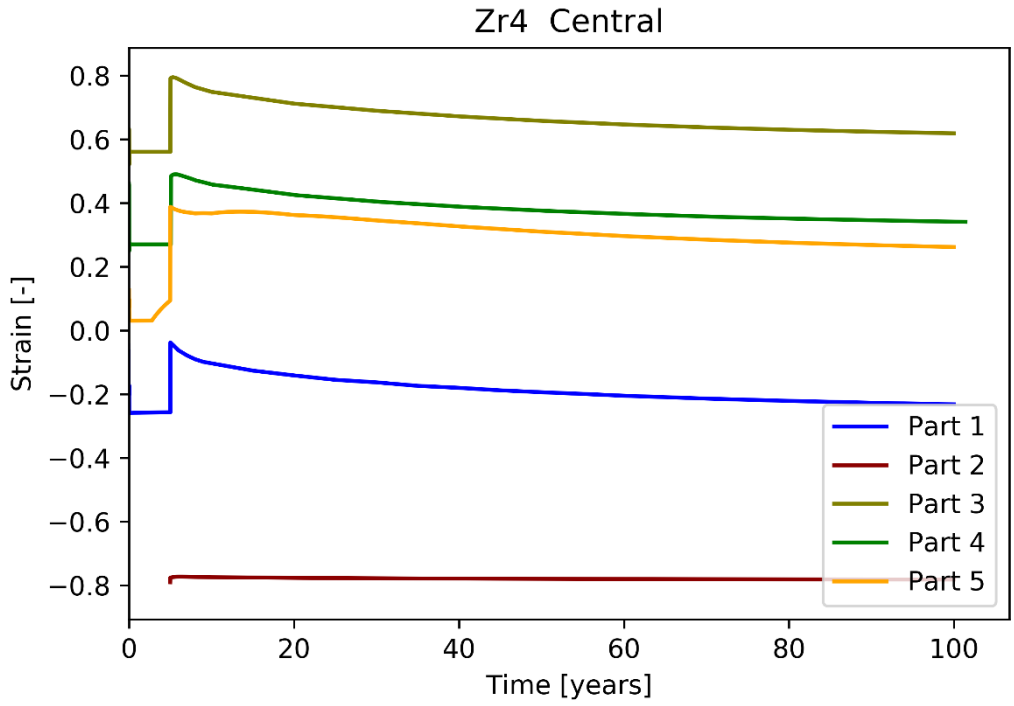

Fig. 3.23 Cladding total hoop strain (ECTH) of Zry-4 central rod during storage

The cladding's total hoop strain (ECTH) is shown in Fig. 3.23. All results show an offset depending on the different predictions during operation and wet storage. Part 1, 3, 4, and 5 show a sharp increase during the drying process, which could be caused by two effects: The increase of the temperature leads to a thermal expansion of cladding and fuel especially for the case of closed pallet-cladding gaps and on the other hand due to the temperature increase causing an increase of the internal pressure and in turn increasing the hoop stresses of the cladding for an open pellet-cladding gap. This effect can also be observed for Part 2, but to a lesser extent. For Part 5, one can observe a similar behaviour as seen in Fig. 3.21, ECTH and RCI start to increase midway through the wet storage resulting from a pellet-cladding gap closure.

The results for the cladding plastic deformation (ECP) show an equivalent offset, presented in Fig. 3.24. Part 1 shows negative plastic deformation possibly related to the creep down of cladding during the operation due to over pressure, while the cladding creep out due to PCMI is not sufficient to overcome previous creep down. The other codes predict a very small or positive outward deformation related to thermal expansion. Especially Part 2 and 6 show an increased plastic deformation during drying process. Comparing these results to Fig. 3.22, one can observe that there are results for plastic deformation even with an open pellet-cladding gap.

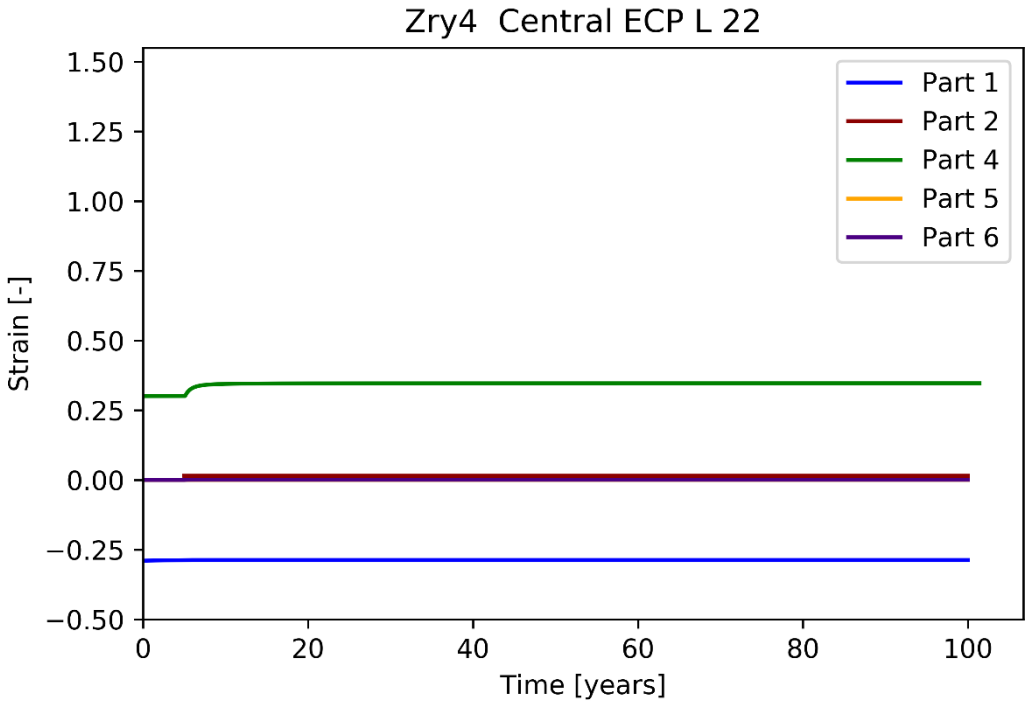

Fig. 3.24 Cladding plastic deformation (ECP) of Zry-4 central rod during storage

Fig. 3.25 shows the results for the cladding hoop stress (SCH). Most of the codes show very similar results except for Part 5: As seen for RCI and ECTH the cladding stresses rise during the wet storage period due to a rigid body pressure between pellet and cladding (gap closure). This effect is caused due to alpha-decay induced fuel swelling, which causes a stress increase even before the drying effect. With the onset of the drying procedure the thermal expansion of the pellet leads to an additional pressure resulting in a local peak stress of SCH ≈ 170 MPa. After a local minimum SCH increases to a maximum stress at t ≈ 25 years with an SCH ≈ 220 MPa. The other results show rather low stress in the range of 40 MPa to 55 MPa. The results of Part 3 exhibit an offset of stress already during wet storage.

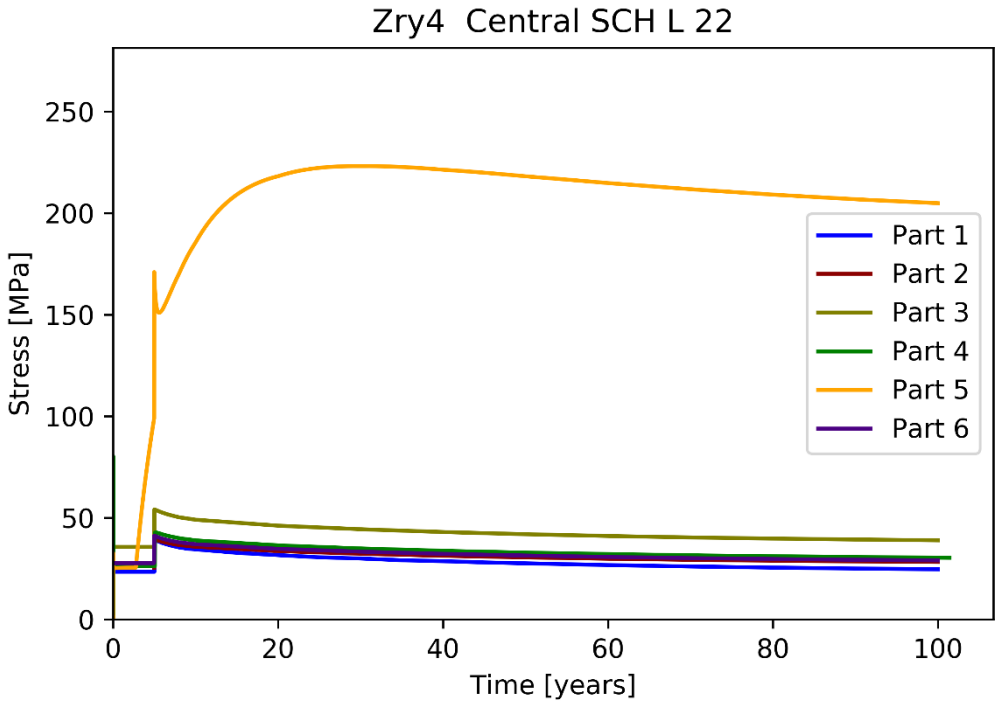

Fig. 3.25 Cladding hoop stress (SCH) of Zry-4 central rod during storage

The results for the gas pressure (PRG) shown in Fig. 3.26 are presented for the full rod, not for a single axial zone, since all participating codes assume axial gas communication over the fuel rod length. Equivalently to the results for hoop stress in Fig. 3.25, an offset of pressure can be observed for Part 3, beginning with higher pressures during wet storage which leads to a shifted result compared to the other codes. Part 5 shows a larger increase during drying process compared to the other solution. Parts 1 to 4 predict decreasing pressures mainly related to the cool-down of the fuel rod over the complete storage period. Part 5 shows a decreasing pressure which stabilizes around 65 years and starts to increase afterwards. According to Fig. 3.19, the temperature decreases over the whole storage period, therefore the increasing pressure cannot be related solely to gas thermal expansion. The additional pressure should result from either gas production or gas release from the pellet.

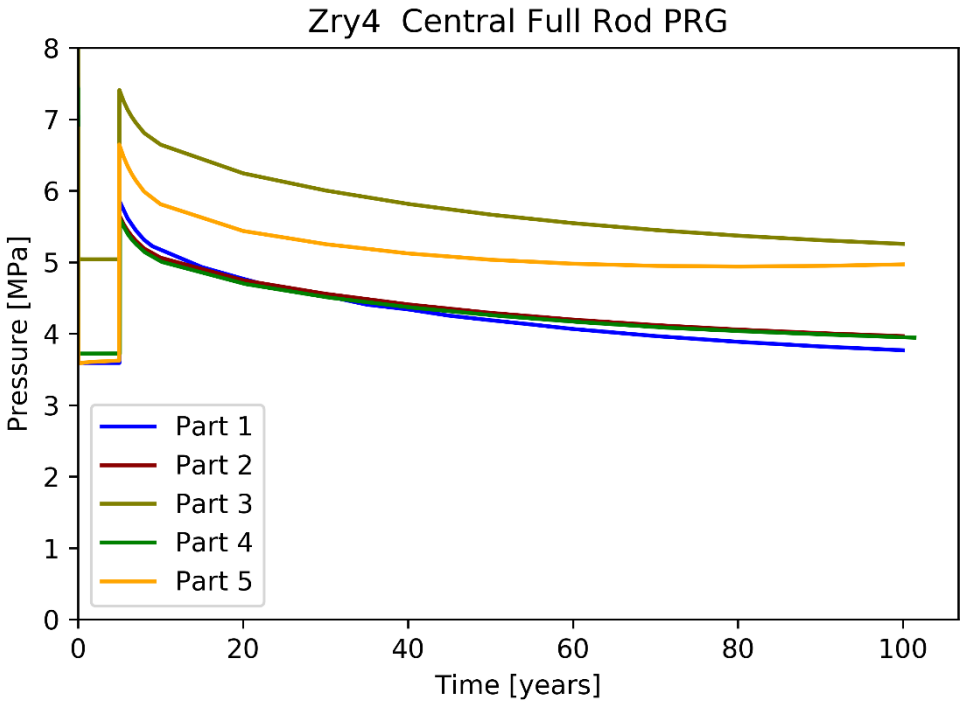

Fig. 3.26 Fuel rod gas pressure (PRG) of Zry-4 central rod during storage

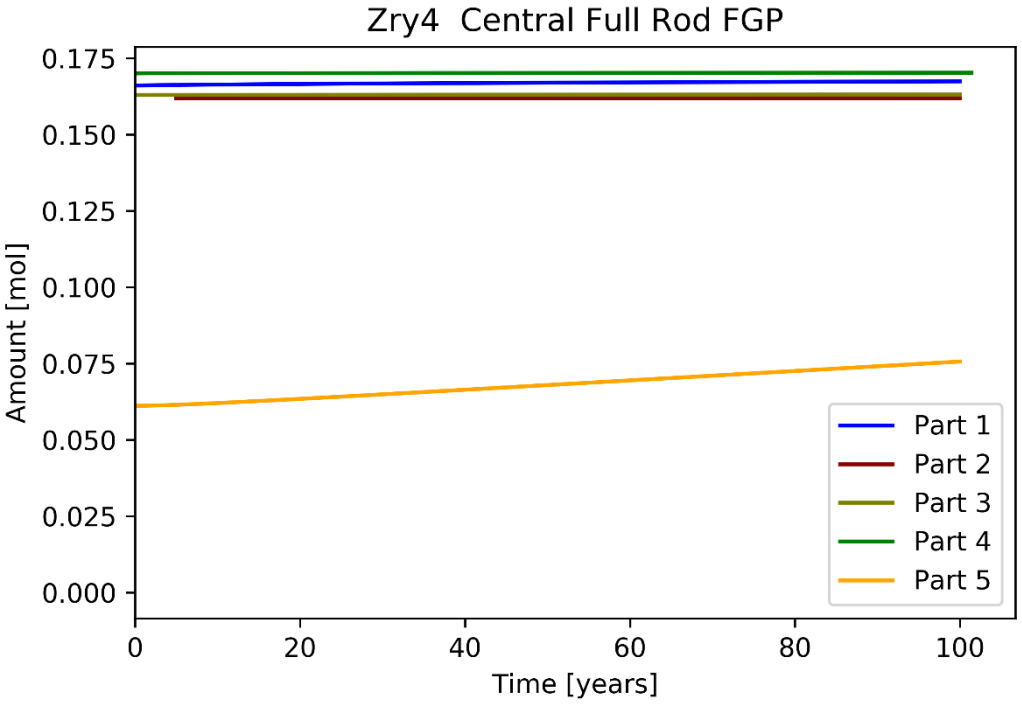

Fig. 3.27 Fission gas production (FGP) of Zry-4 central rod during storage

In Fig. 3.27**,** the fission gas production FGP is shown in moles. Depending on the definition of fission gas production, it might apply exclusively to the gaseous fission products during operation, or it includes the additional source of helium due to the alpha-decay. Parts 1 to 4 predict a constant amount of fission gases during the storage period since this is a post operation scenario. Part 5 shows a lower amount of fission gas (approximately one third of the mole mass predicted by other codes), but with a steady increase over the storage period. This is due to the inclusion of helium release.

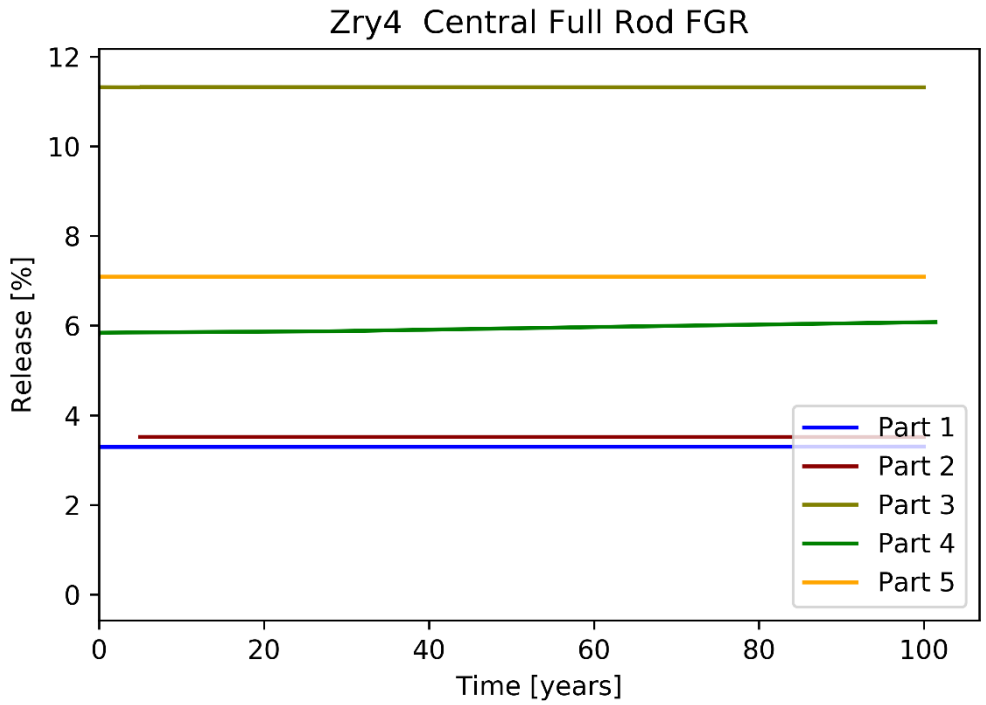

Fig. 3.28 Fission gas release (FGR) of Zry-4 central rod during storage

Fig. 3.28 presents the fission gas release, which is nearly constant over the storage period. Only Part 4 shows a slight increase of fission gas release during the storage period. Other codes show a more constant share of released fission gases.

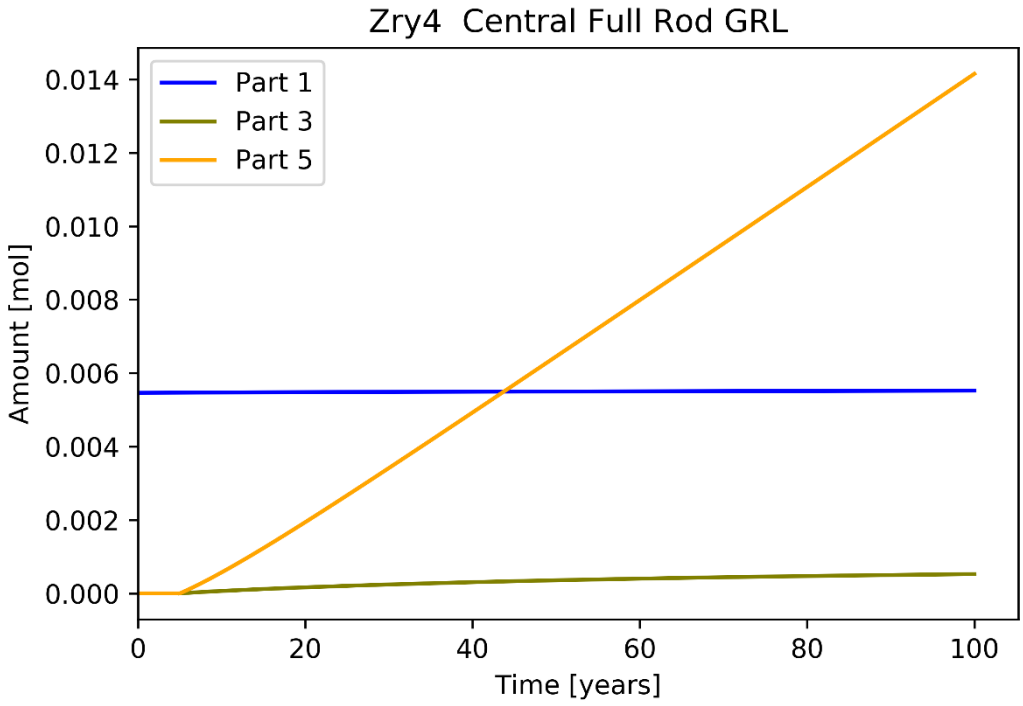

Fig. 3.29 Gas release (GRL) of Zry-4 central rod during storage

The gas release during storage is shown in Fig. 3.29 for Part 1, 3 and 5 over the storage period. This parameter describes the additional part of helium originated from alpha-decay and released from the fuel. Part 5 shows a strong and steady increase beginning with the dry storage period. The increase in Fig. 3.27 for Part 5 results from GRL. Part 3 shows a minor gas release, slightly increasing. Part 1 shows no additional gas release during storage (such as Helium), while it showed a minimal FGP as shown in Fig. 3.27.

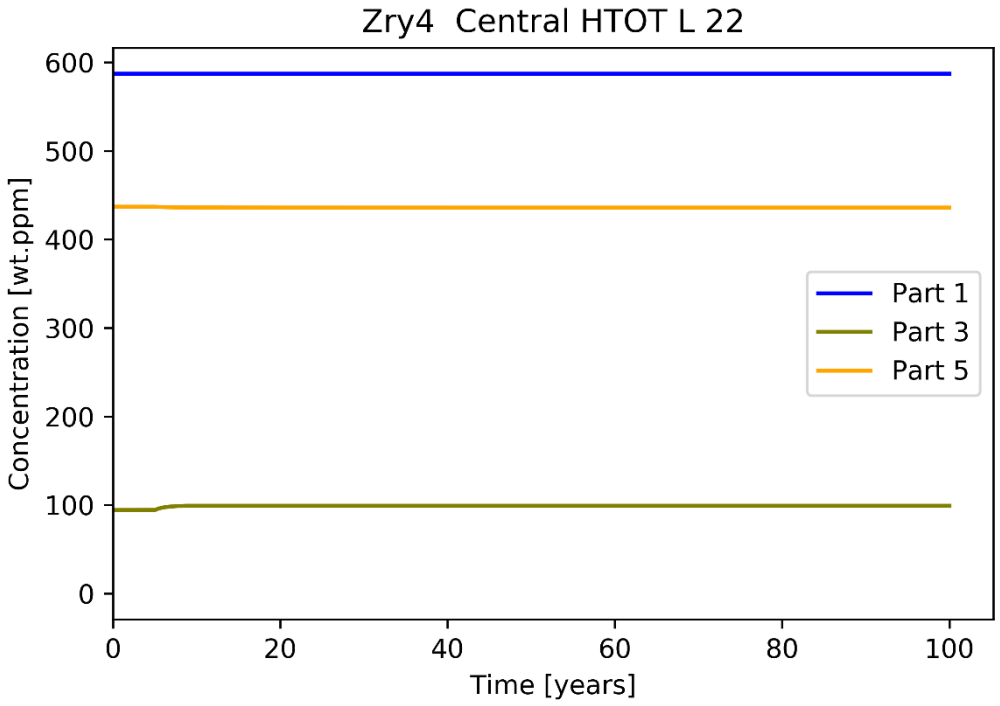

Fig. 3.30 Total hydrogen content (HTOT) of Zry-4 central rod during storage

The total hydrogen uptake (HTOT) is predicted differently by all three results, shown in Fig. 3.30. During dry storage, no further cladding oxidation occurs and thus hydrogen uptake should stop. Even though the oxidation thickness resulting from operation was part of the specification, not all codes imposed this value on their models as Part 1 did. Therefore, hydrogen content differs also between the three codes. Part 3 predicts a small increase of hydrogen at the beginning of the drying process, which could have multiple reasons. If the corrosion model in this code is not deactivated after reactor operation or wet storage, an additional oxidation is predicted with increasing temperatures during drying process. Another possibility would be the hydrogen diffusion along the axial direction of the fuel rod since the hydrogen mobility is increased with increasing temperature. Since the axial level 22 is one of the hottest, diffusion processes should lead to decreasing values if this effect is considered.

Fig. 3.31 describes the share of dissolved hydrogen of the total amount of hydrogen (HDIS). Only two results for this parameter were received. The temperature dependent effect is similar in both codes for the drying process where up to 21 % of the hydrogen is dissolved. The decreasing temperatures lead to a reprecipitation of hydrogen in the following decades. Part 5 describes a faster precipitation than Part 1.

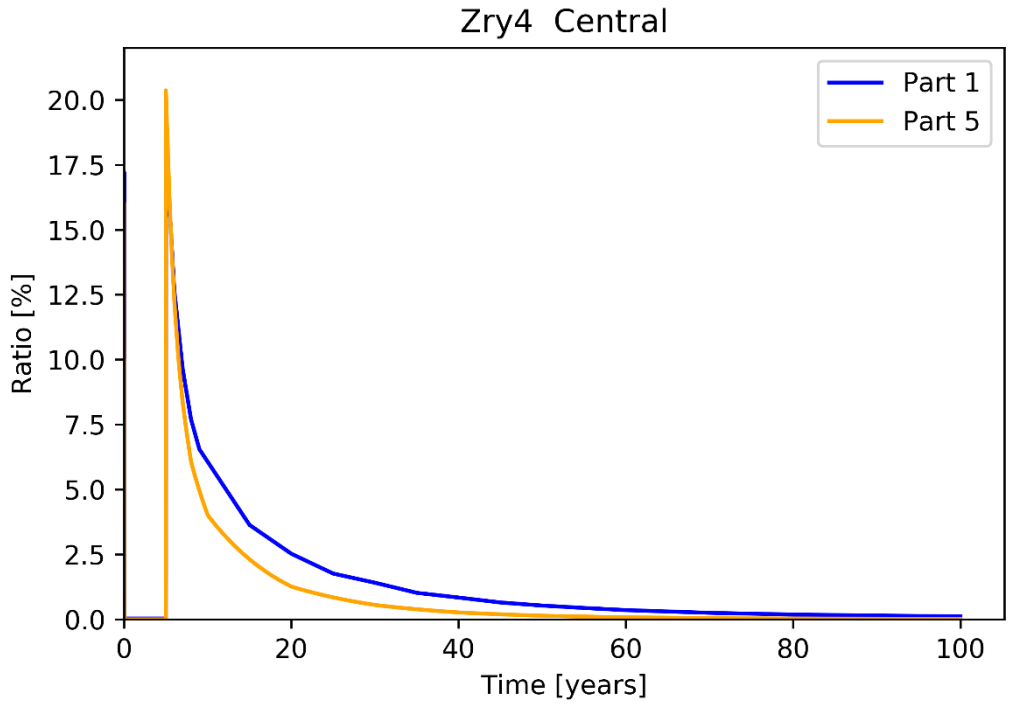

Fig. 3.31 Share of dissolved hydrogen (HDIS) of Zry-4 central rod during storage

Hydrogen may be existent as hydride precipitated or in a dissolved state. The hydride orientation, radial or circumferential may have a significant impact on the cladding mechanical properties. The amount of circumferential hydrides (HCIR) is depicted in Fig. 3.32. During the wet storage, Part 1 predicted 100 % of circumferential hydrides, whereas approximately 90 % are present for Part 5. After the drying process, the number of circumferential hydrides recovers for Part 1, i.e., hydrogen reprecipitates in the same orientation as it was before: all hydrides are circumferentially oriented. For Part 5 the share of circumferential hydrides remains constant over the rest of the dry storage period, by 80 %.

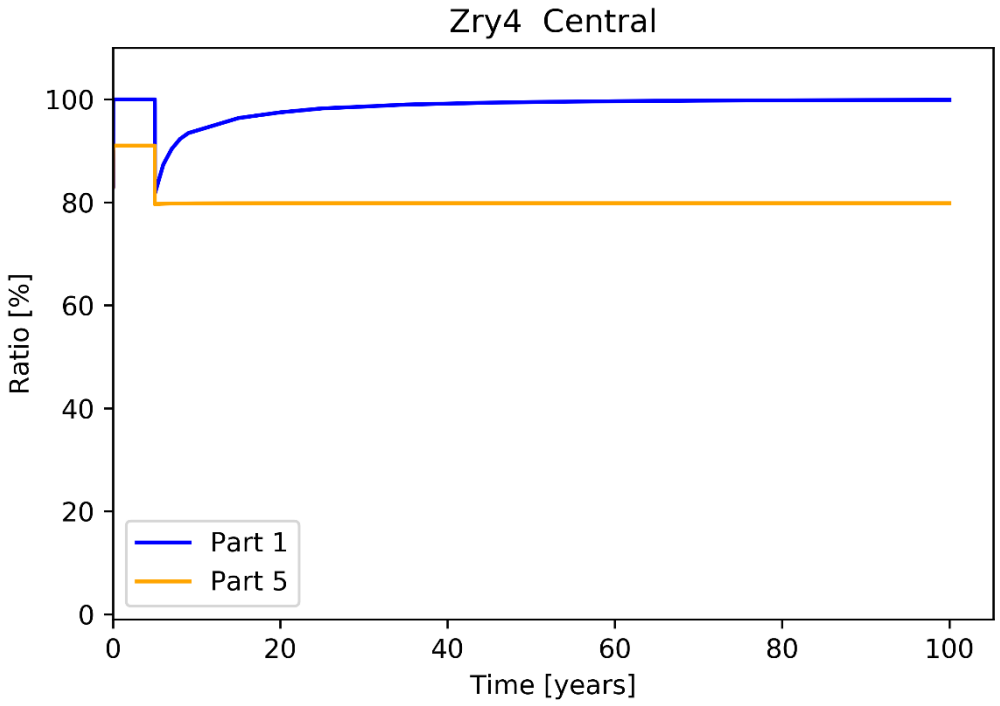

Fig. 3.32 Share of circumferential hydrides (HCIR) of Zry-4 central rod during storage

The dissolved hydrogen of Part 5 forms radial hydrides (HRAD) during the cooldown instead, as shown in Fig. 3.33. The stress state in the cladding is high enough to cause radial hydride precipitation. Only the solutions of Part 1 exhibit stresses too low to form any radially oriented hydrides. Most hydrides which precipitated during reactor operation or at the end of operation, remain precipitated during the full period of storage. They do not dissolve during the drying process, the orientation of precipitated hydrides remains the same.

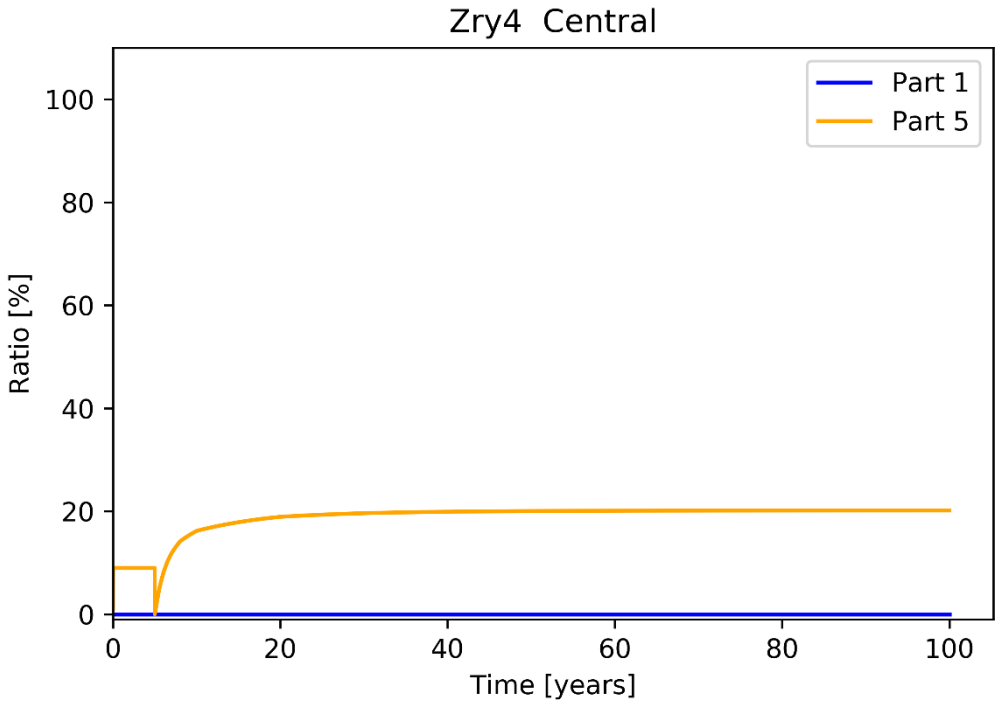

Fig. 3.33 Share of radial hydrides (HRAD) of Zry-4 central rod during storage

3.3 Storage behaviour for Zircaloy-4 corner rod

The corner rod as part of the central fuel assembly exhibits lower temperatures than the central rod. Besides that, the conditions for this rod are very similar. These lower temperatures directly influence the geometry of the fuel pellet and cladding and further the balance of hydrogen and hydrides in the cladding.

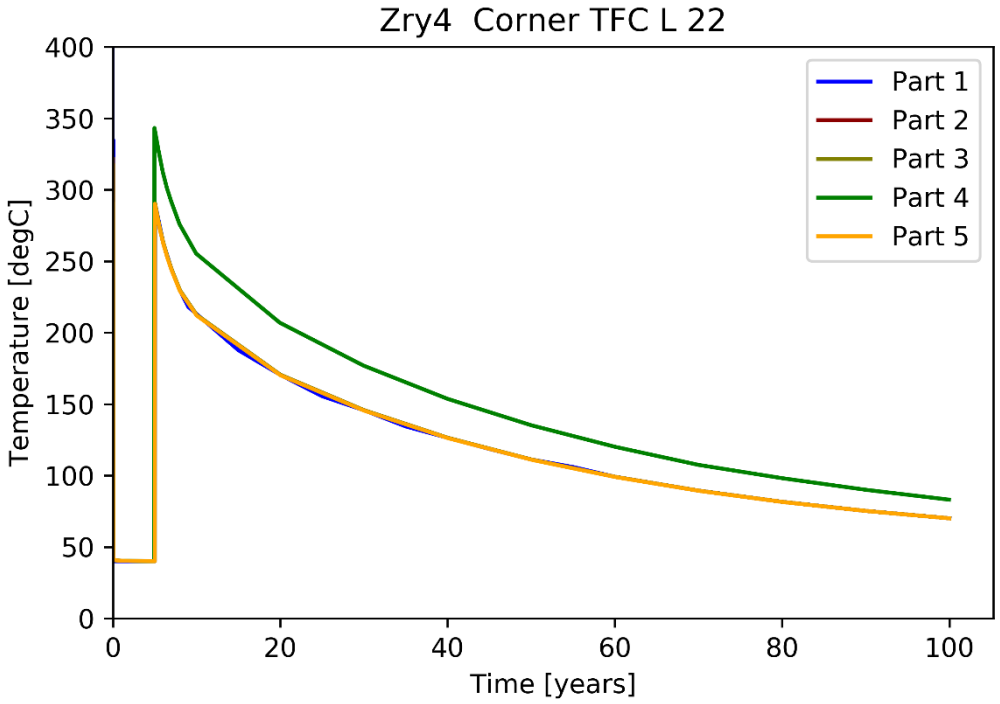

Fig. 3.34 Fuel centreline temperature (TFC) of Zry-4 corner rod during storage

Fig. 3.34 shows the fuel centreline temperature, imposed by the input parameters. Part 3 exhibits a higher fuel temperature compared to others. These may result from the same temperature distribution used for the central rod (on the hotter position). This effect is directly linked to TFO and TCO in Fig. 3.35 and Fig. 3.36, respectively.

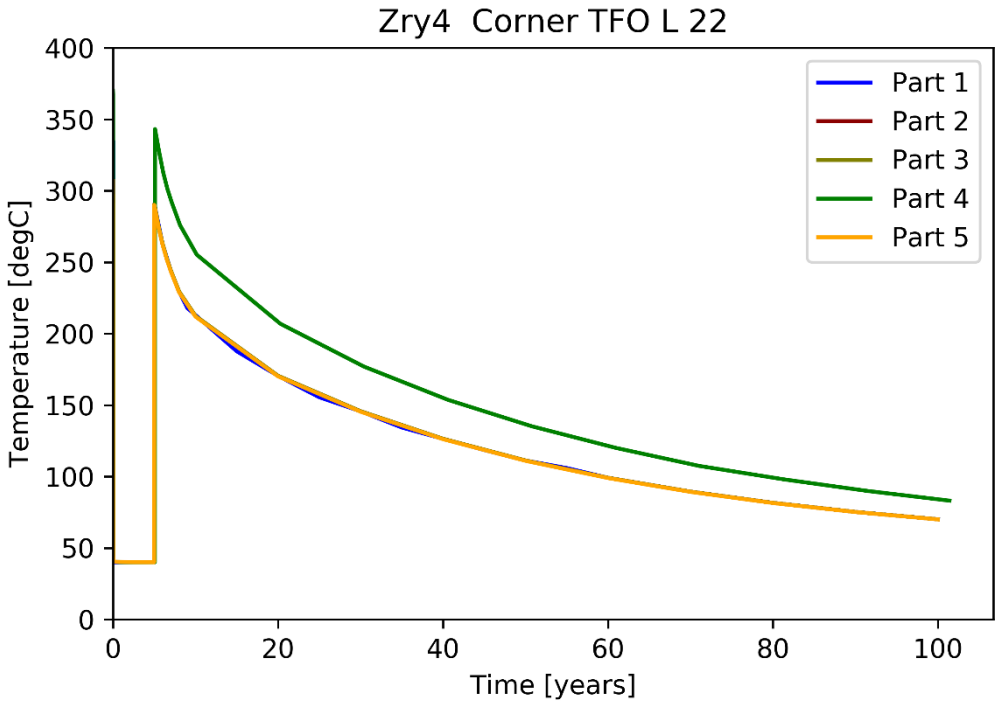

Fig. 3.35 Fuel outer temperature (TFO) of Zry-4 corner rod during storage

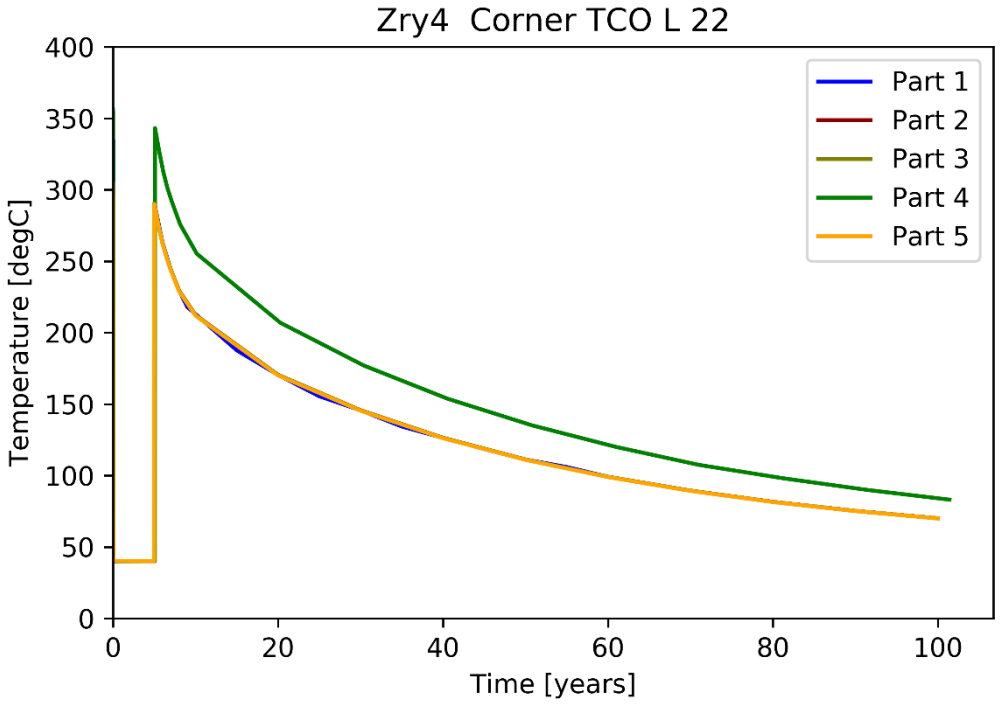

Fig. 3.36 Cladding outer temperature (TCO) of Zry-4 corner rod during storage

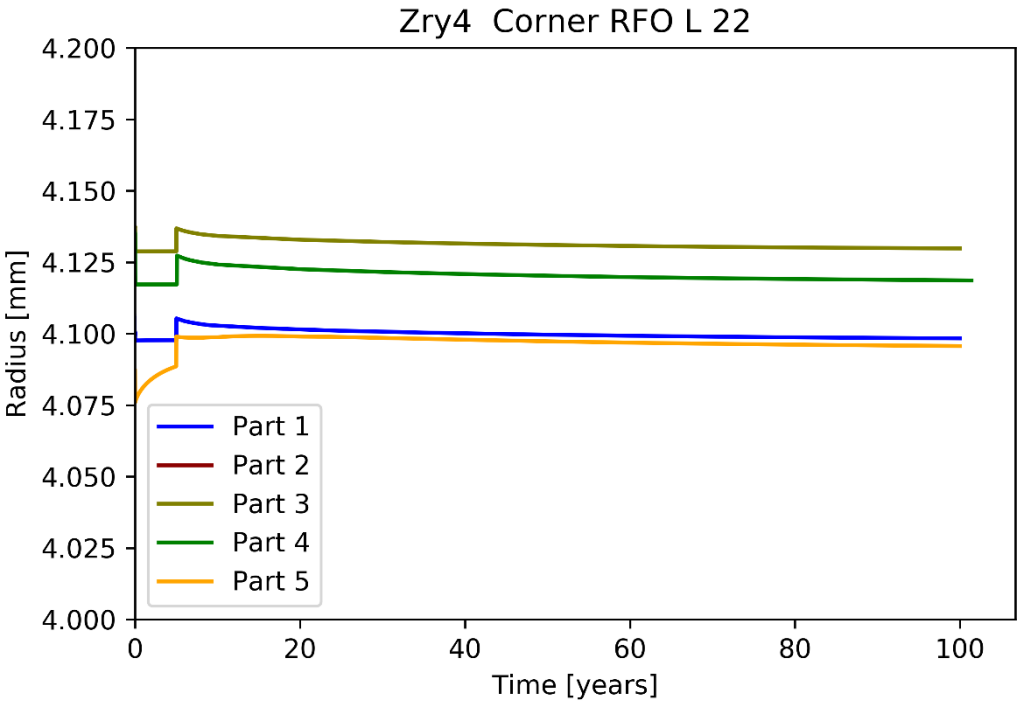

Fig. 3.37 Fuel outer radius (RFO) of Zry-4 corner rod during storage

The fuel outer radius is shown in Fig. 3.37, which shows a similar behaviour as for the central rod in Fig. 3.20. Part 4 should have a slightly higher RFO since the assumed temperature is higher as for the other codes. Analogue results are shown for the cladding inner radius in Fig. 3.38.

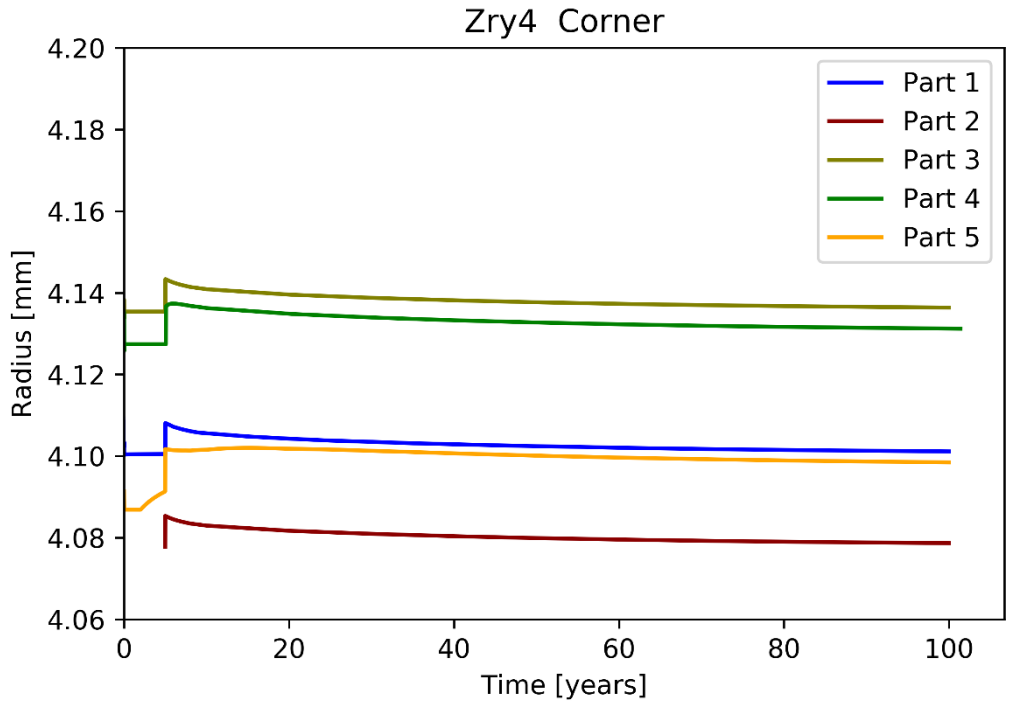

Fig. 3.38 Cladding inner radius (RCI) of Zry-4 corner rod during storage

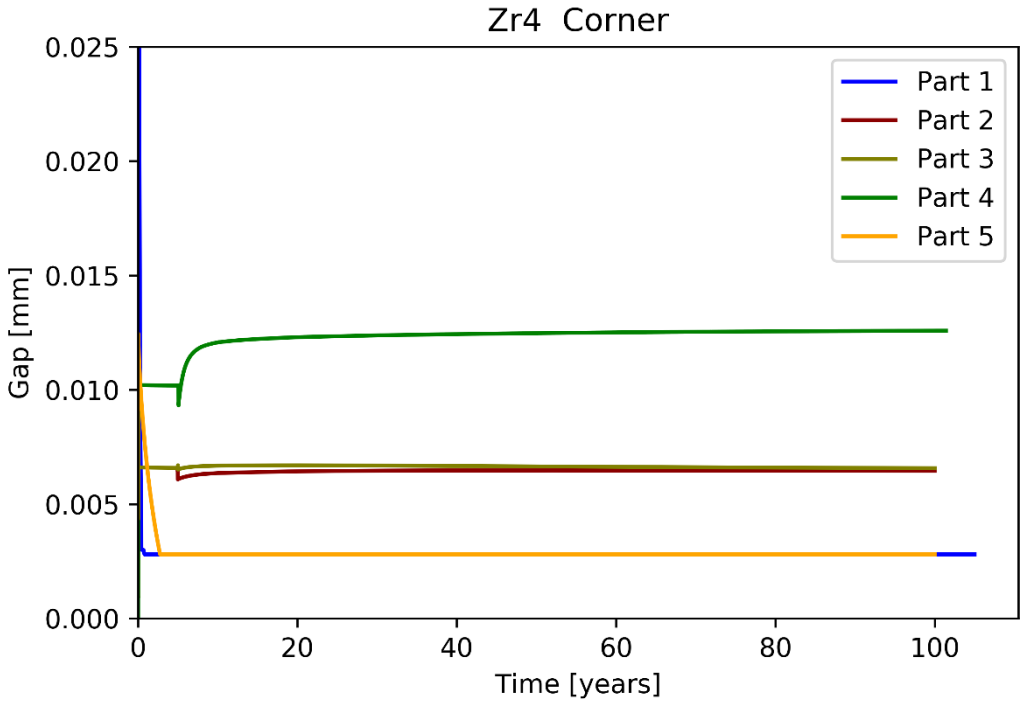

Fig. 3.39 Pellet-cladding gap (GAP) of Zry-4 corner rod during storage

The pellet-cladding gap shows similar effects for Part 2 and 3 compared to the central rod, but is less pronounced due to the lower temperatures achieved during drying process. Part 1 and 5 show gap closure during wet storage at 2.8 µm.

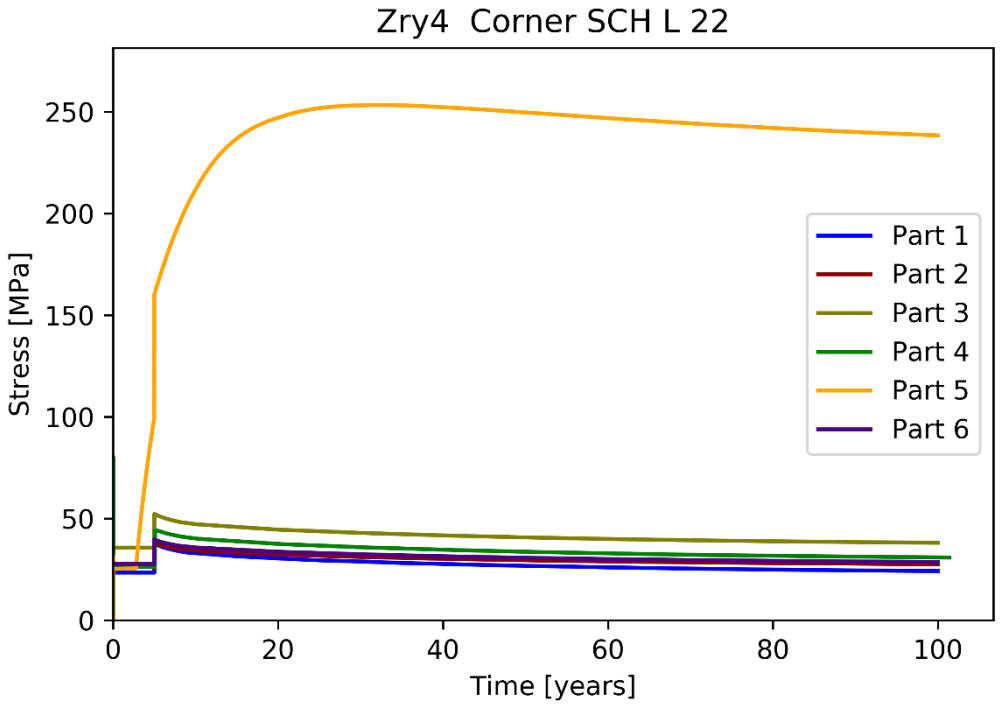

Fig. 3.40 Cladding hoop stress (SCH) of Zry-4 corner rod during storage

Fig. 3.40 shows the total cladding hoop stress during storage. The drying process leads to an increase in stress for Part 1 to 4 and 6. Part 5 shows a stress increase due to pellet-cladding gap closure during wet storage and a constant increase during the drying process and the first years of dry storage. Compared to the central rod (Fig. 3.25) there is no small peak at the end of the drying procedure.

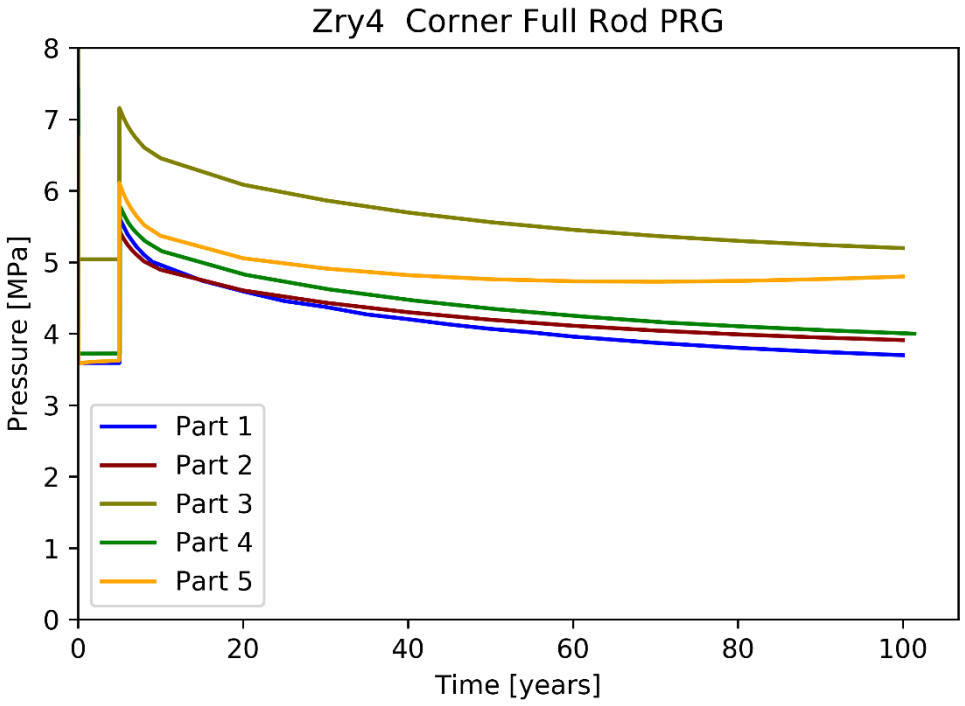

Fig. 3.41 Fuel rod gas pressure (PRG) of Zry-4 corner rod during storage

The fuel rod pressure is shown in Fig. 3.41 starting for Part 1, 2, 4 and 5 around 3.8 MPa inner pressure and for Part 3 at around 5.1 MPa pressure. All codes present a significant pressure increase of about 2 MPa during the drying process, followed by a decrease of pressure after the beginning of dry storage. Part 5 shows a late increase of pressure as observed for the central rod, as in Fig. 3.26. The higher temperatures for Part 4 seem to have no significant impact on the fuel rod gas pressure when compared to Part 2 and 1.

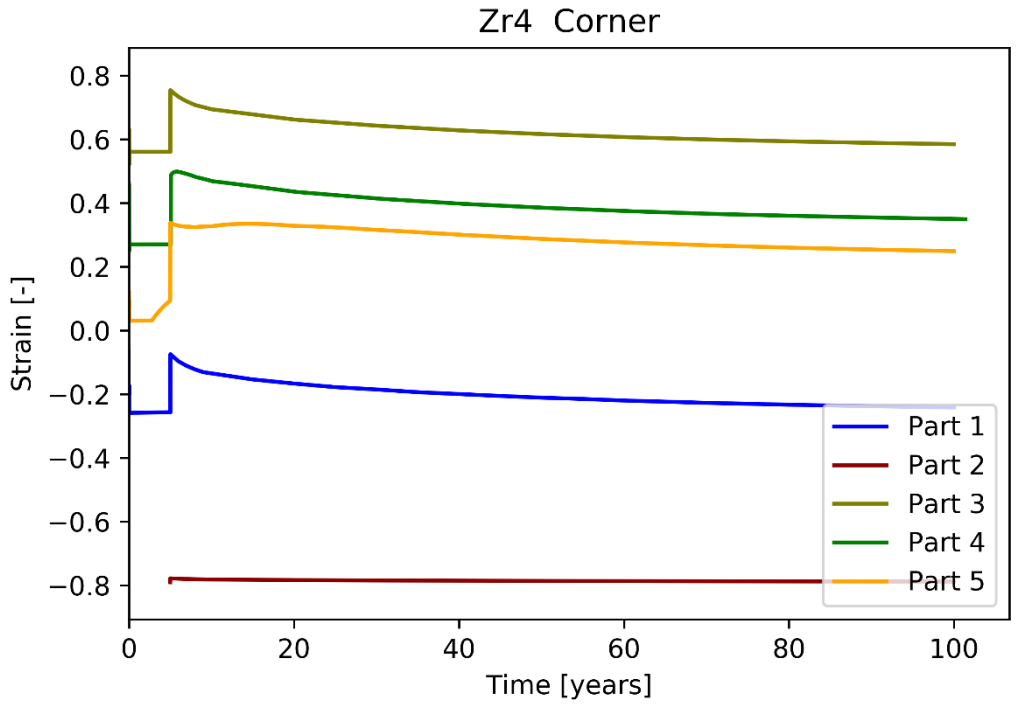

Fig. 3.42 Cladding total hoop strain (ECTH) of Zry-4 corner rod during storage

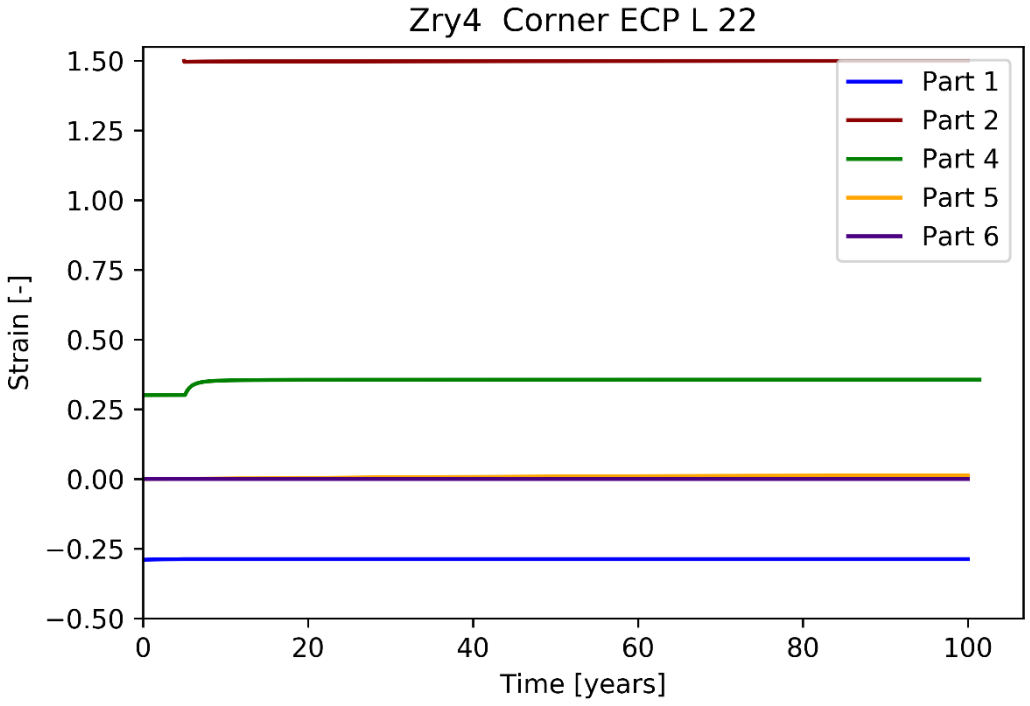

Fig. 3.43 Cladding plastic deformation (ECP) of Zry-4 corner rod during storage

The cladding total hoop strain (Fig. 3.42) and plastic deformation (Fig. 3.43) show a similar effect as for the central rod.

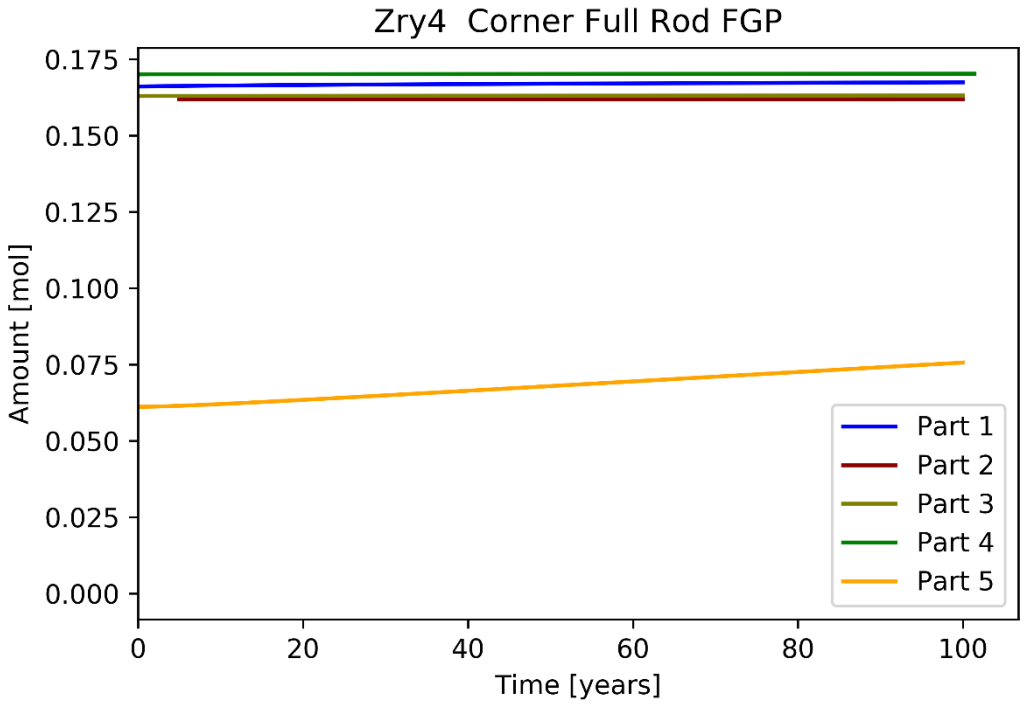

Fig. 3.44 Fission gas production (FGP) of Zry-4 corner rod during storage

The fission gas behaviour in Fig. 3.44and Fig. 3.45 is the same as for the central rod since the fuel has the same operational history.

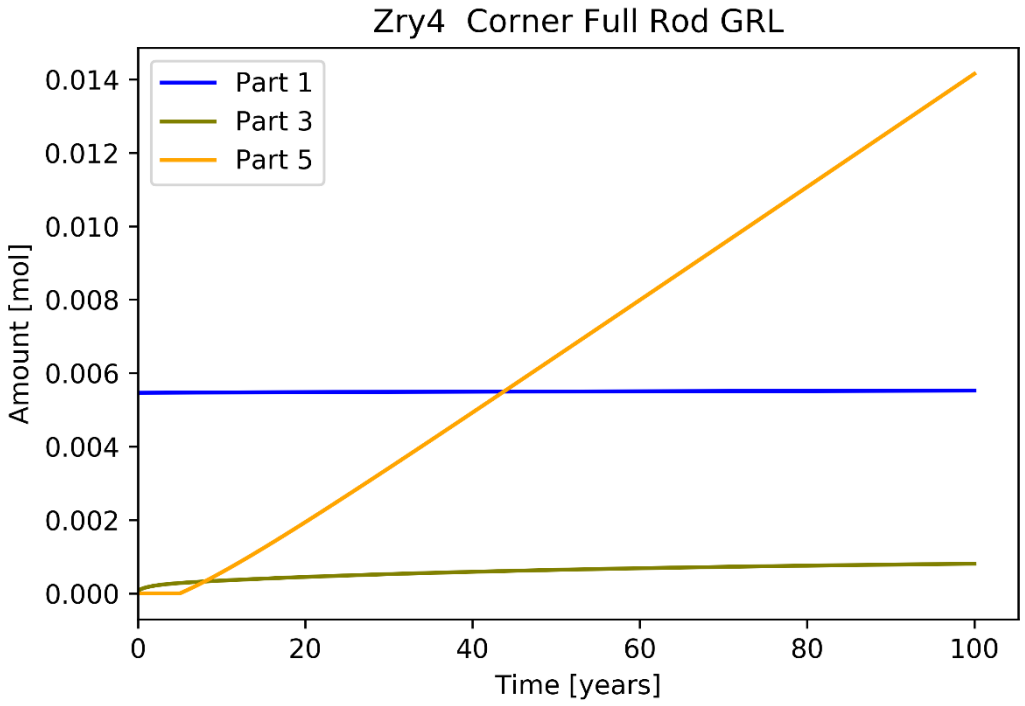

Fig. 3.45 Gas release (GRL) of Zry-4 corner rod during storage

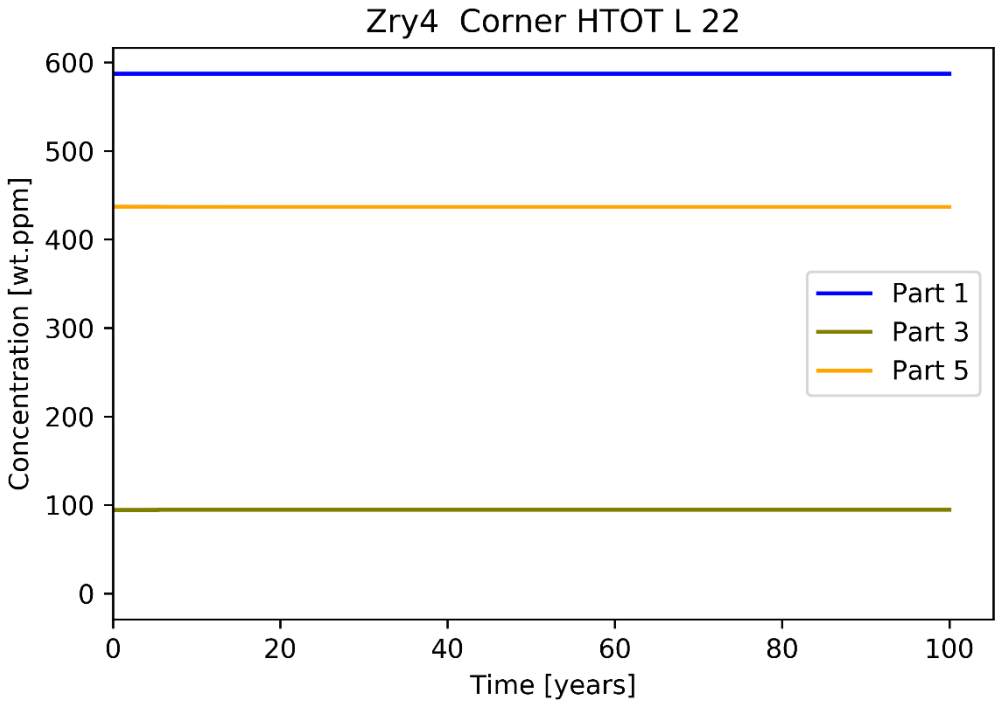

Fig. 3.46 Total hydrogen content (HTOT) of Zry-4 corner rod during storage

The hydrogen content during the storage period is not affected, as shown in Fig. 3.46. The share of dissolved hydrogen in Fig. 3.47 reaches lower maxima for Part 1 and 5 due to the lower temperatures of the corner rod. The circumferential hydrides behave similar as for the central rod, presented in Fig. 3.48. Part 1 shows a decrease of circumferential hydrides during drying and a total recovery within approximately 40 years. Part 5 shows a decrease of circumferential hydrides from 90 % before drying process to 85 % afterwards. Then the share of circumferential hydrides stays constant for the whole dry storage period. Part 5 predicts that the hydrides dissolved during the drying process reprecipitate as radial hydrides during the dry storage, as shown in Fig. 3.49. Part 1 does not predict radial hydrides during the full storage period.

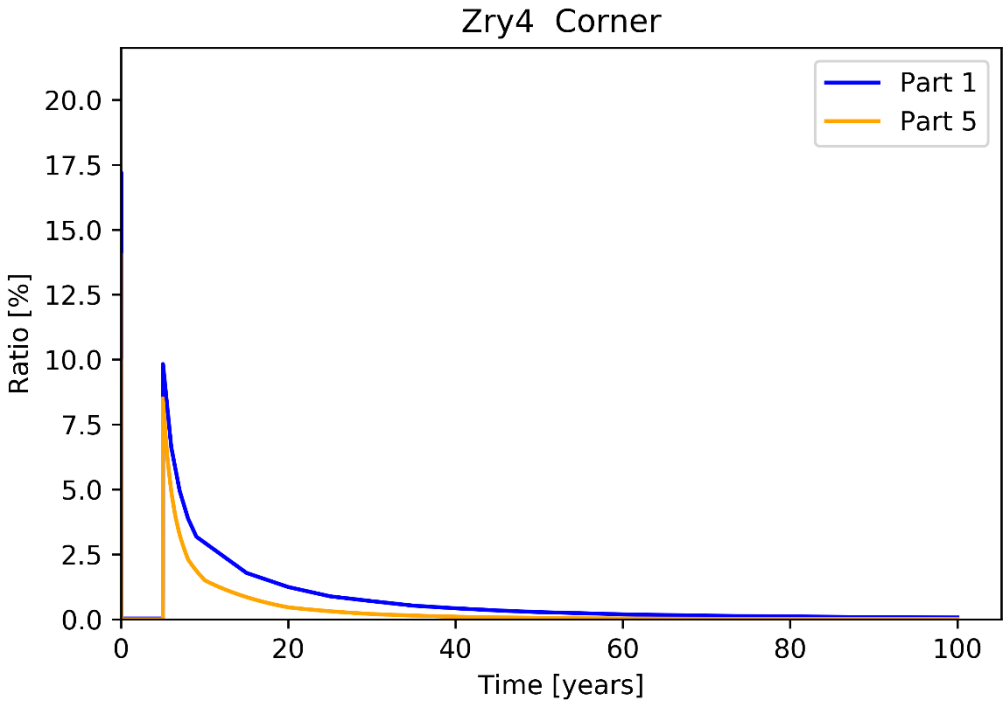

Fig. 3.47 Share of dissolved hydrides (HDIS) of Zry-4 corner rod during storage

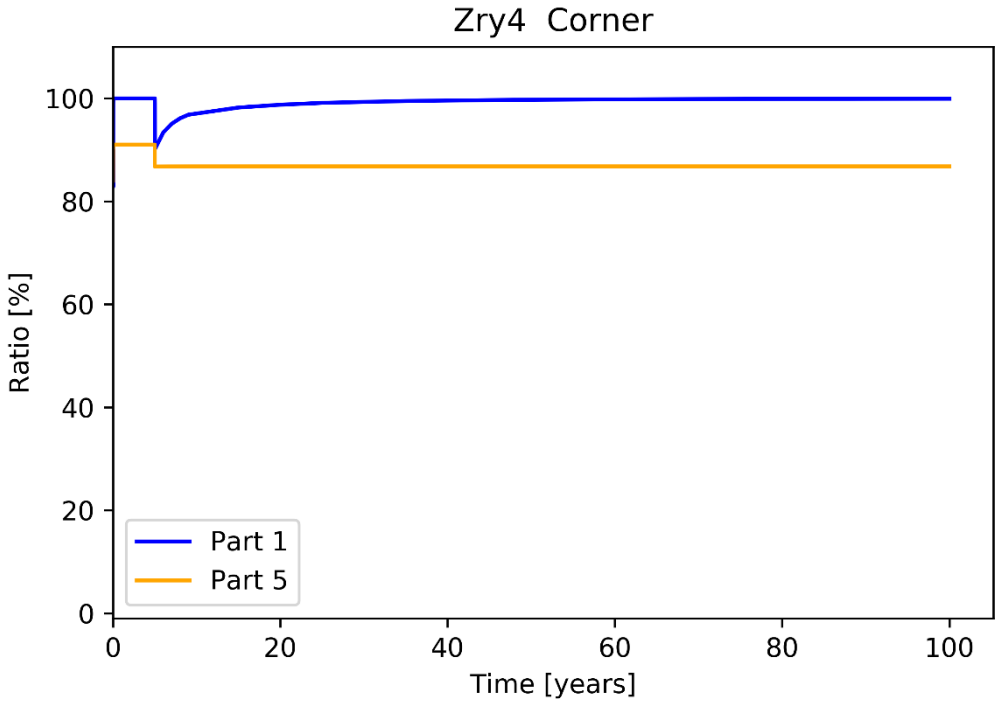

Fig. 3.48 Share of circumferential hydrides (HCIR) of Zry-4 corner rod during storage

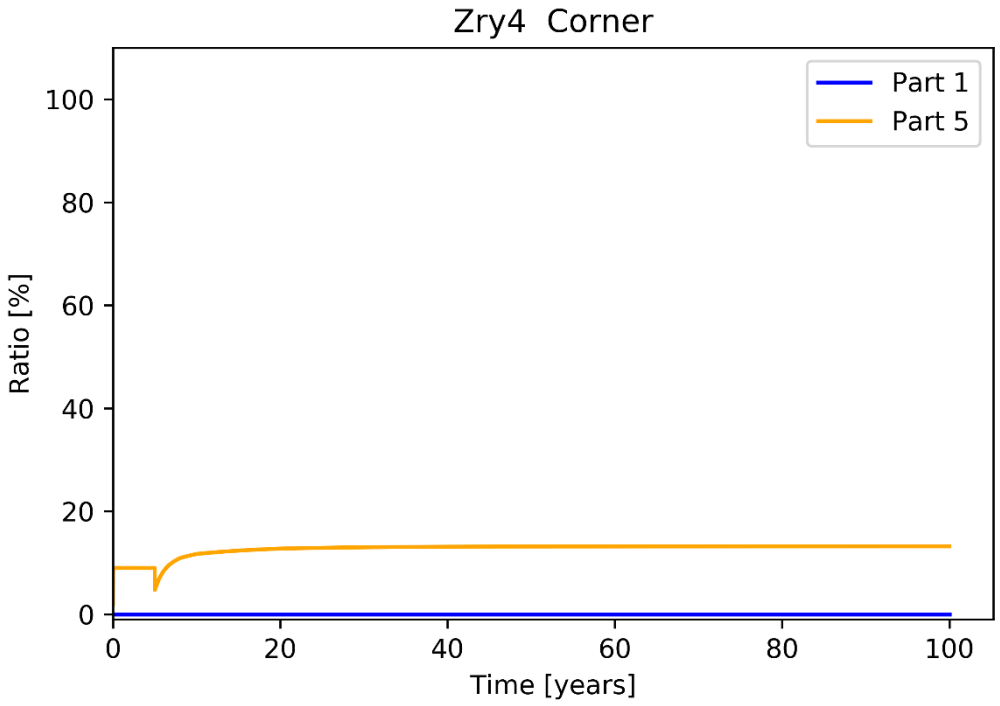

Fig. 3.49 Share of radial hydrides (HRAD) of Zry-4 corner rod during storage

3.4 Operational behaviour for M5

The M5 rod is exposed to the same conditions as the Zry-4 rod in the subsequent sub-chapters. The main difference with the M5 rod is the lower oxidation rate in PWR conditions. For this scenario, only Part 4 delivered solutions which will be presented here. The temperature predictions in Fig. 3.50, Fig. 3.51 and Fig. 3.52 exhibit analogue results as for the Zry-4 results.

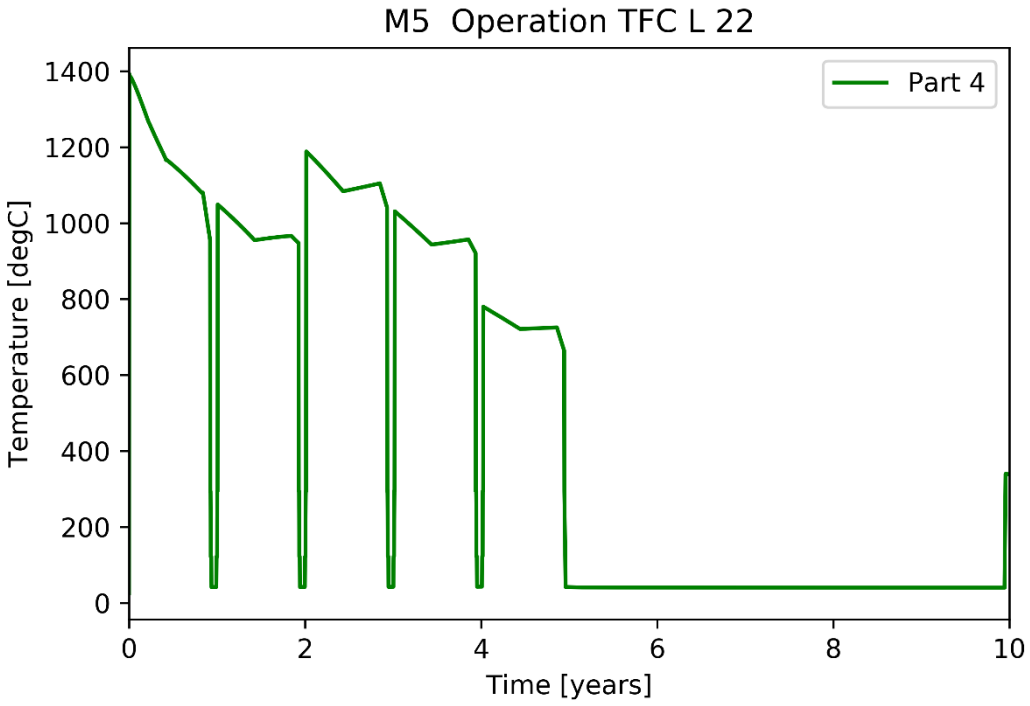

Fig. 3.50 Fuel centreline temperature (TFC) of M5 rod during operation

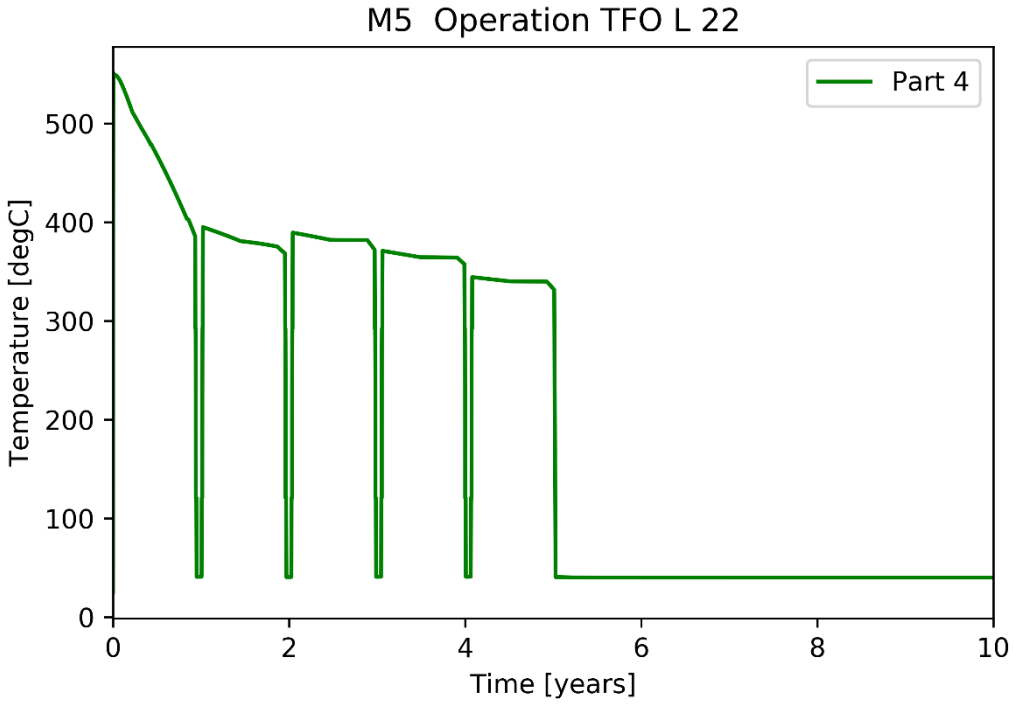

Fig. 3.51 Fuel outer temperature (TFO) of M5 rod during operation

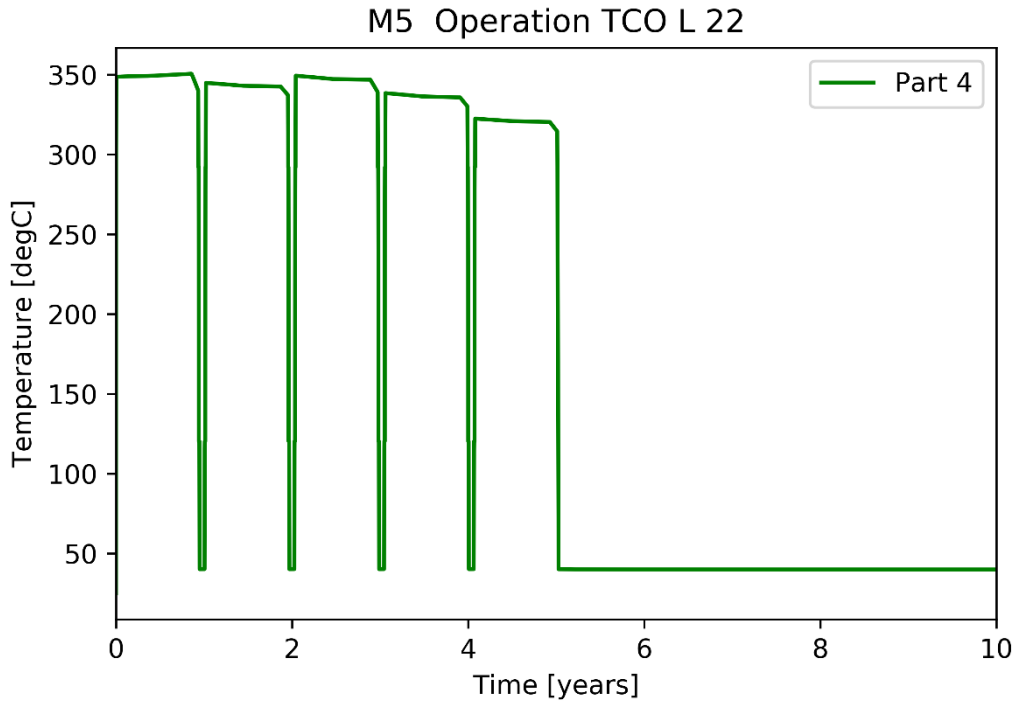

Fig. 3.52 Cladding outer temperature (TCO) of M5 rod during operation

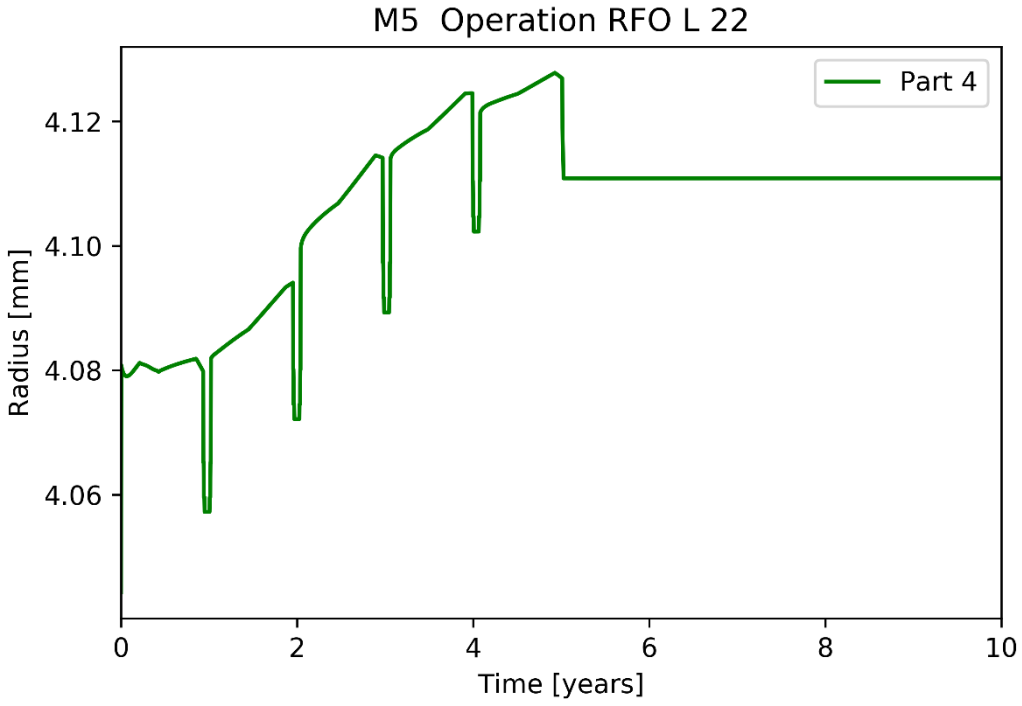

Fig. 3.53 Fuel outer radius (RFO) of M5 rod during operation

Fig. 3.54 Cladding inner radius (RCI) of M5 rod during operation

In Fig. 3.54 one can see the cladding inner radius (RCI) of the M5 rod, which shows compared to Fig. 3.5 slightly smaller values after approximately one year of operation and also during wet storage. The pellet-cladding gap shown in Fig. 3.55 differs slightly from the results for Zry-4 as in Fig. 3.8. The gap of the M5 rod closes already at the end of the first cycle and reopens with every reactor outage at the end of each cycle. The Zry-4 rod shows a small gap during the beginning of the second cycle. Furthermore, the cladding hoop stress in the Zry-4 cladding is larger (Fig. 3.9) than for M5 (Fig. 3.56). Different cladding creep models could have an influence on the gap and the relaxation due to a forced displacement due to PCMI.

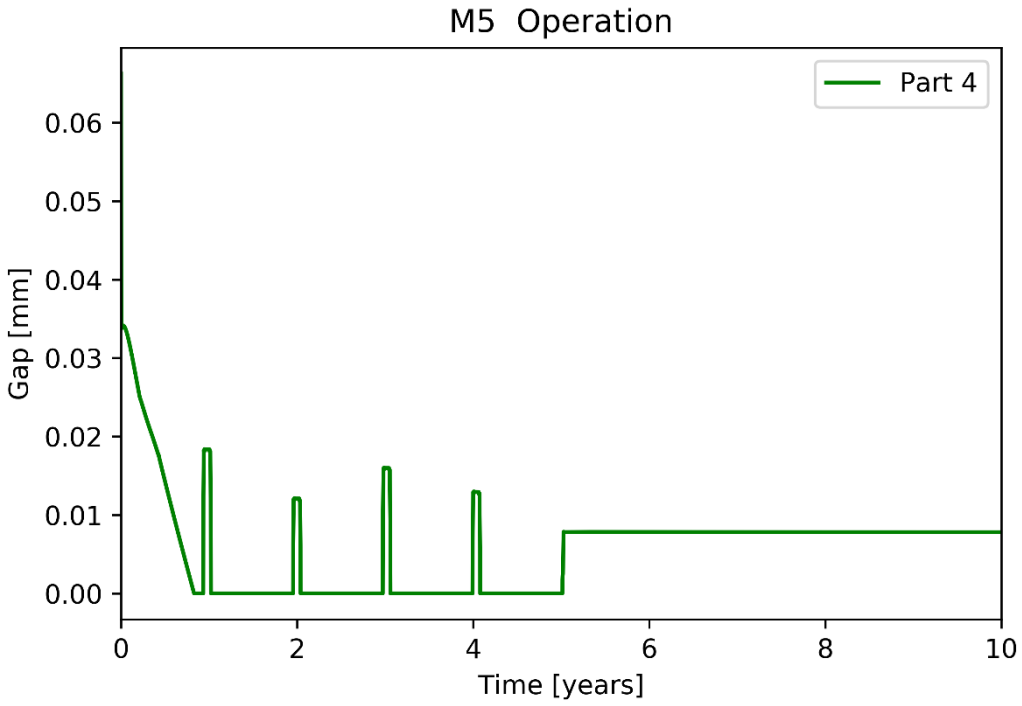

Fig. 3.55 Pellet-cladding gap (GAP) of M5 rod during operation

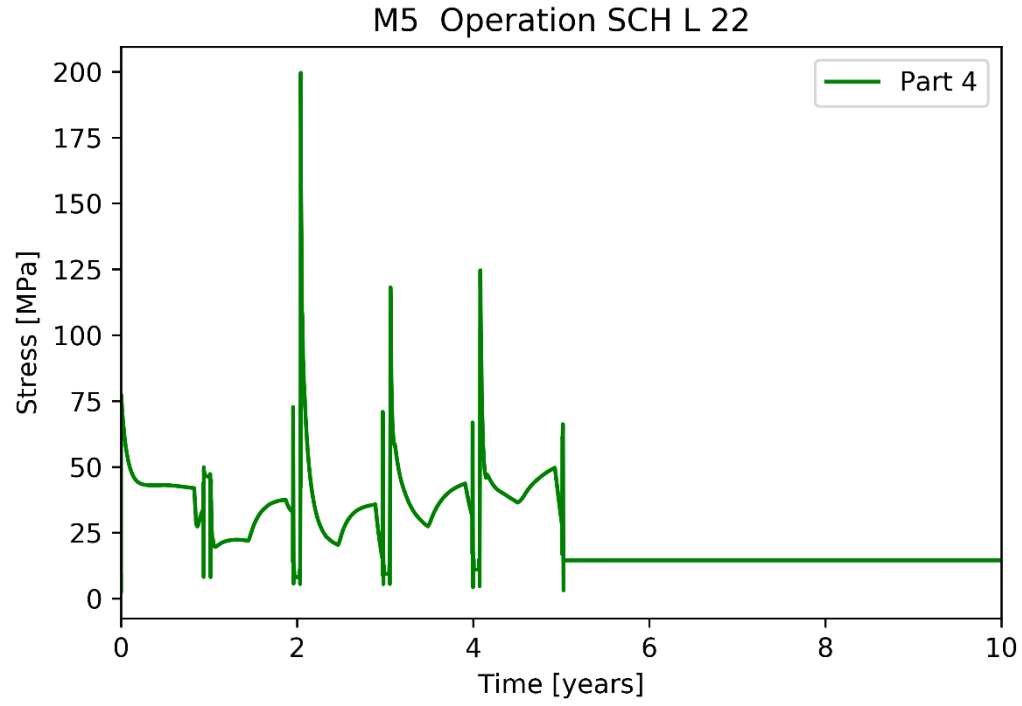

Fig. 3.56 Cladding hoop stress (SCH) of M5 rod during operation

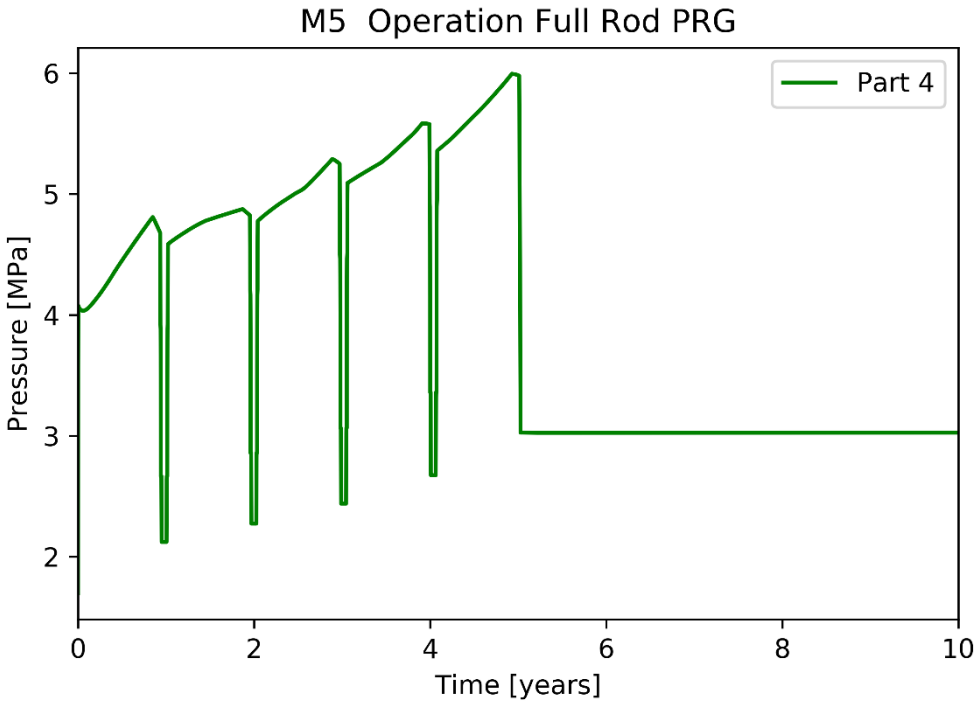

Fig. 3.57 Fuel rod gas pressure (PRG) of M5 rod during operation

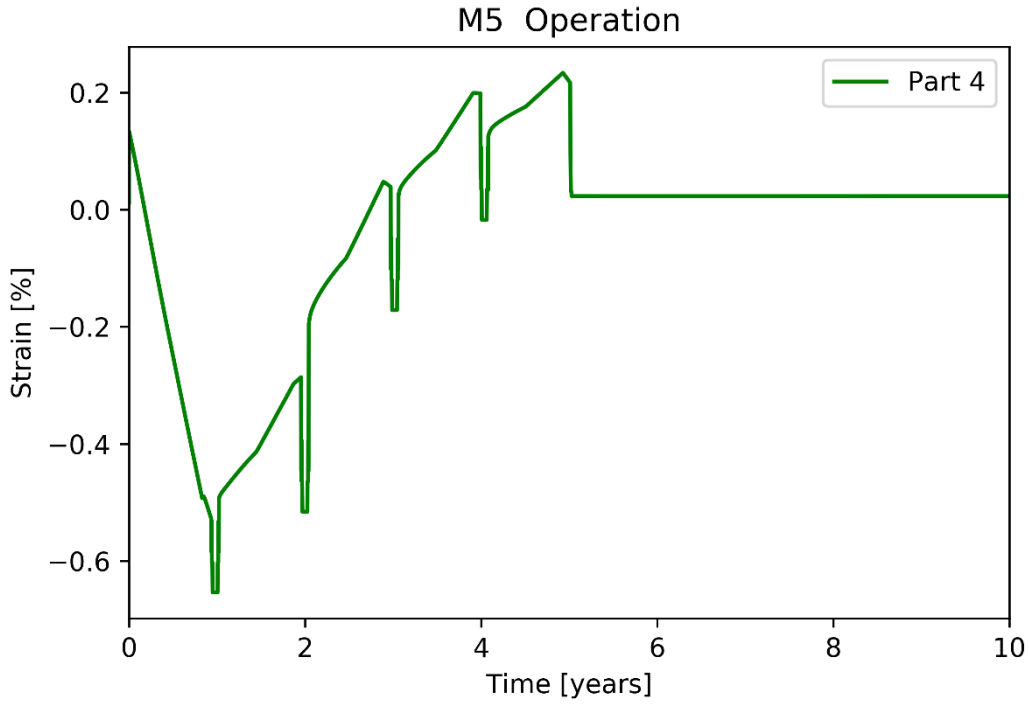

Fig. 3.58 Cladding total hoop strain (ECTH) of M5 rod during operation

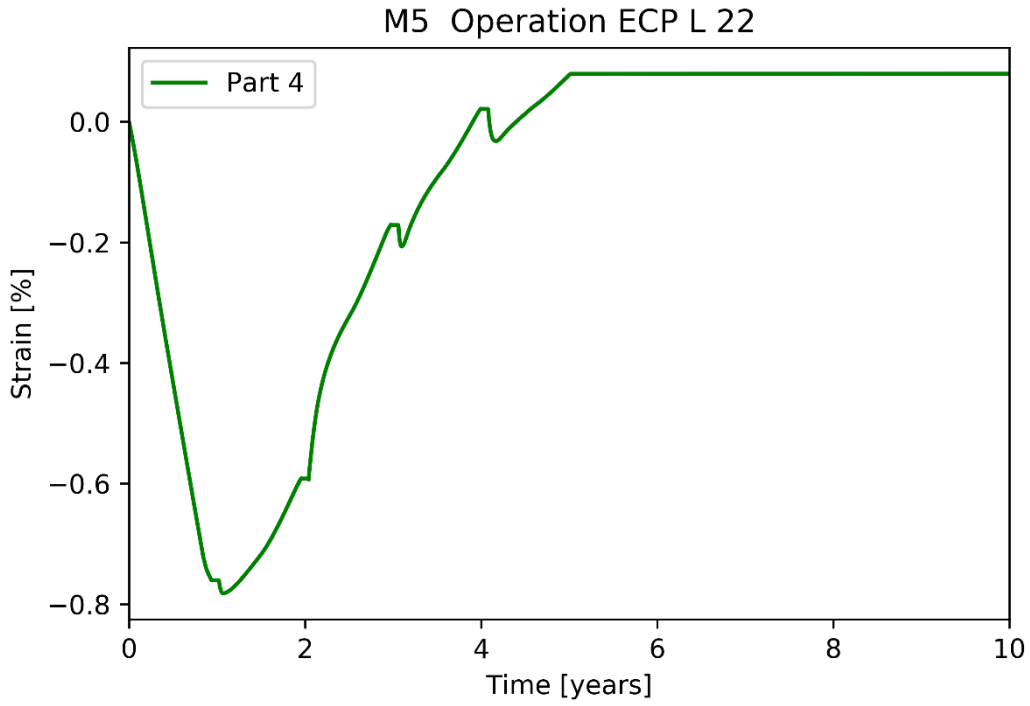

Fig. 3.59 Cladding plastic deformation (ECP) of M5 rod during operation

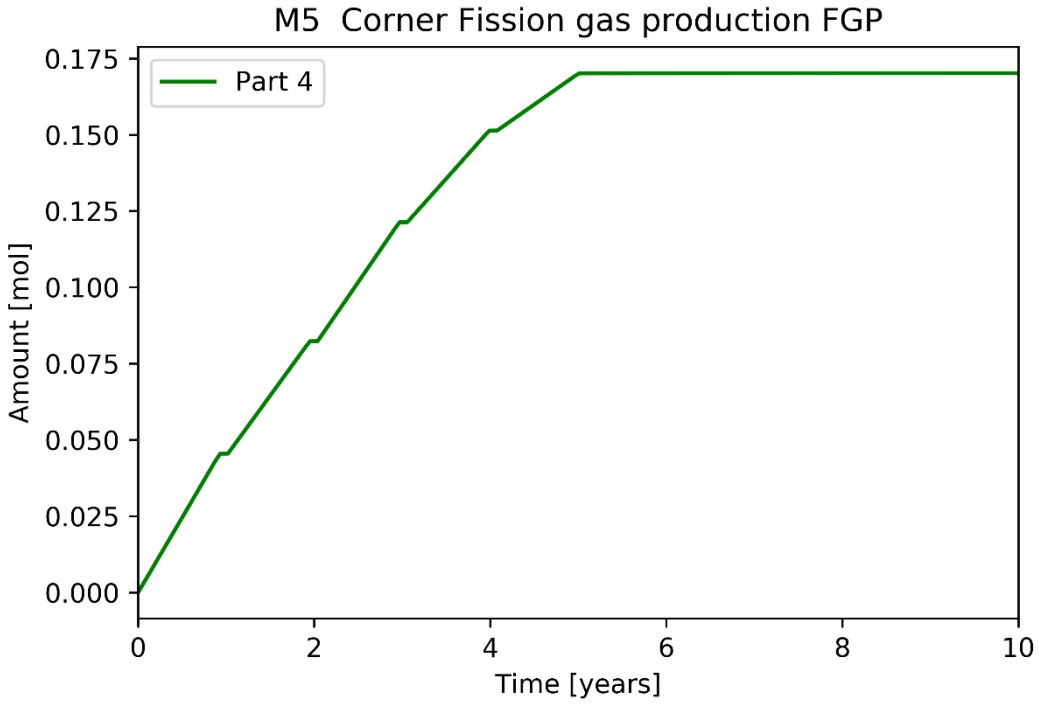

Fig. 3.60 Fission gas production (FGP) of M5 rod during operation

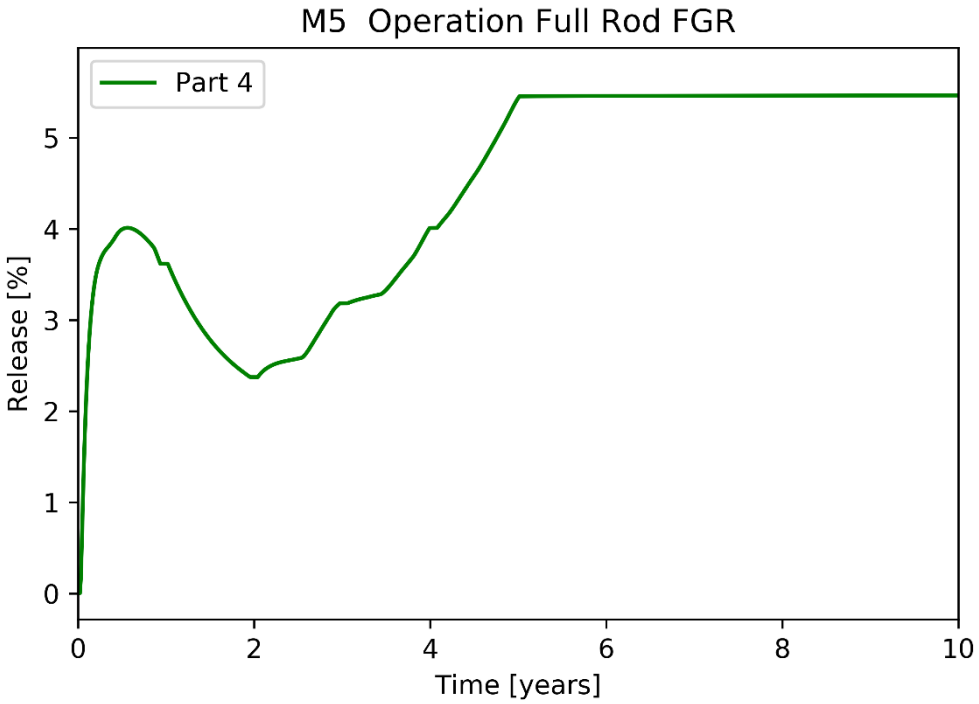

Fig. 3.61 Fission gas release (FGR) of M5 rod during operation

3.5 Storage behavior for M5 central rod

The storage behaviour is predicted by Part 4, Part 5, and Part 6. The Part 4 data set consists of a combined calculation of operation and storage. For the predictions of Part 5 the same starting conditions were assumed as for Zry-4, a closed gap at the end of operation and a reduced oxide thickness compared to Zry-4. As for the operation, the temperature conditions are imposed, hence only minor deviations between the codes are expected. Fig. 3.62, Fig. 3.63 and Fig. 3.64 show consistent results for Part 4 and Part 5. Part 6 contributed to hoop stress SCH (Fig. 3.68) and plastic deformation ECP (Fig. 3.71).

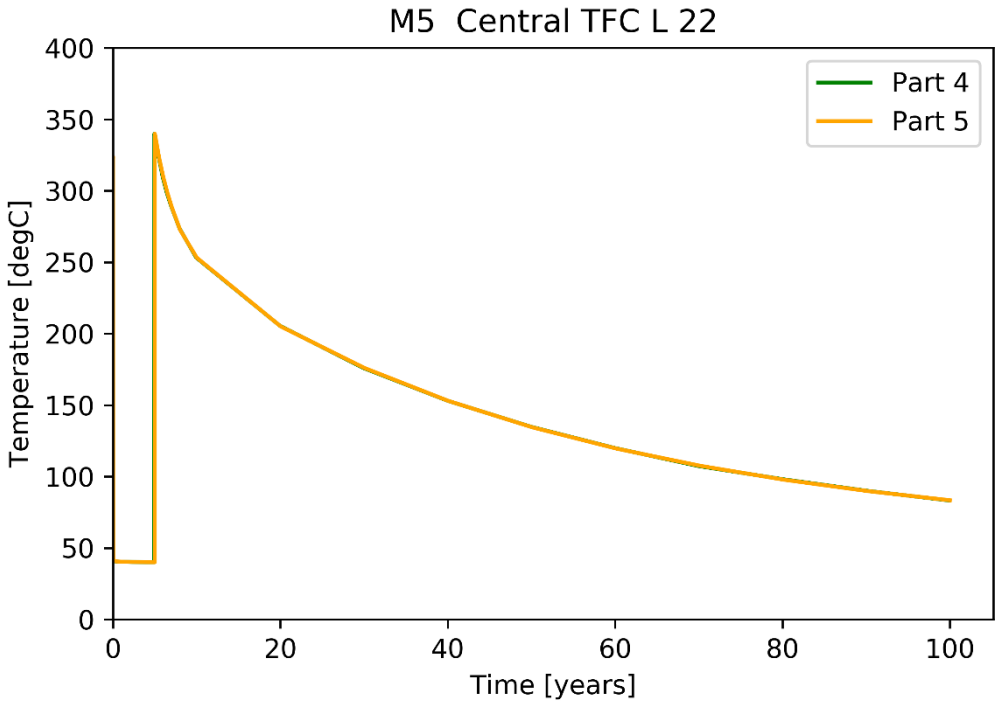

Fig. 3.62 Fuel centreline temperature (TFC) of M5 central rod during storage

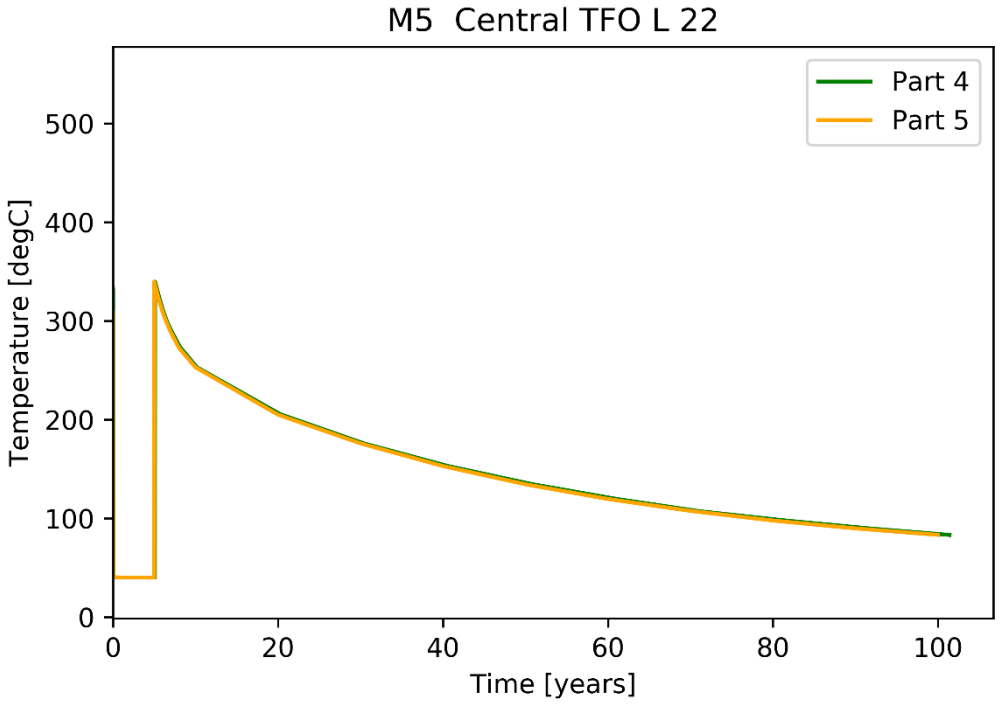

Fig. 3.63 Fuel outer temperature (TFO) of M5 central rod during storage

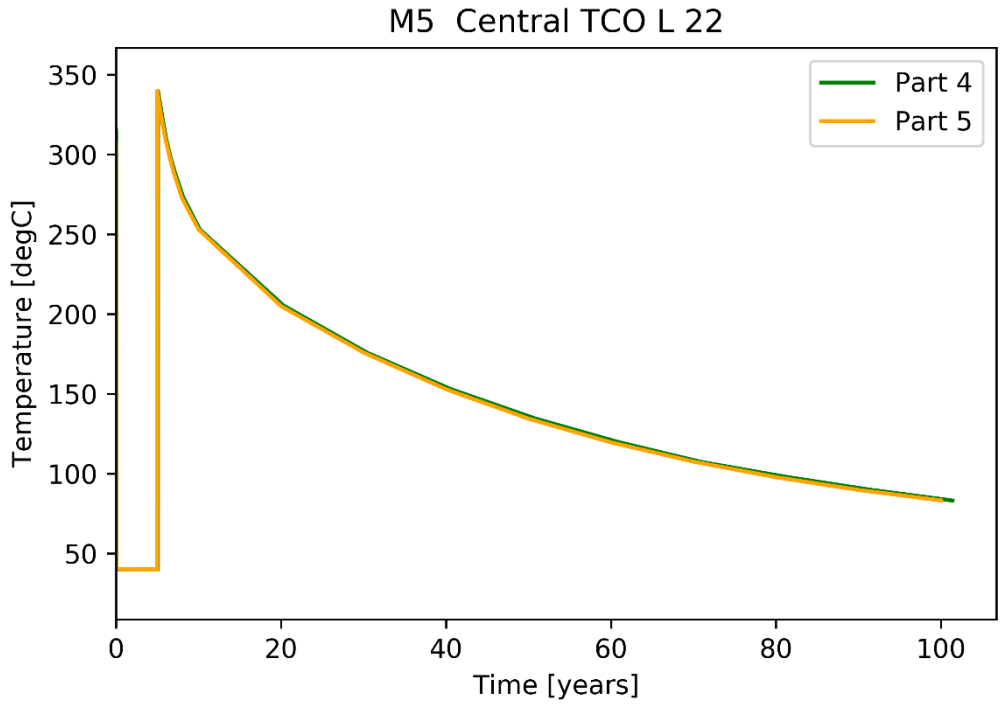

Fig. 3.64 Cladding outer temperature (TCO) of M5 central rod during storage

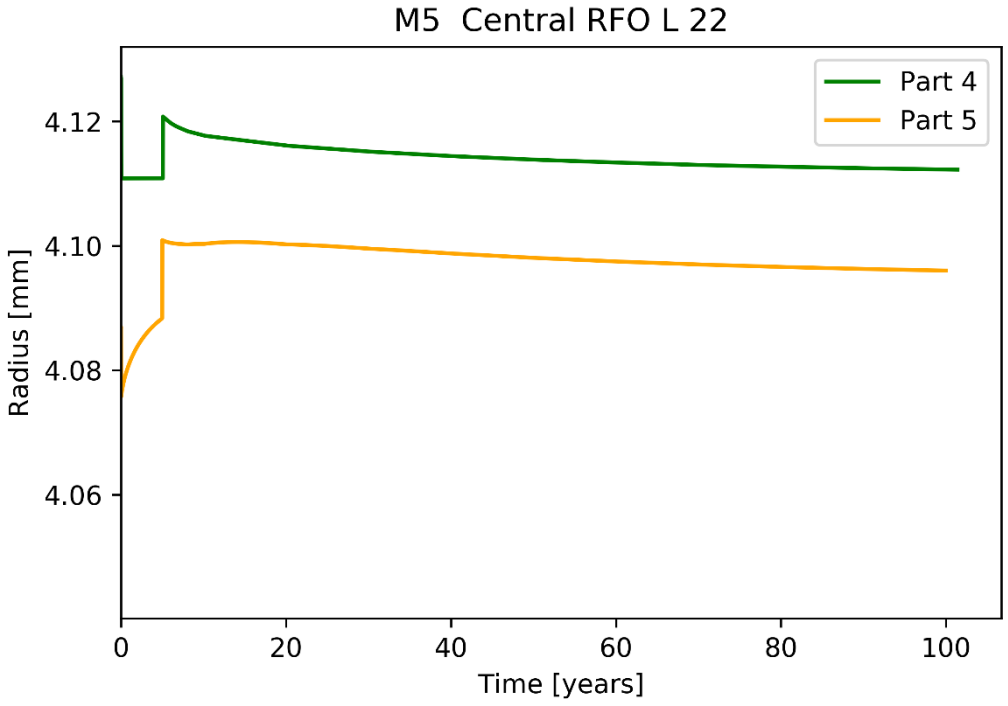

Fig. 3.65 Fuel outer radius (RFO) of M5 central rod during storage

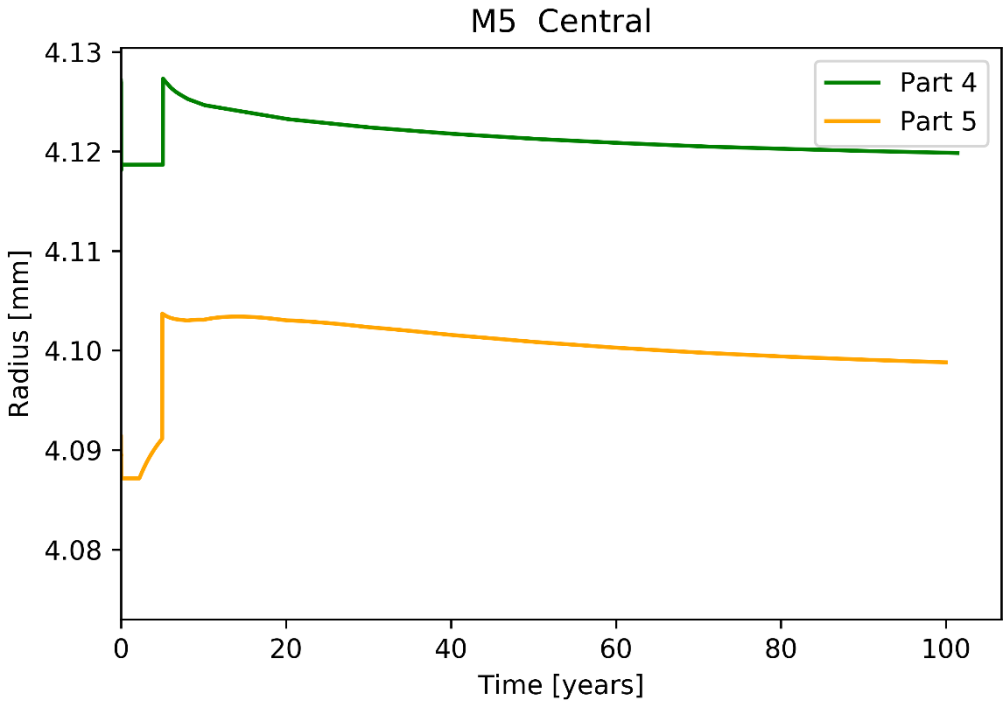

Fig. 3.66 Cladding inner radius (RCI) of M5 central rod during storage

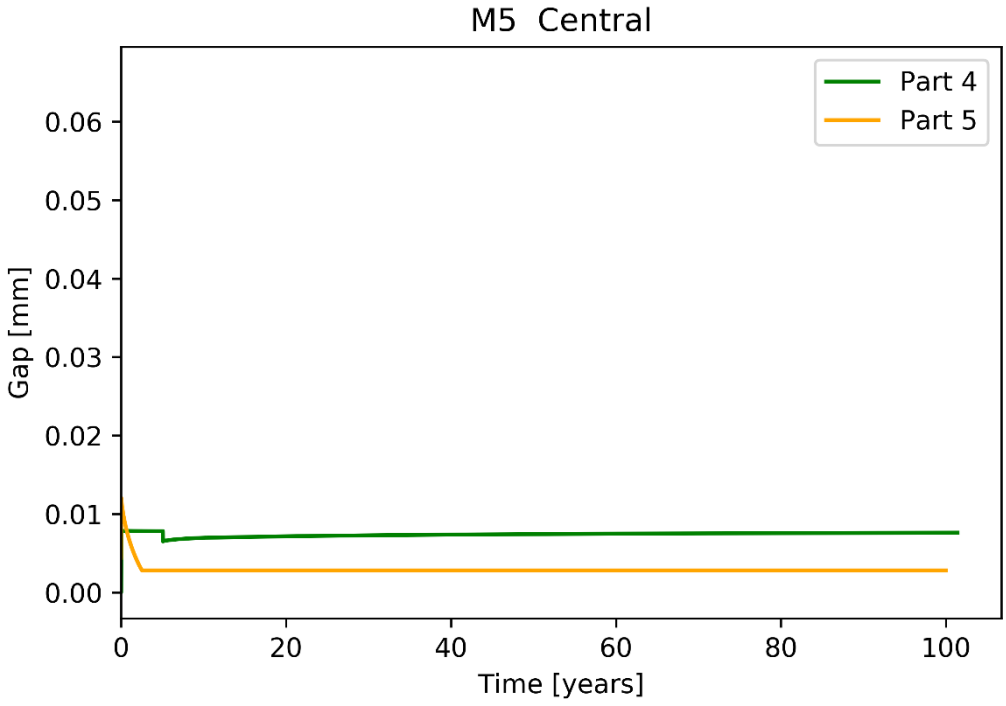

Fig. 3.67 Pellet-cladding gap (GAP) of M5 central rod during storage

Fig. 3.67 presents the results for the pellet cladding gap. Part 5 predicted a gap closure during the wet storage period and no more change afterwards during dry storage. For

Part 4, the gap remains unchanged during wet storage, but presents a small reduction during the drying process. Part 4 predicted a slight increase of the gap over the first years of dry storage, which could be related to temperature effects.

Fig. 3.68 shows the cladding hoop stress. Compared to the Zry-4 results (see Fig. 3.25), similar values are shown here: Part 4 and 6 show a very small increase of the stress during the drying process, as the pellet-cladding gap remains open. For Part 5 the pellet cladding gap closes and results in very high stresses due to a rigid-body pressure. Furthermore, the first maximum stress for Zry-4 occurs during the storage period after approximately 30 years, which is significantly higher as the first peak during the drying process (see Fig. 3.25). The M5 cladding shows two local maxima close to 200 MPa each during drying and after 30 years. Here, different creep behaviour may lead to differences in stress relaxation.

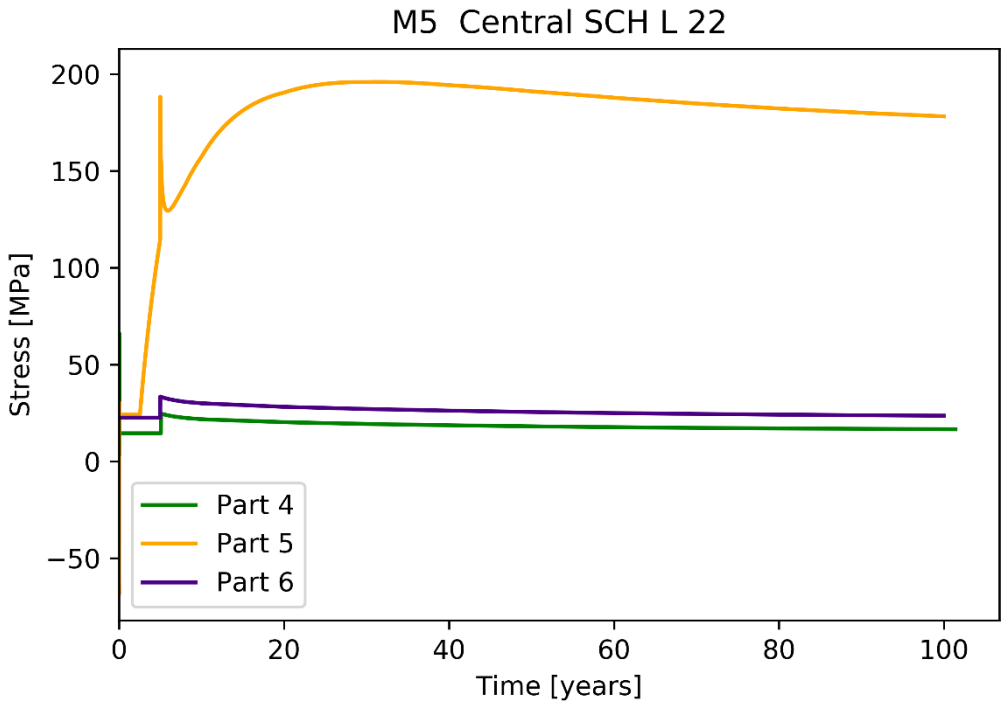

Fig. 3.68 Cladding hoop stress (SCH) of M5 central rod during storage

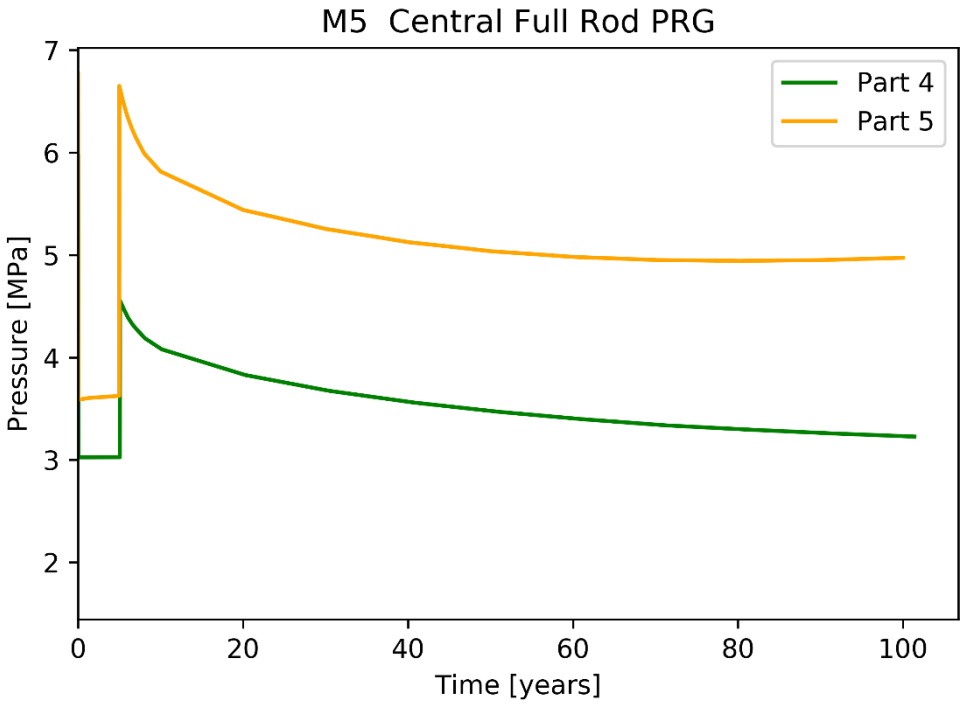

Fig. 3.69 Fuel rod gas pressure (PRG) of M5 central rod during storage

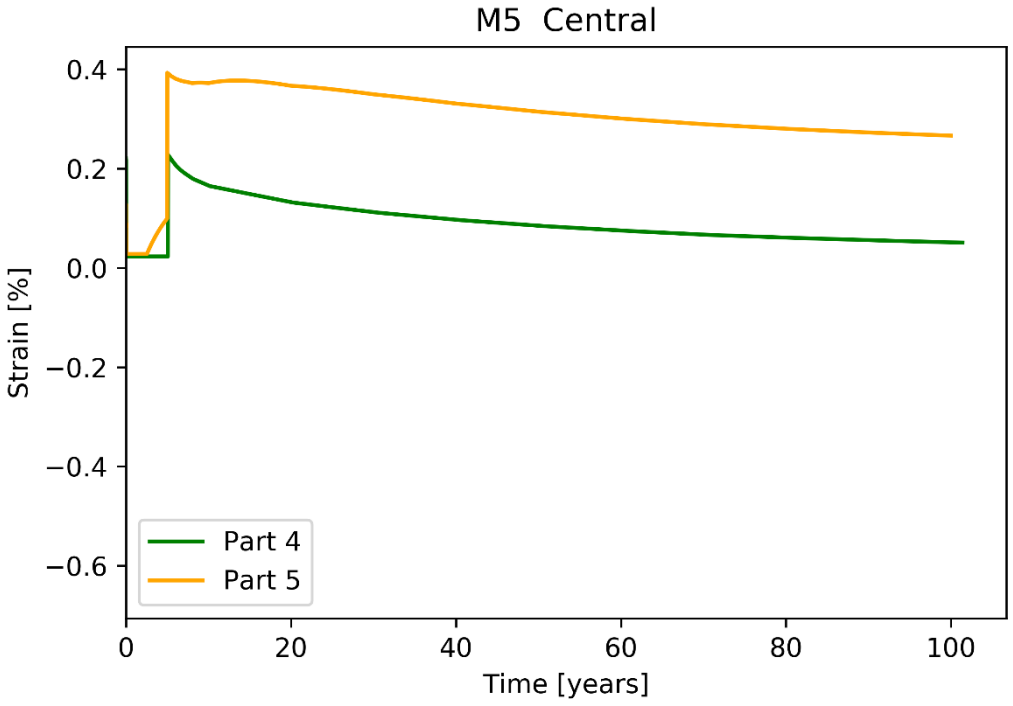

Fig. 3.70 Cladding total hoop strain (ECTH) of M5 central rod during storage

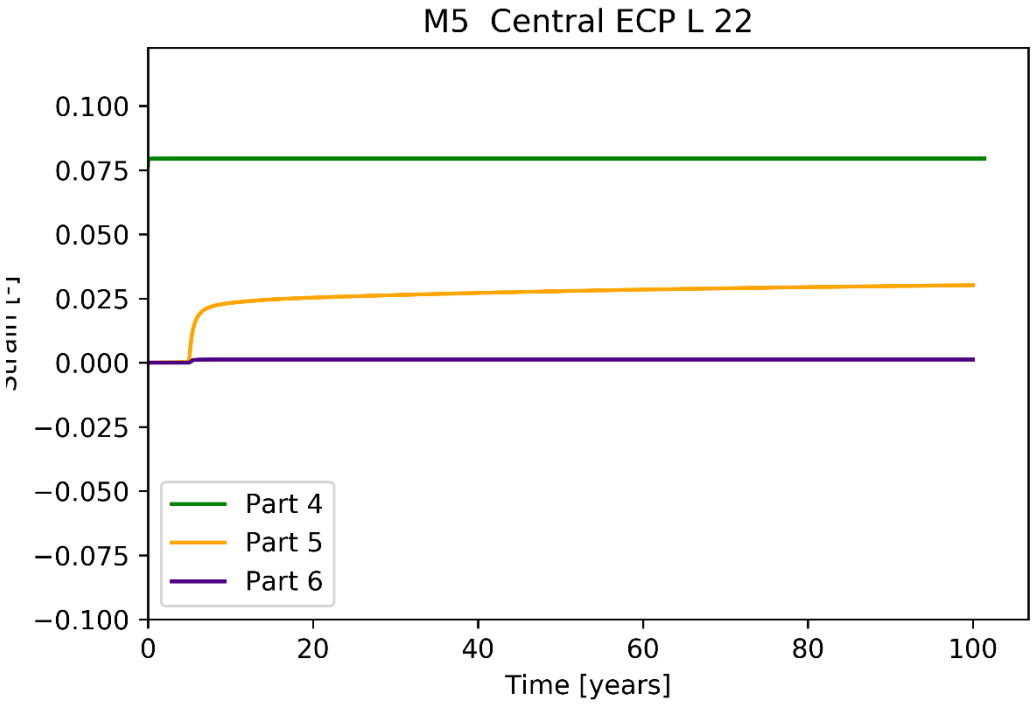

Fig. 3.71 Cladding plastic deformation (ECP) of M5 central rod during storage

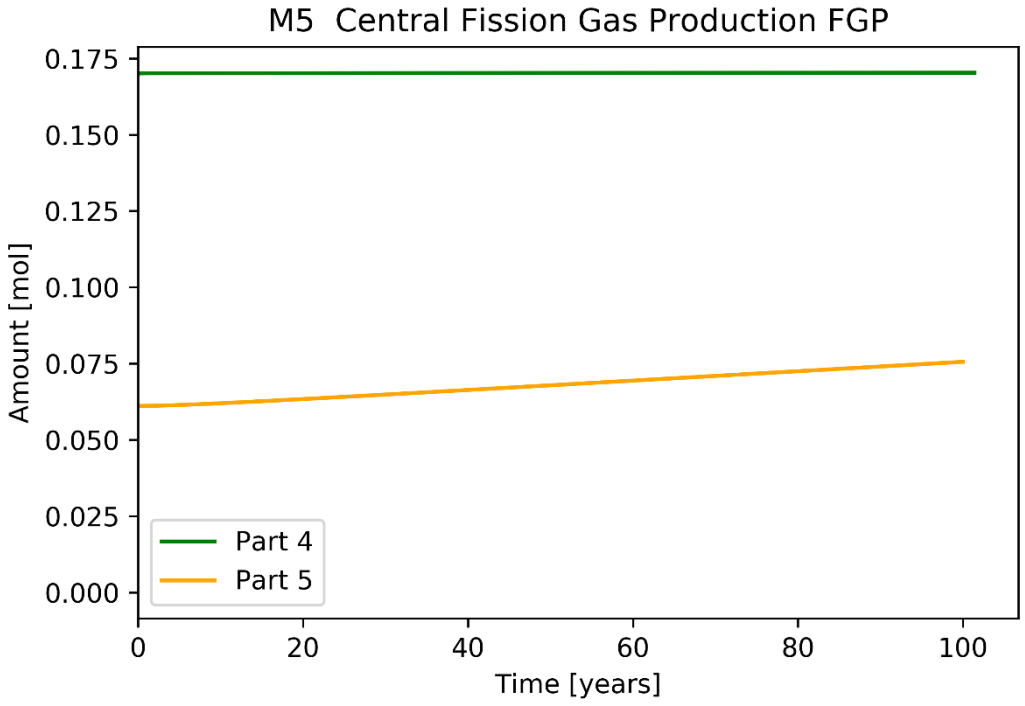

Fig. 3.72 Fission gas production (FGP) of M5 central rod during storage

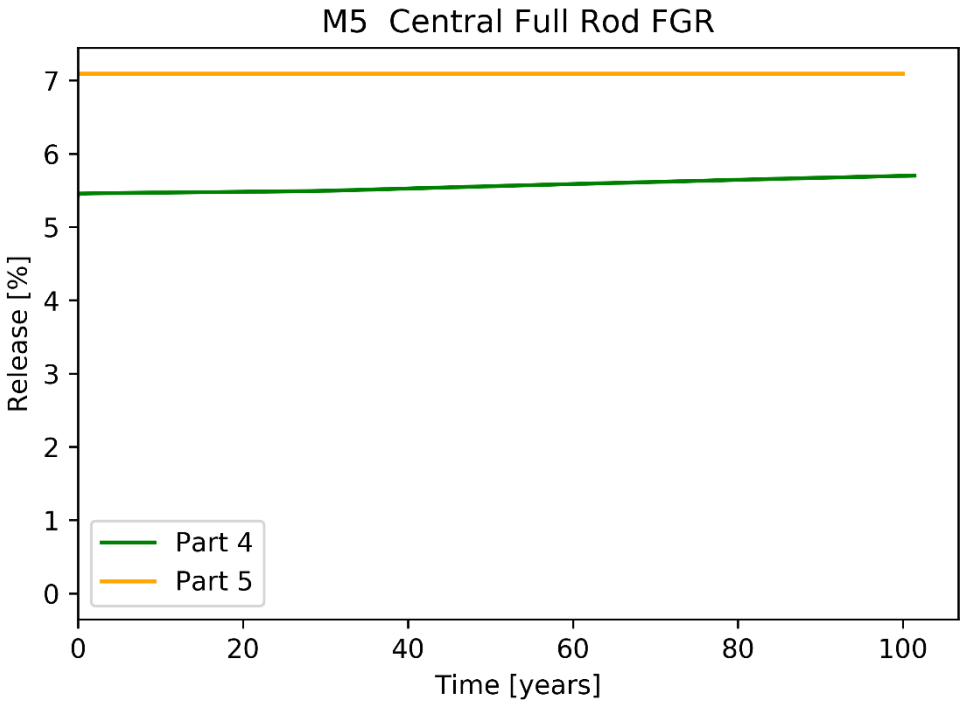

Fig. 3.73 Fission gas release (FGR) of M5 central rod during storage

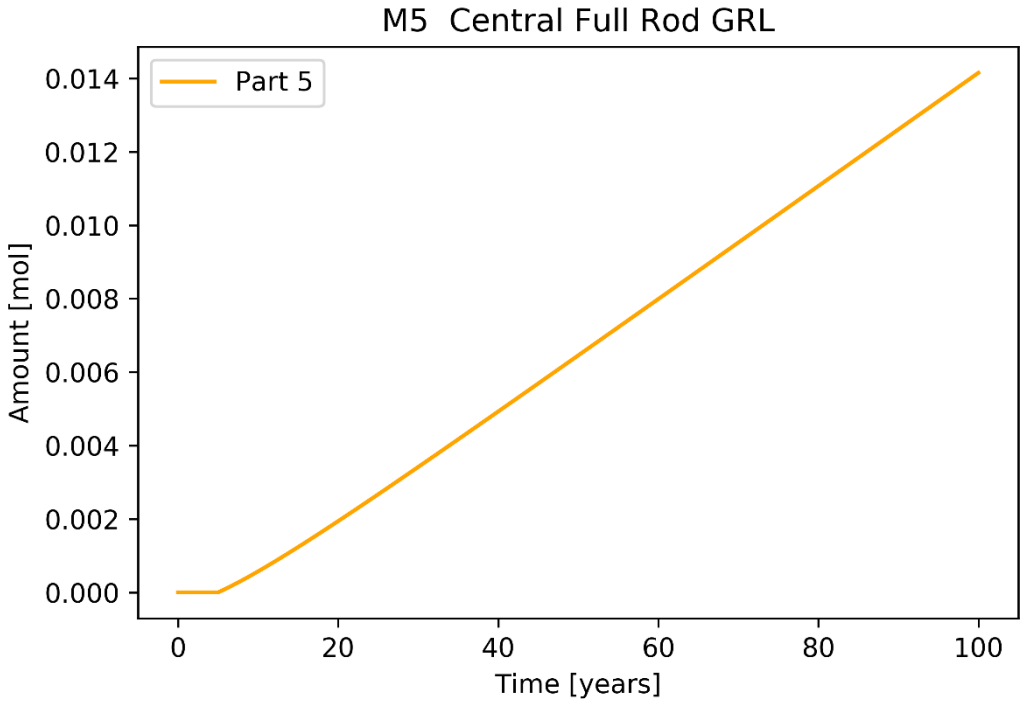

Fig. 3.74 Gas release (GRL) of M5 central rod during storage

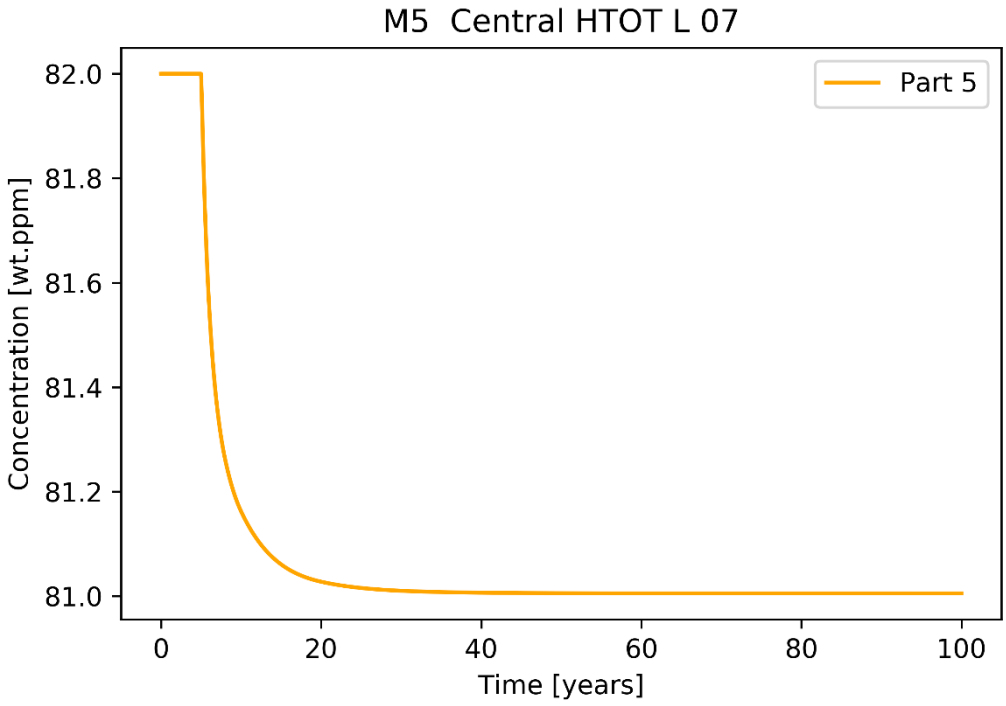

Fig. 3.75 Total hydrogen content (HTOT) of M5 central rod during storage

The total hydrogen concentration was predicted by Part 5 and is shown in Fig. 3.75. Due to the reduced oxidation of the cladding, the total hydrogen content is much lower than for Zry-4 rods, it amounts to 82 wt.ppm. With beginning of the drying process, the amount of hydrogen drops to 81 wt.ppm which may result from an axial diffusion of dissolved hydrogen within the cladding. This small effect should have no impact on the mechanical properties of the fuel rod. In Fig. 3.76 the share of dissolved hydrogen is presented. All hydrogen dissolves during drying process. This effect shows that the total amount of hydrogen is lower than the terminal solid solubility for hydrogen in M5 at the given temperatures.

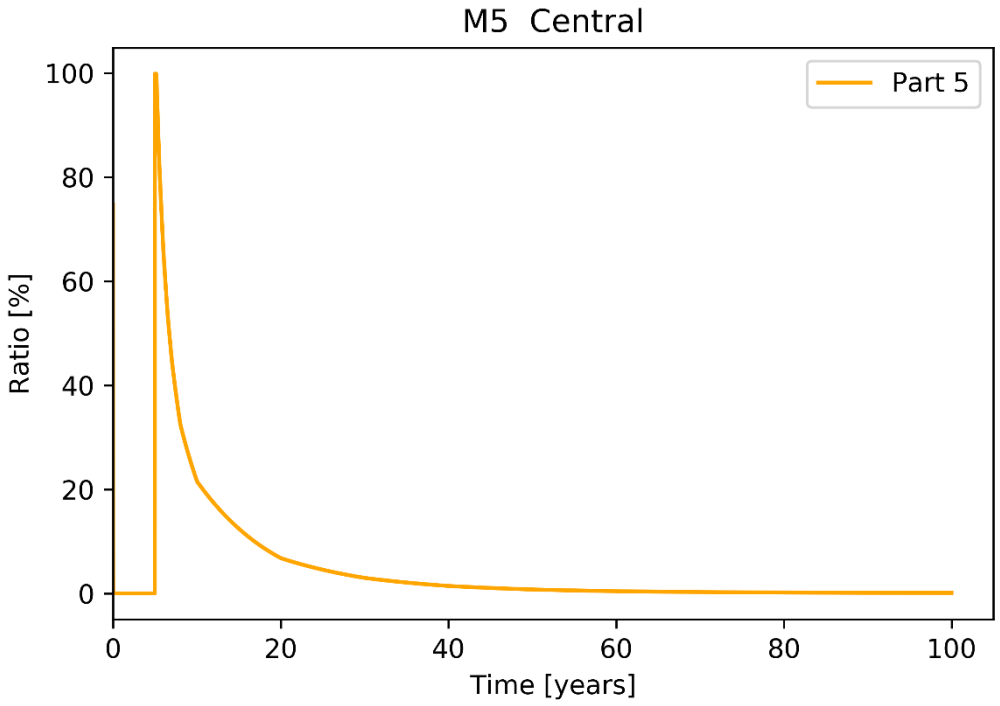

Fig. 3.76 Share of dissolved hydrogen (HDIS) of M5 central rod during storage

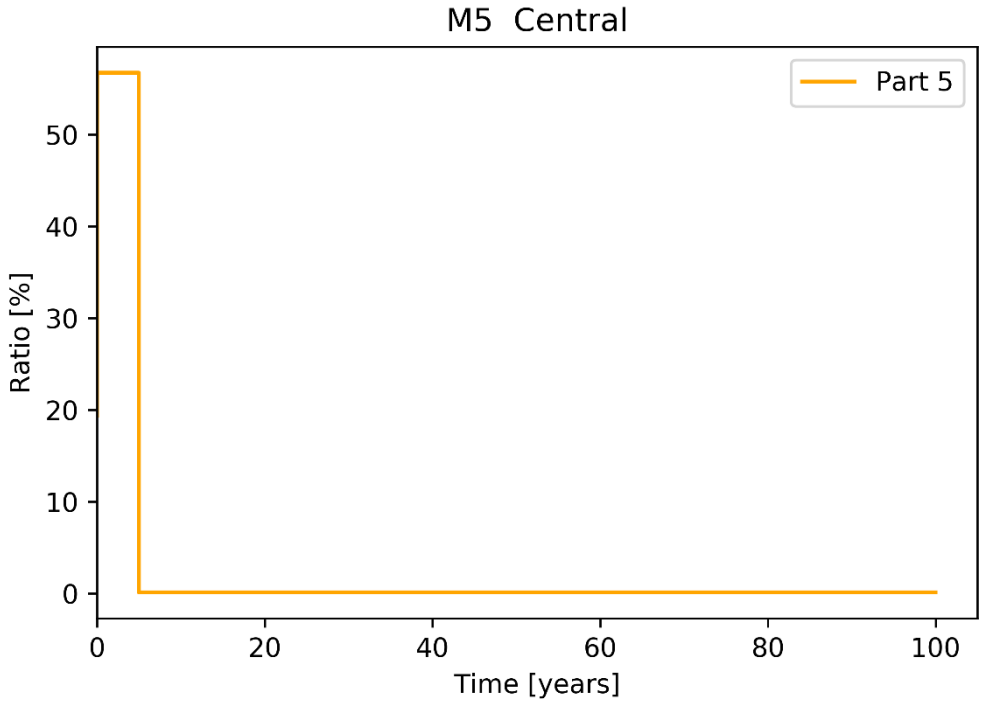

Fig. 3.77 Share of circumferential hydrides (HCIR) of M5 central rod during storage

The ratio of circumferential hydrides is shown in Fig. 3.77, starting at approximately 58 % and reducing to 0 % due to the dissolution of all hydrides during the drying process.

During the dry storage period, all hydrides precipitate in radial orientation as shown in Fig. 3.78, independent of the original distribution of circumferentially and radial oriented hydrides.

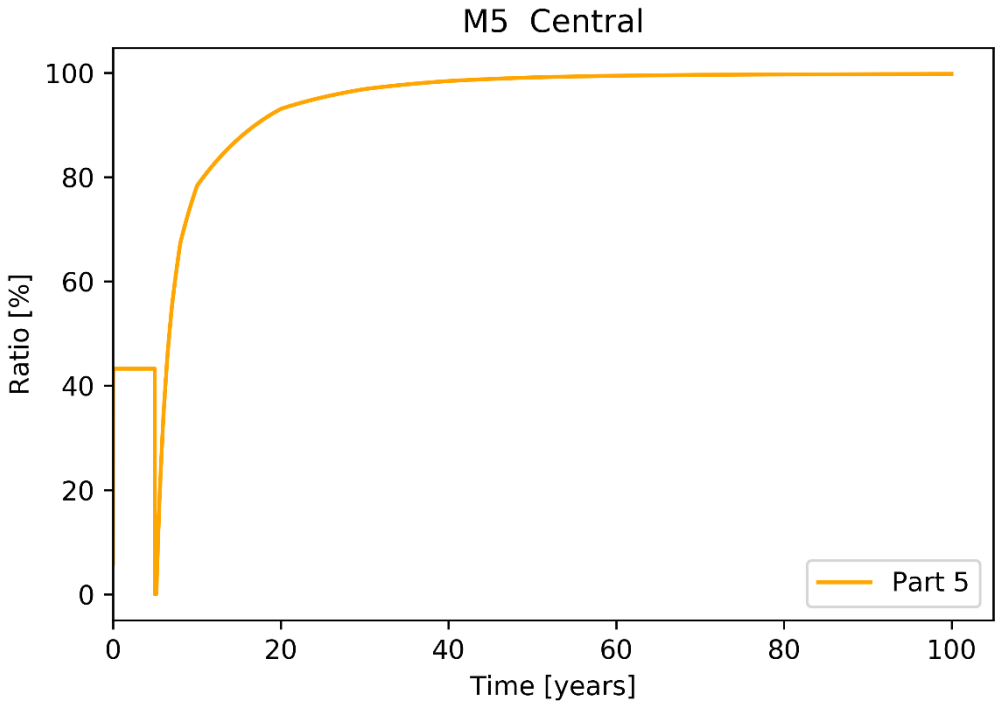

Fig. 3.78 Share of radial hydrides (HRAD) of M5 central rod during storage

3.6 Storage behaviour for M5 corner rod

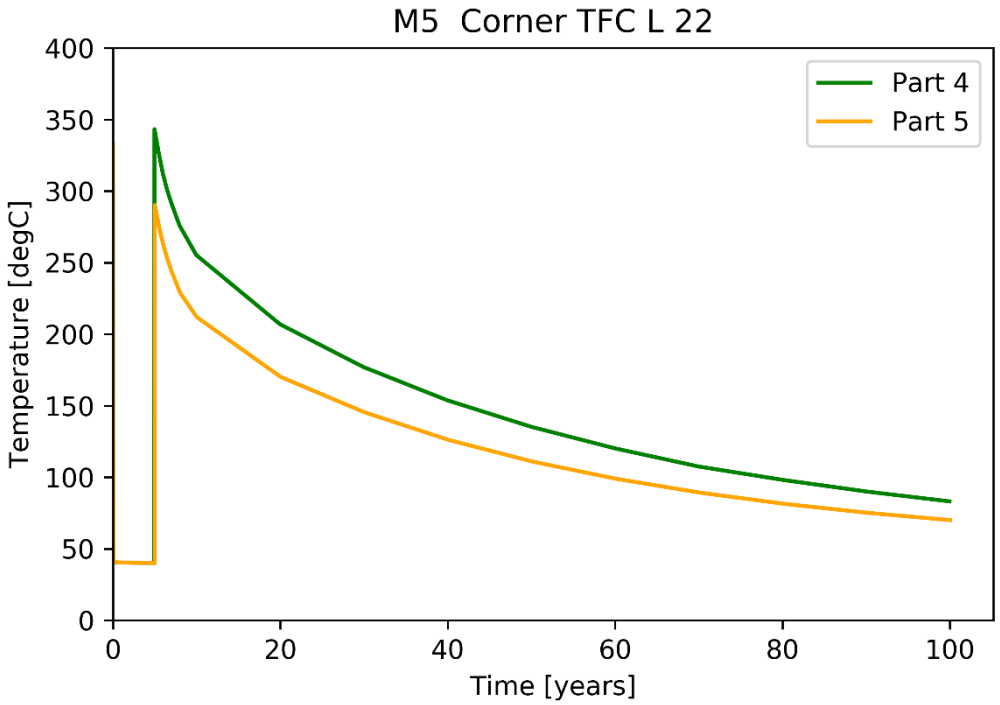

Fig. 3.79 Fuel centreline temperature (TFC) of M5 corner rod during storage

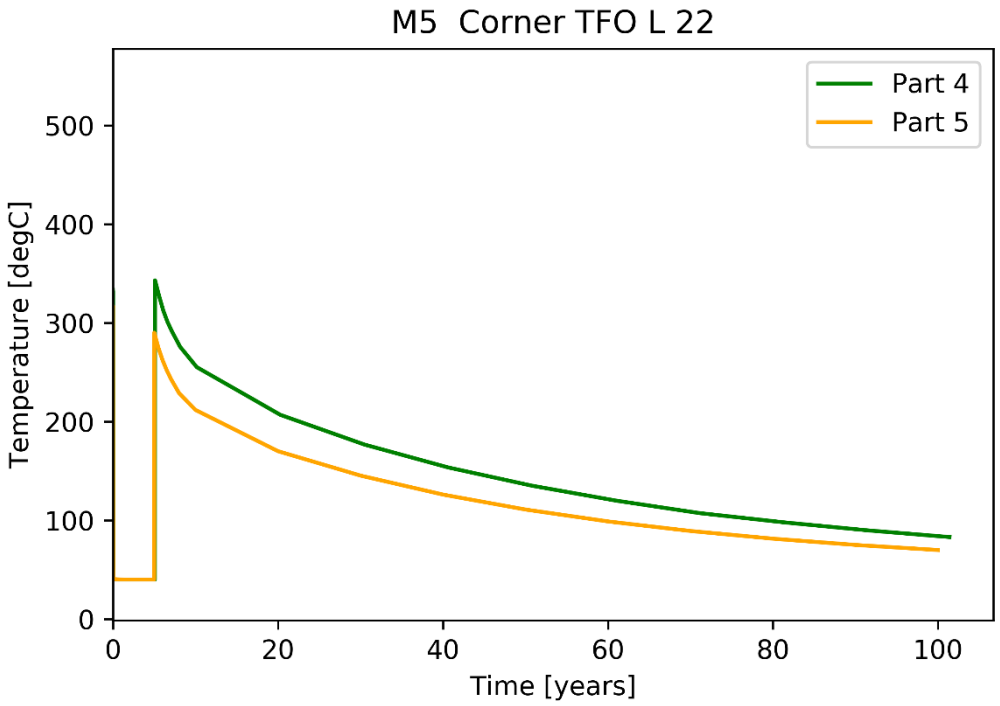

Fig. 3.80 Fuel outer temperature (TFO) of M5 corner rod during storage

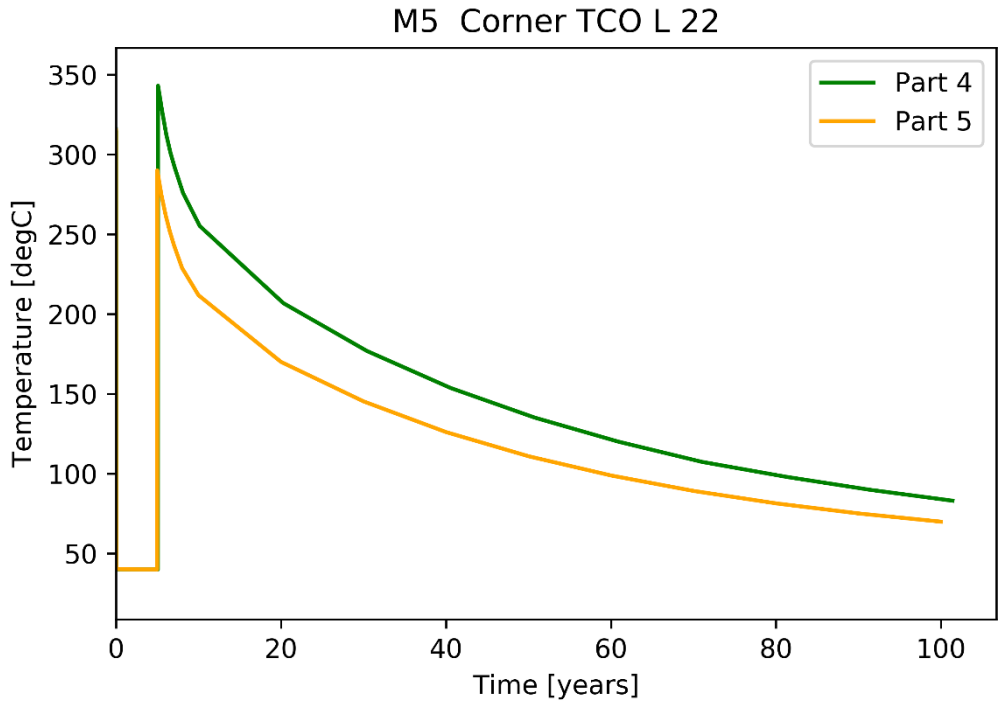

Fig. 3.81 Cladding outer temperature (TCO) of M5 corner rod during storage

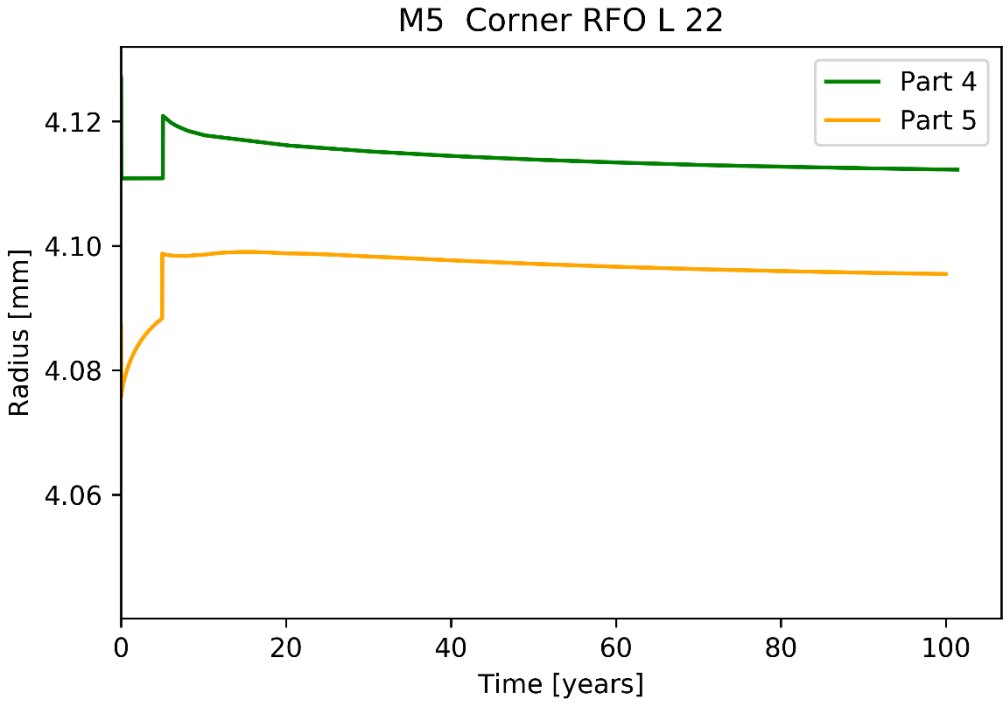

Fig. 3.82 Fuel outer radius (RFO) of M5 corner rod during storage

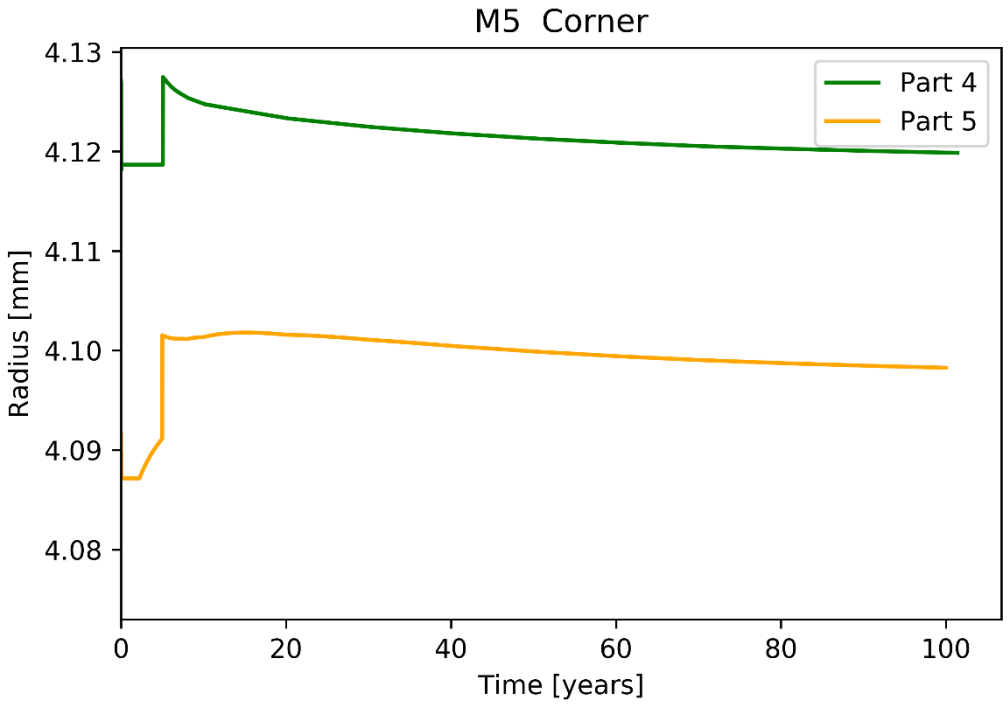

Fig. 3.83 Cladding inner radius (RCI) of M5 corner rod during storage

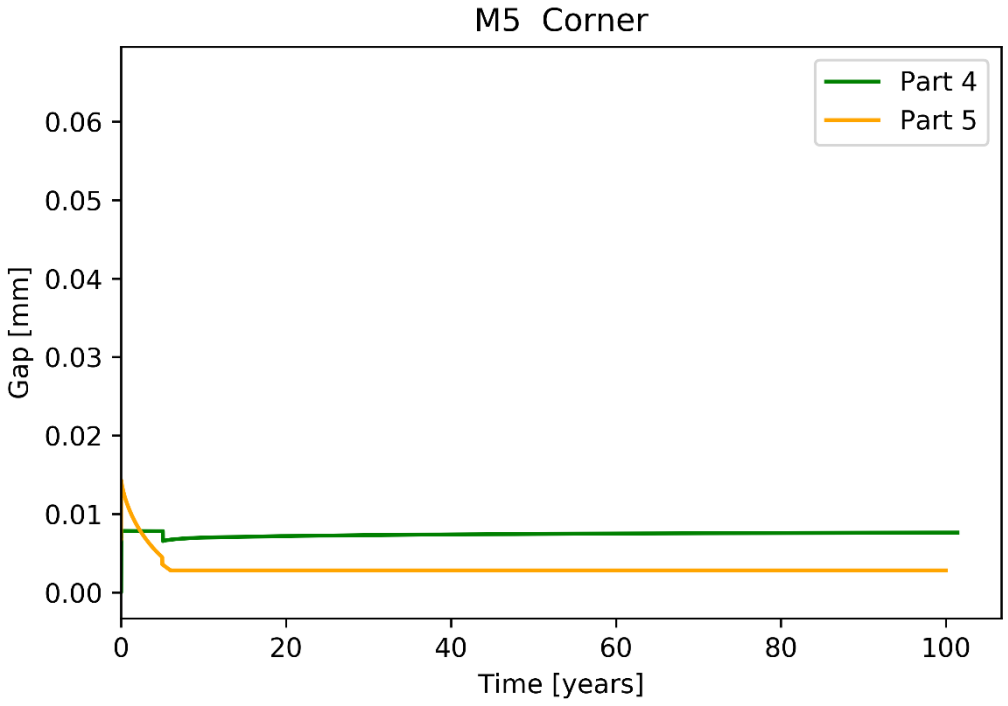

Fig. 3.84 Pellet-cladding gap (GAP) of M5 corner rod during storage

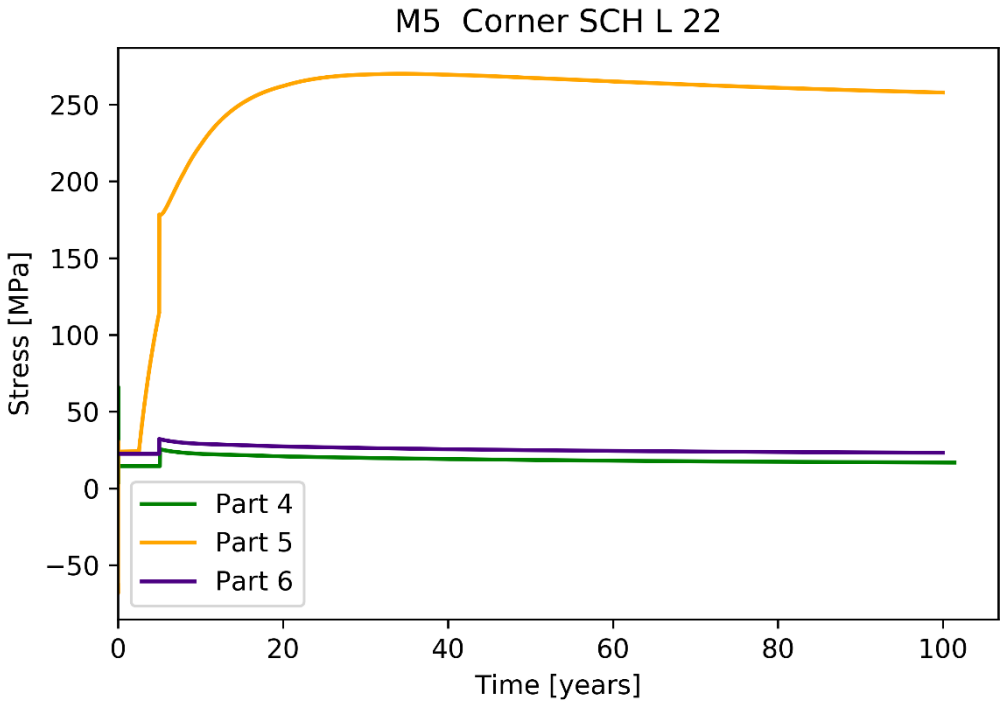

Fig. 3.85 Cladding hoop stress (SCH) of M5 corner rod during storage

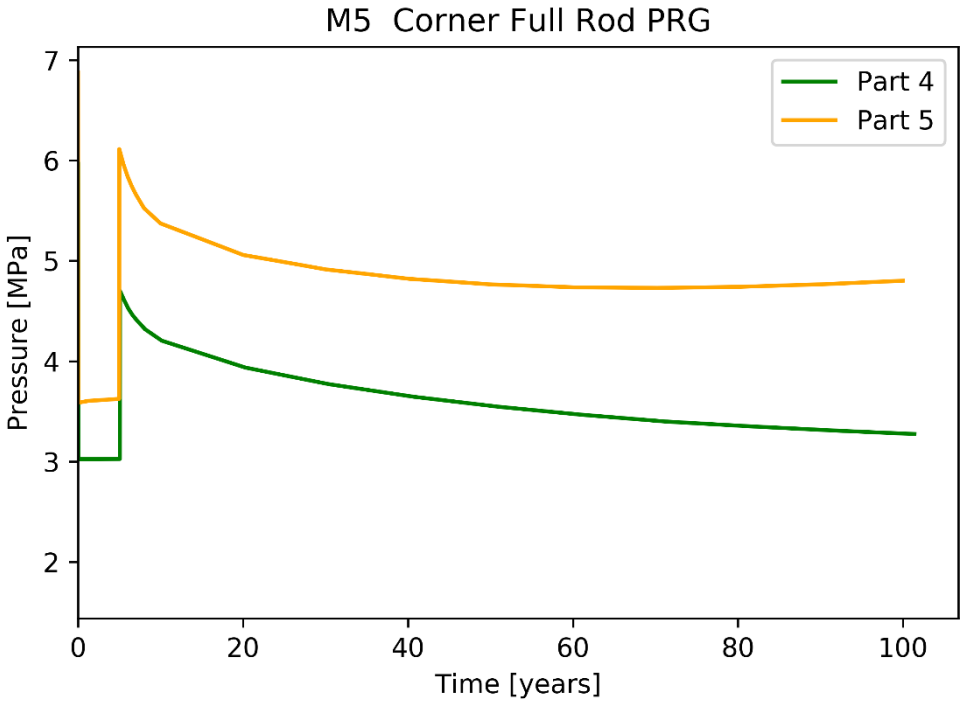

Fig. 3.86 Fuel rod gas pressure (PRG) of M5 corner rod during storage

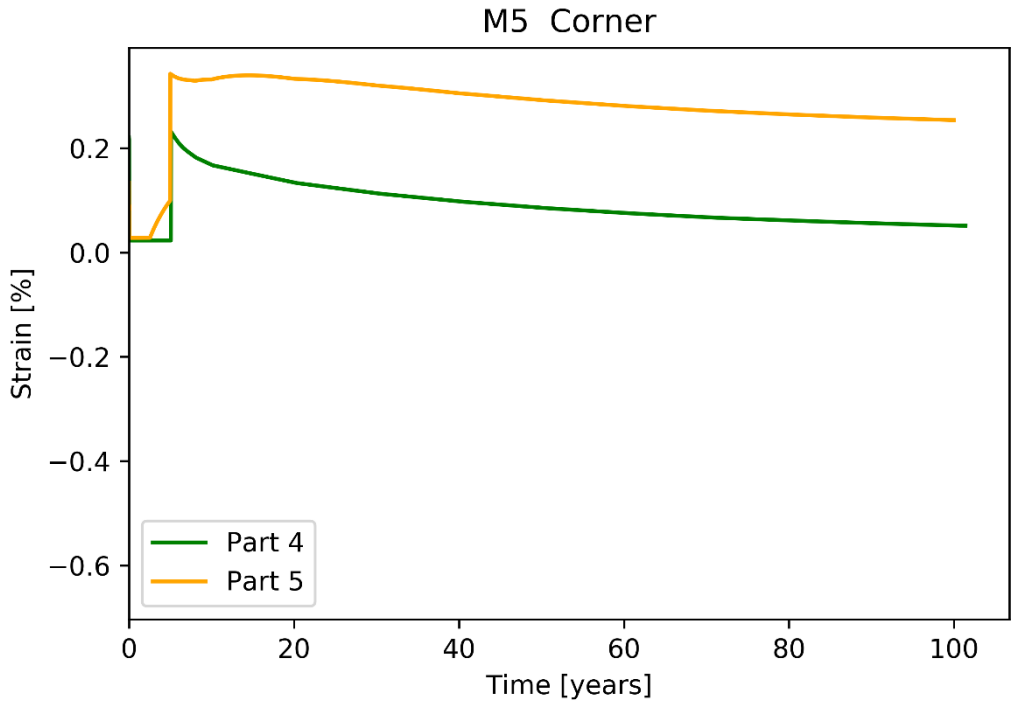

Fig. 3.87 Cladding total hoop strain (ECTH) of M5 corner rod during storage

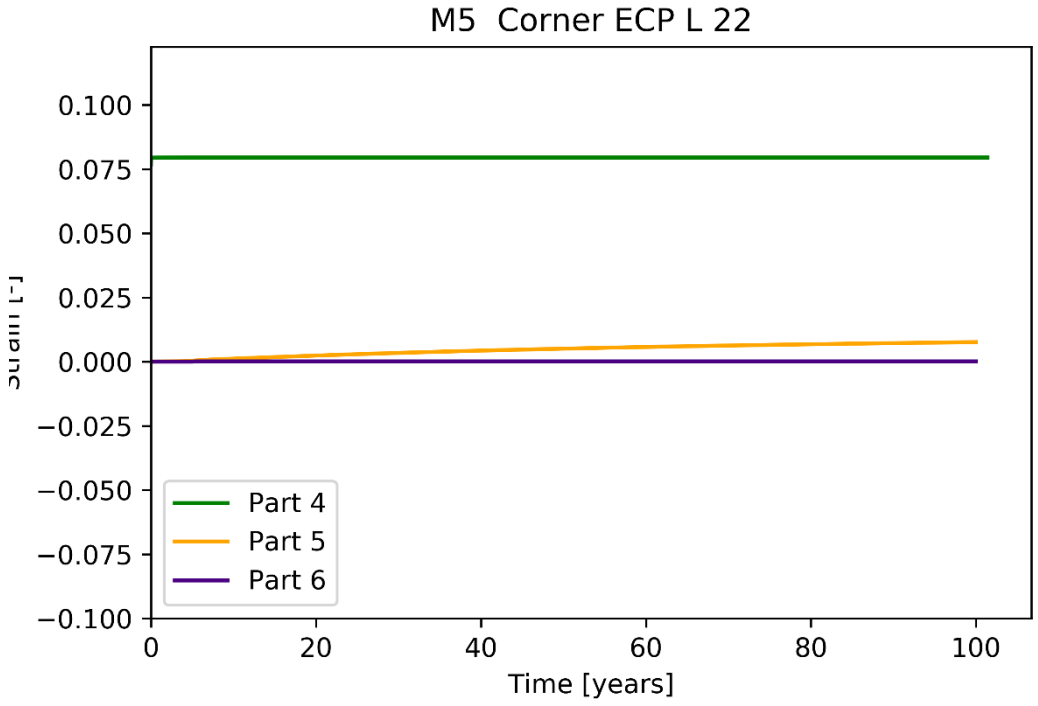

Fig. 3.88 Cladding plastic deformation (ECP) of M5 corner rod during storage

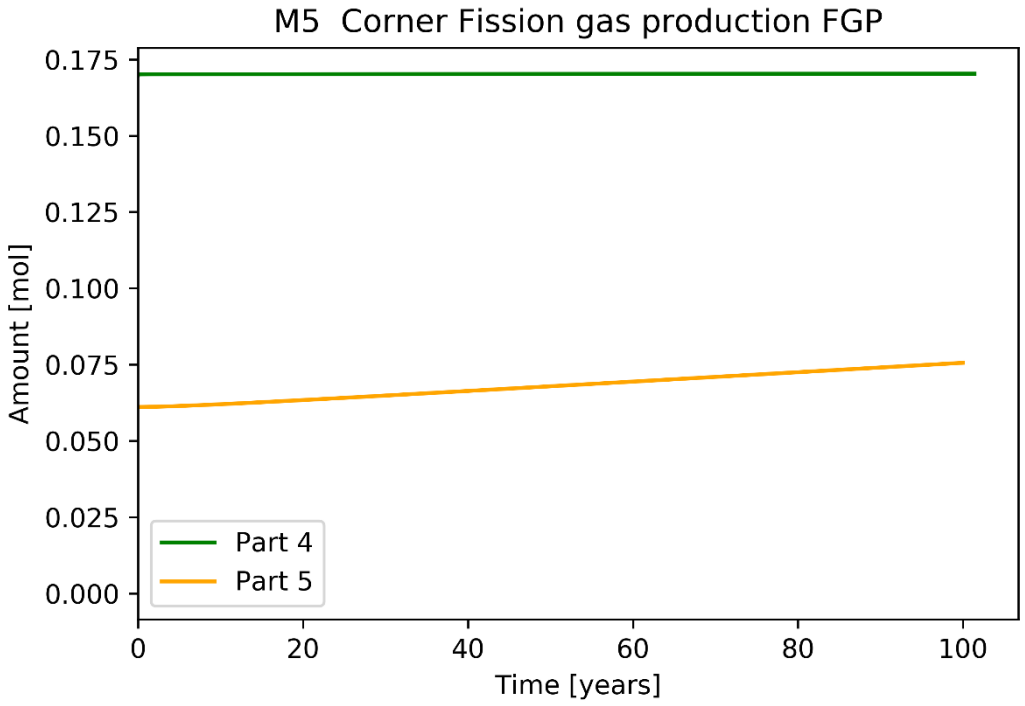

Fig. 3.89 Fission gas production (FGP) of M5 corner rod during storage

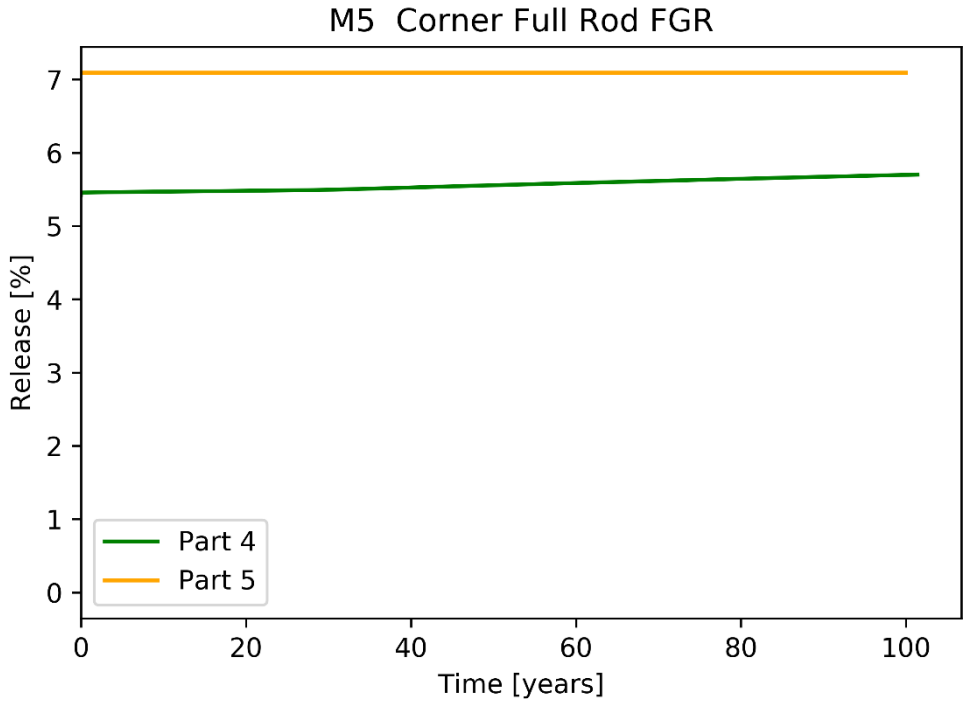

Fig. 3.90 Fission gas release (FGR) of M5 corner rod during storage

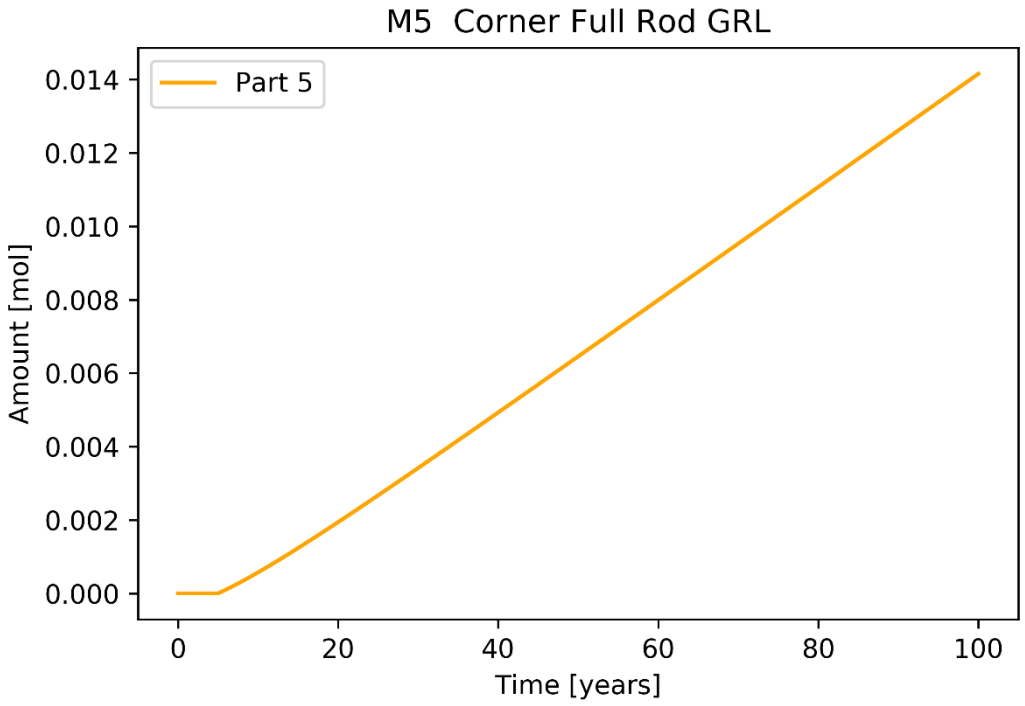

Fig. 3.91 Gas release (GRL) of M5 corner rod during storage

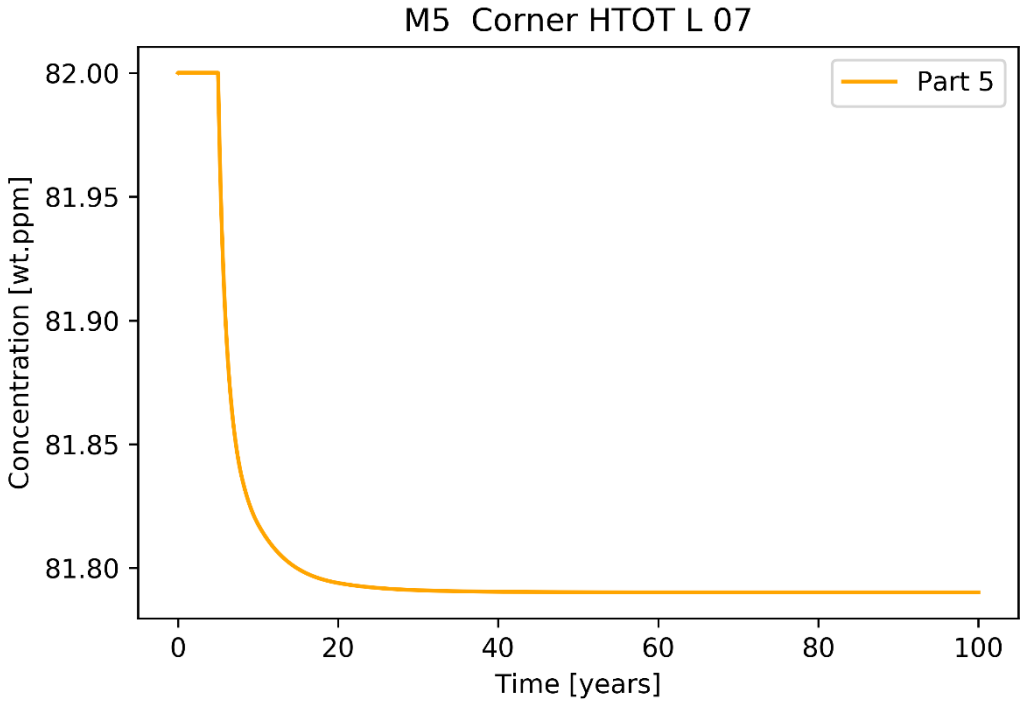

Fig. 3.92 Total hydrogen content (HTOT) of M5 corner rod during storage

The amount of hydrogen starts with the same conditions as given in the central rod position with 82 wt.ppm. Due to the lower temperatures the diffusion effect is still visible, but with a drop of 0.2 wt.ppm even smaller than for the central rod.

In Fig. 3.93, the share of dissolved hydrides is shown for Part 5. Unlike the case of the central rod, not all hydrides dissolve during the drying process: a share of about 45 % of hydrides dissolves, while the rest remains precipitated. Fig. 3.94 and Fig. 3.95 show the share of circumferential and radial hydrides, respectively. While the drying process leads to dissolution of both circumferential and radial hydrides, only radial hydrides are formed during the following dry storage period. Thus, the ratio circumferential/radial hydrides get reversed: from 57 % to 43 % in wet storage, the ratio changes to 34 % to 66 % in dry storage.

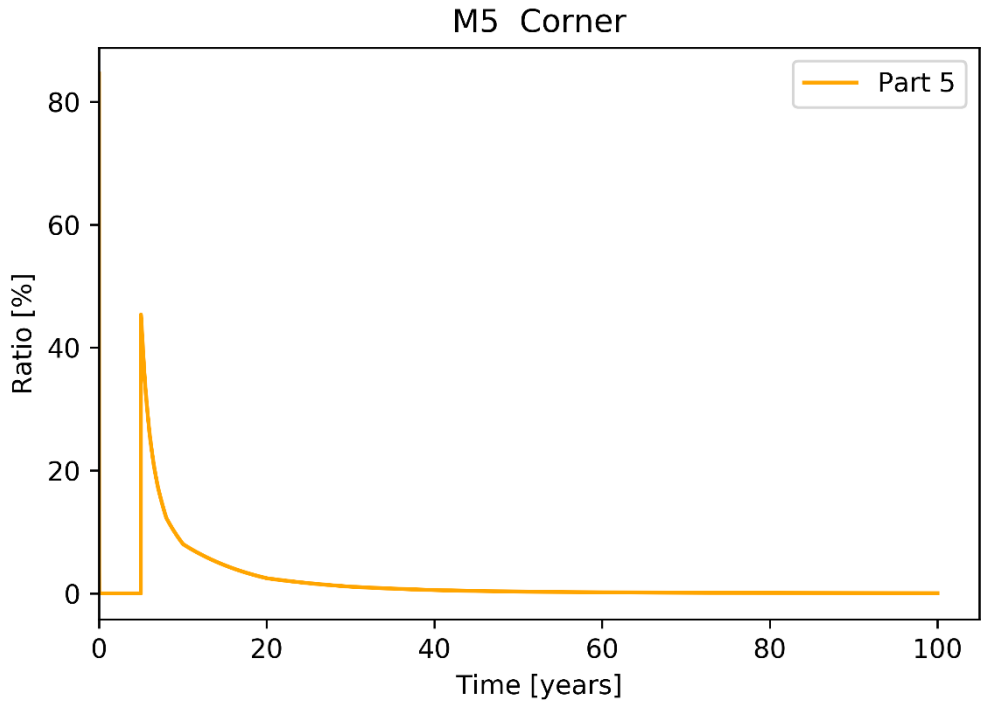

Fig. 3.93 Share of dissolved hydrogen (HDIS) of M5 corner rod during storage

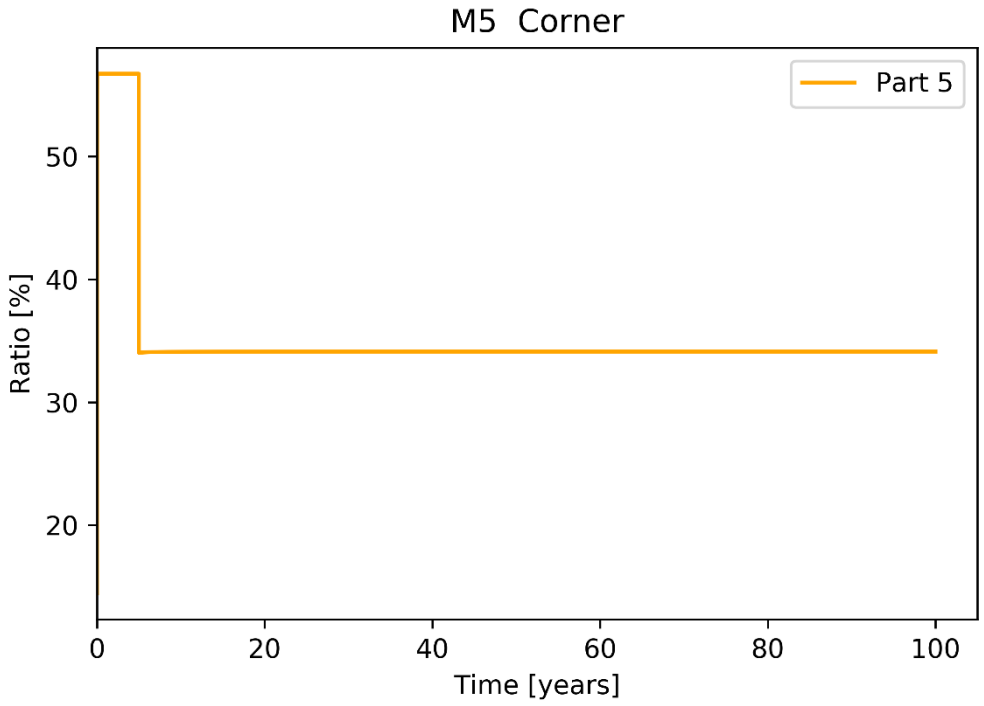

Fig. 3.94 Share of circumferential hydrides (HCIR) of M5 corner rod during storage

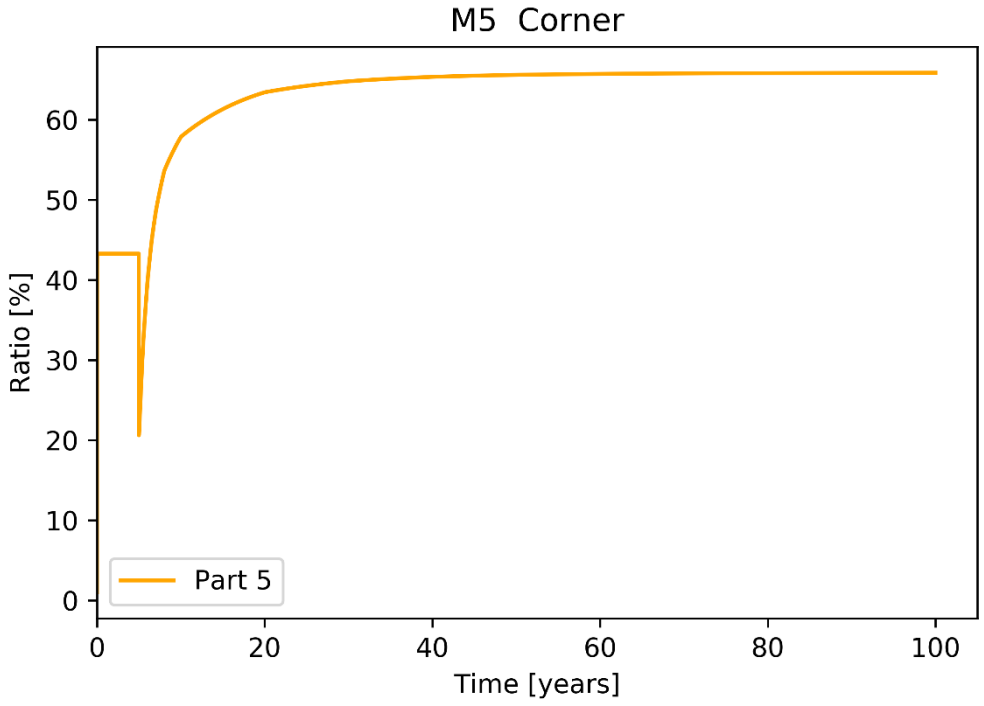

Fig. 3.95 Share of radial hydrides (HRAD) of M5 corner rod during storage

4 Discussion

These results show the calculated basic thermo-mechanical parameters of a fuel rod during operation, wet and dry storage. Some of the parameters show the imposed boundary conditions such as fuel centreline temperature. Other parameters, such as gap size, total hoop strain or cladding hoop stress are indirect parameters, which depend on models incorporated by the codes.

The codes used for this benchmark were originally developed for the reactor operation or accident analysis. Given the imposed boundary conditions the codes show some major deviation during the operation period. Some large deviations were observed for the same type of code (e.g., FALCON and TRANSURANUS) used in different versions by two participants. Differences in modelling approaches and a user effect must be considered when analysing these results.

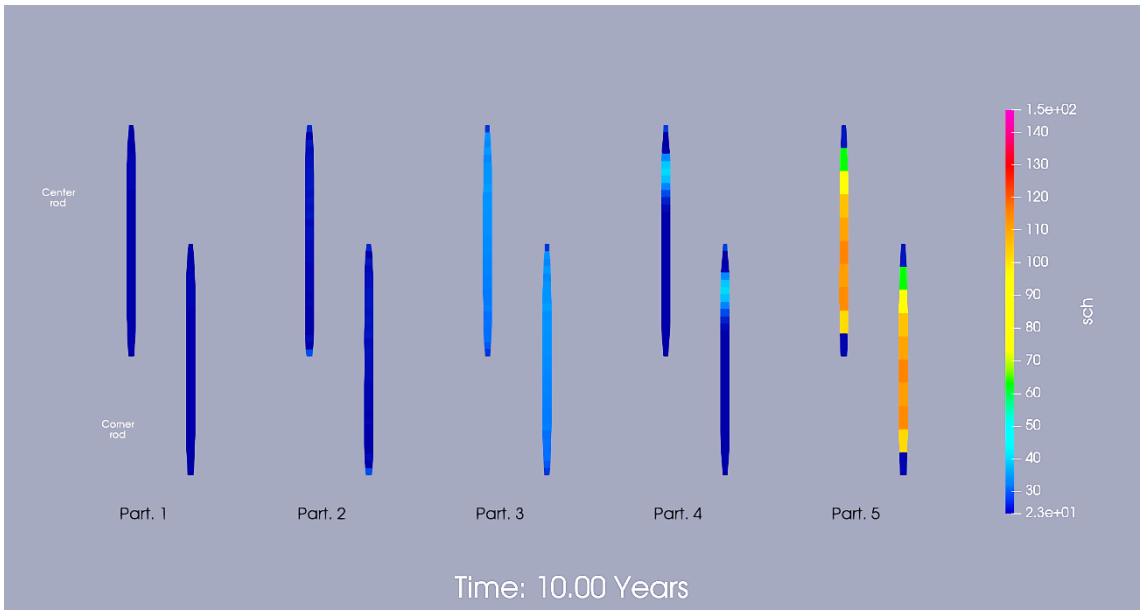

Fig. 4.1 Axial distribution of Cladding hoop strain (SCH) for Zry-4 after 10 years of storage (end of wet storage)

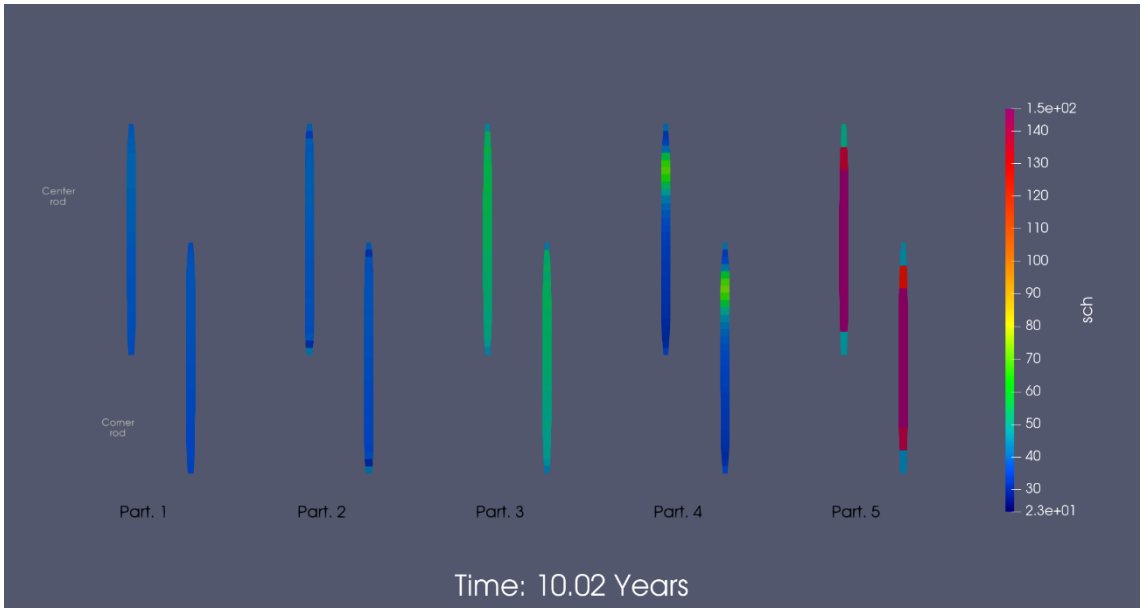

Fig. 4.2 Axial distribution of Cladding hoop strain (SCH) for Zry-4 after 10.02 years of storage (end of drying process / beginning of dry storage)

Fig. 4.1 to Fig. 4.4 show the axial distribution of selected parameters at selected time points. The colour-coded axial segments of the rod illustrate the selected parameters, whereas the width of the segment is the relative cladding radius, intentionally magnified to visualize any changes. Fig. 4.1 shows the axial distribution of the axial hoop stress for the Zry-4 rod after 10 years, which refers to the end of dry storage. Part 1, 2 and 3 show rather small changes, while Part 4 shows elevated stresses in the upper part of the rod. Part 5 shows large stresses, with a maximum stress in the lower half of the rod. Fig. 4.2 shows the axial hoop stress after the drying process. The cladding stress increases over the drying process for all fuel rods. The axial effects remain present as they were before the drying process.

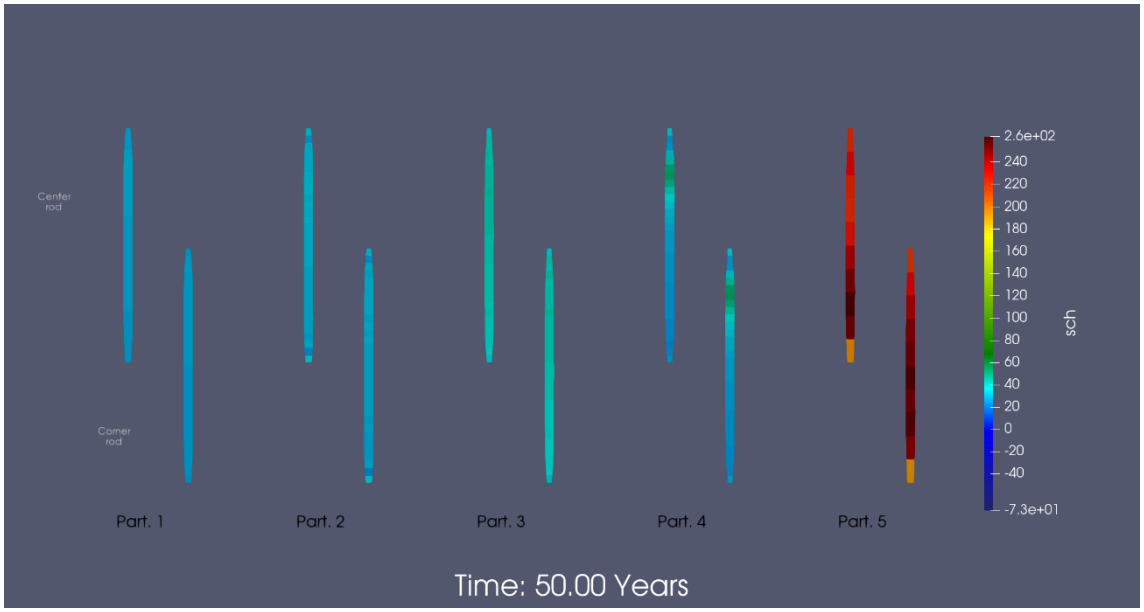

Fig. 4.3 Axial distribution of Cladding hoop strain (SCH) for Zry-4 after 50 years of storage

During the storage period the fuel rods cool down slowly and the stresses decrease. Fig. 4.3 and Fig. 4.4 show axial hoop stress after 50 and 100 years. The axial distribution becomes more pronounced for Part 4 and 5. Since Part 5 shows the highest hoop stresses, the differences between central rod and corner rod are visible. The corner rod exhibits very high hoop stresses above 240 MPa along two thirds of the length. The central rod shows these values only in the lower half of the fuel rod. The temperature difference along the fuel rod length may have an influence on the cladding creep models, leading to a stronger relaxation in the upper part of the fuel rod.

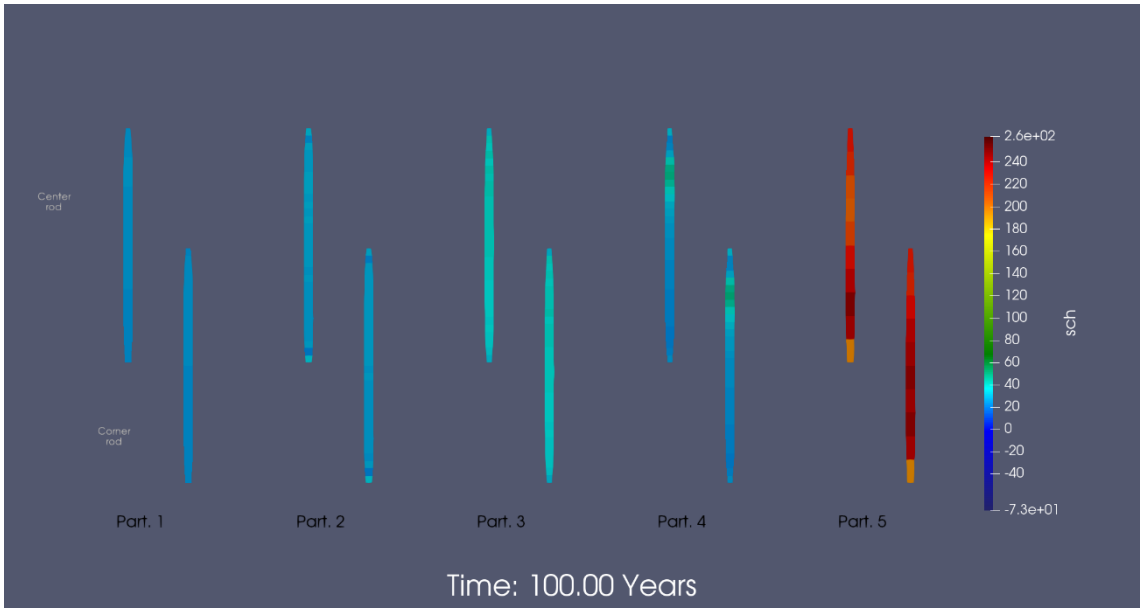

Fig. 4.4 Axial distribution of Cladding hoop strain (SCH) for Zry-4 after 100 years of storage

Remarkable results for the Zircaloy-4 central rod case are the plastic deformation in combination with the gap size. The results of Part 1 show a permanently closed gap during the entire storage period and neither changes in plastic deformation during drying process nor large hoop stress increases. This implies, the cladding follows the pellet in its deformation and remains in close contact.

Due to the large offset in temperature for Part 2, it can be assumed that the imposed temperatures are different to the other codes, which may cause also the small cladding radii. The cladding plastic deformation is at the maximum compared to all results and should be even larger if a higher temperature would be imposed to the fuel rod.

Part 3 shows an open pellet-cladding gap, even during drying process. At the same time, plastic deformation of the cladding changes significantly. In this case the fuel rod gas pressure seems to be sufficiently high to cause plastic deformation in the cladding.

Large pellet-cladding gaps are observed for Part 4, but the total strain (ECTH) is rather low compared to other code predictions. These effects show a rather small pellet diameter compared to the other codes. Possibly some geometric effects such as radial fuel relocation and pellet swelling may influence the evolution of the pellet diameter to lesser extent as compared to other codes.

Part 5 shows a closed pellet cladding gap during wet storage and an increased stress, which outreaches all other participant's results. A possibly non-thermal effect leads to a swelling of the pellet during the entire storage period. Besides the geometric effect the fuel rod gas pressure shrinks less compared to other solutions and starts to increase after approximately 65 years. Part 6 results are limited to plastic cladding deformation and hoop stress and show only minor effects over the whole storage period.

The hydride effects are shown for Part 1 and Part 5 and follow a comparable behaviour. The high hoop stresses in the cladding of Part 5 causes radially oriented hydride precipitation, whereas Part 1 has only circumferentially precipitated hydrides during the entire period of storage.

5 Conclusion and outlook

The results of the SEDS Benchmark on fuel rod behaviour during dry storage have been presented and discussed. The results for Zircaloy-4 corner and central rods were provided by seven participants using different codes and show for some of the variables of interest large deviations in the predicted results. For the M5 fuel rods only three participants provided results. Since the operational behaviour is not the main focus of this task, it shows large deviation in some of the fuel rod results, especially the geometric parameters, such as strain, gap size and plastic deformation. This leads to strong deviations in the starting conditions for the long-term storage period. However, most participants predicted a similar trend, such as a decreasing pressure or temperature over the storage period. The gap closure between pellet and cladding is predicted differently but shows only minor effect on creep deformation and cladding stresses. All results foresee only small or no plastic deformation due to creep. Some codes predict deviating effects, resulting either from the code input or individual modelling choices.

Furthermore, the definition of fuel rod strain should be a topic for discussion. The variety of parameters which influence the size of the fuel rod is large – from thermal expansion to elastic and plastic deformations. The latter may or may not include deformation due to creep mechanisms. All definitions are valid on their own but could lead to wrong conclusions if used to compare fuel rod data, especially if any quantitative value of strain is used for regulatory purposes. For this benchmark purpose, a reliable parameter describing the evolution of the cladding deformation is the cladding inner diameter. This parameter does not change due to oxidation processes and remains comparable for this benchmark task. Any other requirement of strain investigation should be made separately.

In this compilation of results and the subsequent analysis, the authors did not have the resources and time to study the code models in detail yet, allowing for a rigorous comparison and analysis of results. Most importantly, not all codes were capable of simulating and predicting all relevant physical effects to date, which leads to deviations in the resulting predictions. To close these gaps, further meetings to discuss the results are scheduled.

Most notably, only two results were provided to predict the hydride behaviour in the cladding, an effect believed to be important for the prediction of cladding integrity during the dry storage period. Hydrogen and hydride behaviour within the fuel rod cladding remains an intensely discussed topic in the nuclear community. New experimental findings and

mechanistic models are expected to be published within the midterm future, which will in return address the code developers and users to expand their modelling capacities.

This benchmark presents the challenges of giving a simplified but realistic benchmark task to all participants, taking part with different simulation tools. Furthermore, it exhibits the general difficulties of assessing the fuel rod state at the beginning of the dry storage. It was shown that the physical phenomena involved in this task were manifold and turned this benchmark in a multi-physics multi-scale[1] problem.

Based on the outcome of this benchmark, a Phase II is in discussion. Its focus is addressing the details of the different modelling assumptions in various code in greater detail.

[1] Multi-scale regarding time scales

References

/BOL 19/ Boldt, F., Stuke, M.: Benchmark for thermo-mechanical fuel rod behaviour during dry storage, Specifications, Version 3. Hrsg.: Gesellschaft für Anlagen- und Reaktorsicherheit (GRS) gGmbH (GRS), Dezember 2019.

/BOL 20/ Boldt, F., Péridis, M., Stuke, M.: SEDS benchmark for fuel rod behaviour during dry storage – preliminary results. Kerntechnik, Bd. 85, Nr. 6, S. 426–432, DOI 10.3139/124.200073, 2020.

/HES 86/ Hesse, U., Denk, W., Deitenbeck, H.: OREST - eine direkte Kopplung von HAMMER und ORIGEN zur Abbrandsimulation von LWR-Brennstoffen. Gesellschaft für Anlagen- und Reaktorsicherheit (GRS) gGmbH (GRS), GRS-63, November 1986.

/MIC 17/ Michener, T. E., Rector, D. R., Cuta, J. M., Atkins, H. E., JR.: COBRA-Sfs: A Thermal-Hydraulic Anlaysis Code for Spent Fuel Storage and Transportation Casks Cycle 4a. Pacific Northwest National Lab. (PNNL), PNNL-24841, Oktober 2017.

/NEA 06/ OECD Nuclear Energy Agency (NEA): OREST96, LWR Burnup Simulation Using Program HAMMER and ORIGEN. NEA Data Bank, NEA-1324, 2006.

/STU 19/ Stuke, M. (Hrsg.): SEDS2019 - 3rd Workshop on Safety of Extended Dry Storage of Spent Nuclear Fuel, Abstract Book. Gesellschaft für Anlagen- und Reaktorsicherheit (GRS) gGmbH (GRS), Garching, 5. - Juni 2019, 2019.

List of figures

List of tables

A Participants' contribution to simulation benchmark

A.1 CIEMAT results

Benchmark for thermo-mechanical fuel rod behaviour during dry storage

CIEMAT

C. Aguado, F. Feria, L.E. Herranz

July 2020

Code system used

CIEMAT's contribution to the Benchmark is based on FRAPCON-xt calculations; this is a CIEMAT´s extension of PNNL's FRAPCON-4.0 code to dry storage conditions (Feria et al., 2020; Geelhood et al., 2015). FRAPCON-4.0 has been developed for calculating steady-state fuel behaviour at high burnup; it has been validated up to a rod-average burnup of 62 GWd/MTU, although it should give reasonable predictions for burnup beyond this level for some parameters (Geelhood et al. 2015). Some main features of FRAPCON-4.0, which apply also to FRAPCON-xt, are the following:

- 1.5D code, that is to say, only radial heat flow calculations; axial heat exchange considered through the coolant flow.
- Axisymmetric fuel rod with no axial constraints.
- Thin wall approach (no cladding radial nodalization).

Specific models

- Fission gas release model

MASSIH model (PNNL's modification of Forsbeg and Massih (Forsberg and Massih, 1985)) has been used for Fission Gas Release calculations as the one recommended by the developers (Geelhood et al., 2015).

- Mechanical model

FRACAS-I (Bohn, 1977) is selected as mechanical model, also based on developers' recommendations.

Own developments/changes in models

- Cladding creep law

A creep law for dry storage conditions is implemented in FRAPCON-xt. It was derived from Zircaloy-4 data obtained from the literature for irradiated (low and high burnups) and unirradiated cladding material. The primary variables taken into account are temperature (T), cladding hoop stress (σ_θ), storage time (t) and fast neutron fluence (φt). A more complete description of this model can be found elsewhere (Feria and Herranz 2011).

- In-Clad hydrogen behavior

The in-clad hydrogen behavior modelling carried out is coupled with FRAPCON-xt. It is based on two models focused on the hydrogen migration/precipitation in the radial direction and the hydride radial reorientation.

Hydrogen migration along irradiation and dry storage is modelled through a 1D model (radial transport) based on Fick's and Soret's laws. The hydrogen precipitation is modelled through solubility limits found in the literature, taking into account the precipitation kinetics.

In order to predict the radial hydrides content in dry storage, an empirical model from IRSN (Desquines et al., 2014), supported on unirradiated Zircaloy-4 data, is implemented based on CIEMAT´s assumptions to apply it to irradiated claddings. A detailed description of in-clad hydrogen behavior modelling in FRAPCON-xt has been recently published (Feria et al., 2020).

- Cladding corrosion

Cladding corrosion model is deactivated for Dry Storage stage.

Specific boundary conditions/assumption used for the calculation

Most of initial and boundary conditions for irradiation and dry storage have been imposed by the Benchmark's specifications (Boldt and Stuke, 2019). However,

some of these conditions have been assumed due to the characteristics of FRAPCON modelling or to the lack of information in the specifications:

- Irradiation conditions:
    - Plenum – Spring:

Due to the absence of double plenum design in FRAPCON, and in order to meet the total (upper and lower) plenum void volume, the dimensions given to the plenum and spring are the following:

Plenum Dimensions		
Plenum Length	399	mm
Spring Dimensions		
Spring outer diameter	7.190	mm
Spring wire diameter	1.22	mm
Number of spring turns	28	

    - Densification:

An expected density increase of 0.9% of the UO_2 Theoretical Density (TD) has been considered (Geelhood et al., 2009).

- Dry Storage conditions:
    - Cladding oxidation:

A correction factor of 0.766 has been added to the corrosion model in order to meet the specifications (maximum oxide layer of 90 μm).

References

Bohn, Michael P. 1977. *FRACAS - A Subcode for the Analysis of Fuel Pellet-Cladding Mechanical Interaction*. TREE-NUREG-1028 TRN: 77-017259.

Boldt, Felix and Maik Stuke. 2019. *Benchmark for Thermo - Mechanical Fuel Rod Behaviour during Dry Storage Specifications*.

Desquines, J., D. Drouan, M. Billone, M. P. Puls, P. March, S. Fourgeaud, C. Getrey, V. Elbaz, and M. Philippe. 2014. "Influence of Temperature and Hydrogen Content on Stress-Induced Radial Hydride Precipitation in Zircaloy-4 Cladding." *Journal of Nuclear Materials* 453(1–3):131–50.

Feria, F., C. Aguado, and L. E. Herranz. 2020. "Annals of Nuclear Energy Methodology for a Realistically Conservative Characterization of Spent Fuel in Dry Storage." *Annals of Nuclear Energy* 140:107148.

Feria, F. and L. E. Herranz. 2011. “Progress in Nuclear Energy Creep Assessment of Zry-4 Cladded High Burnup Fuel under Dry Storage.” *Progress in Nuclear Energy* 53(4):395–400.

Forsberg, K. and A. R. Massih. 1985. “Diffusion Theory of Fission Gas Migration in Irradiated Nuclear Fuel UO2.” *Journal of Nuclear Materials* 135:140–48.

Geelhood, K. J., W. G. Luscher, C. E. Beyer, D. J. Senor, M. E. Cunningham, D. D. Lanning, and H. E. Adkins. 2009. “Predictive Bias and Sensitivity in NRC Fuel Performance Codes Office of Nuclear Regulatory Research.”

Geelhood, K. J., W. G. Luscher, P. A. Raynaud, and I. E. Porter. 2015. *Frapcon-4.0: A Computer Code for the Calculation of Steady-State, Thermal-Mechanical Behavior of Oxide Fuel Rods for High Burnup*. PNNL-19418 Vol.1 Rev.2.

A.2 CNAT results

Benchmark for thermo-mechanical fuel rod behaviour during dry storage
CNAT Model

1. FALCON GENERAL DESCRIPTION

FALCON is a 2D finite element based thermos-mechanical code. Calculates irradiation dependent thermal and mechanical behavior of the fuel, cladding, and internal void regions.

- Fuel centerline temperature
- Cladding stress and strain
- Thermal margins (e.g. departure from nucleate boiling (DNB), critical power ratio (CPR))
- Fuel rod internal pressure and fission gas release
- Cladding axial growth
- Etc...

2. CNAT CALCULATION

Cases:

- Zircaloy-4 Central Rod
- Zircaloy-4 Corner Rod

3. MODELS USED

PROPERTY	MODEL
Densification Model	ESCORE
Relocation Model	ESCORE
Fission Gas Relearse Model	Forsberg and Massih
Iron Particle Size Model	LOWTIN
Cladding Low Temperature Creep Model	LIMBACK
Cladding High Temperature Creep Model	MATPRO
Axial Growth Model	MATPRO
Oxidation Low Temperature Model	MATPRO
Oxidation High Temperature Model	CATHCART

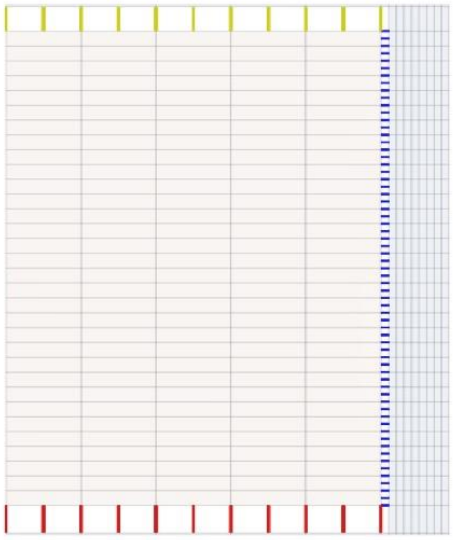

4. MODIFICATIONS AND CONSIDERATIONS

Models input assumptions

- Cold work ratio: 0.1
- Densification - Final fuel density: 96.3%
- Densification - Burnup at which densification is complete: 9 MWd/kgU
- Relocation Power Threshold: 16.4 kw/m
- Cladding Tin Content: 1.3%
- Coolant litium concentration 2.25 ppm

As axial power shapes are set by node in FALCON, axial distributions have been set to middle point of each section and upper and lower bounds have been extrapolated to cover total active length.

Lower	Upper	Node	Node height	BOC	MOC	EOCnat	EOC
		1	0	0.18825	0.38640	0.48495	0.40560
0	121.875	2	60.9375	0.28960	0.52160	0.60770	0.50790
121.875	243.75	3	182.8125	0.49230	0.79200	0.85320	0.71250
243.75	365.625	4	304.6875	0.65900	0.98340	1.02030	0.84410
365.625	487.5	5	426.5625	0.77430	1.07830	1.08900	0.89670
487.5	609.375	6	548.4375	0.85680	1.12030	1.10940	0.91390
609.375	731.25	7	670.3125	0.92310	1.13910	1.11810	0.91980
731.25	853.125	8	792.1875	0.97870	1.14530	1.10450	0.92130
853.125	975	9	914.0625	1.02410	1.14060	1.09300	0.92280
975	1096.875	10	1035.9375	1.06740	1.13670	1.08400	0.92840
1096.875	1218.75	11	1157.8125	1.10630	1.13050	1.07470	0.93510
1218.75	1340.625	12	1279.6875	1.13800	1.12210	1.06500	0.94290

1340.625	1462.5	13	1401.5625	1.16970	1.11630	1.05920	0.95490
1462.5	1584.375	14	1523.4375	1.19820	1.11040	1.05390	0.96780
1584.375	1706.25	15	1645.3125	1.21830	1.10230	1.04720	0.97960
1706.25	1828.125	16	1767.1875	1.23880	1.09740	1.04400	0.99520
1828.125	1950	17	1889.0625	1.25600	1.09270	1.04140	1.01140
1950	2071.875	18	2010.9375	1.26460	1.08610	1.03710	1.02590
2071.875	2193.75	19	2132.8125	1.27240	1.08230	1.03610	1.04420
2193.75	2315.625	20	2254.6875	1.27860	1.07880	1.03600	1.06340
2315.625	2437.5	21	2376.5625	1.27280	1.07360	1.03470	1.08140
2437.5	2559.375	22	2498.4375	1.26500	1.07020	1.03640	1.10320
2559.375	2681.25	23	2620.3125	1.25320	1.06680	1.03940	1.12680
2681.25	2803.125	24	2742.1875	1.23250	1.06120	1.04160	1.15010
2803.125	2925	25	2864.0625	1.20410	1.05560	1.04700	1.17870
2925	3046.875	26	2985.9375	1.16970	1.04850	1.05380	1.21020
3046.875	3168.75	27	3107.8125	1.12470	1.03630	1.05880	1.24100
3168.75	3290.625	28	3229.6875	1.05830	1.01070	1.05650	1.26580
3290.625	3412.5	29	3351.5625	0.96930	0.96900	1.04330	1.28050
3412.5	3534.375	30	3473.4375	0.81610	0.86660	1.00750	1.26310
3534.375	3656.25	31	3595.3125	0.66960	0.73730	0.87480	1.12240
3656.25	3778.125	32	3717.1875	0.49220	0.57570	0.68150	0.89410
3778.125	3900	33	3839.0625	0.26620	0.35250	0.45100	0.59480
		34	3900	0.15320	0.24090	0.33575	0.44515

Other information ask to GRS by mail.

Upper plenum		
Gross Volume	8130	mm^3
Spring volume	1700	mm^3
Free volume	6430	mm^3
Spring volume fraction	0.209102091	
Length	153	Mm
Spring length(FALCON default)	160.65	Mm
Lower plenum		

Gross Volume	17385	mm^3
Isolating pellet + support sleeve Volume	3265	mm^3
Free volume	14120	mm^3
Length	328	mm
Adapted length	266.1	
Plugs		
Length	12	mm

A.3 Framatome results

Benchmark for thermo-mechanical fuel rod behaviour during dry storage

Framatome GmbH
R. Sedláček, D. Deuble, H. Landskron, E. Schweitzer
July 2020

Code system used

Framatome GmbH uses the fuel rod design code CARO-E for simulation of the fuel rod behavior during irradiation. The design code CSAS is used for calculation of cladding stress and strain in storage. A special R&D version of CSAS was used to produce the results presented in the Benchmark.

CARO-E The computer code CARO-E has been developed since about 50 years by Siemens KWU, AREVA GmbH and Framatome GmbH for the analysis of fuel rod behavior under conditions of authorized reactor operation. It is applicable in best estimate calculations as well as Monte Carlo calculations within the Framatome GmbH statistical design methodology.

The code deals with the entire fuel rod in its radial and axial extension. The active length can be subdivided into several axial zones with different fuel properties and each axial zone is subdivided in segments (nodes). Pellets are divided in several radial ring zones of equal mass. Cladding is considered in thin wall approximation.

The radial heat conduction in the rod is solved from the rod surface to pellet center. For the calculation of the rod internal gas pressure, it is assumed that an unhindered exchange of gas is possible between the rod free volumes (plena, dishings, gap, cracks, open pores). Models for heat conduction, fission gas release, dimensional behavior of pellet and cladding and cladding corrosion form a complex nonlinear system that is solved by a fast and robust iterative method. The following variables and their time dependence are analyzed in a CARO-E3 calculation for long-term behavior of fuel rods:

- Cladding tube
  - temperature
  - thermal expansion and elastic strain
  - thermal and irradiation-induced creep
  - irradiation-induced growth
  - corrosion
  - hydrogen pick-up
- Pellet
  - temperature
  - thermal expansion
  - densification and swelling due to irradiation

  - fission gas release (including rim effect)
  - helium absorption
  - release of adsorbed and chemically bonded residual gas
  - radial and axial relocation
  - restructuring
- Fuel rod
  - pressure
  - plenum temperatures
  - gas composition

The exceptional strength of the code resides in the experience accumulated over 50 years of design calculations and its extended validation and verification database comprising several hundreds of fuel rods irradiated in both commercial and research reactors, with their power histories, pool side measurements, hot cell examinations, etc.

CSAS The computer code CSAS conservatively calculates the dry storage design relevant quantities cladding stress and cladding creep strain under given axial temperature profile as a function of time. The input to CSAS is the end-of-life (EOL) state of the fuel rod as calculated by CARO-E:

- amount of gas
- dimensions
- free volumes
- oxide thickness
- fast fluence

The program calculates the cladding hoop creep strain during storage conservatively by choosing an unfavorable combination of conditions (temperature, fluence, oxide). A creep correlation that accounts for irradiation hardening and its annealing has been fitted on data from long-term creep tests on irradiated cladding. The creep strain at the begin of storage is set to zero and an increase in free volume due to creep is conservatively neglected. The stress to be compared with design criterion is calculated conservatively at the highest temperature, using the thick wall formula evaluated at inner cladding radius. Thus, CSAS delivers one conservative value for cladding stress and one for cladding creep strain. Those values can be compared with the corresponding design criteria. The stress criterion guarantees that no substantial hydride reorientation takes place during storage.

CSAS R&D The R&D version of CSAS utilizes the same models as CSAS for calculation of inner pressure and cladding creep strain. As distinct from CSAS, the calculations are performed in all axial nodes with their local values of temperature, fluence and oxide thickness as delivered by CARO-E. The stress is calculated in all axial nodes using thin wall approximation.

CSAS R&D enables to consider additional mechanisms such as

- increase in free volume due to clad creep
- He production due to α-decay (Rondinella 2012)
- Fuel swelling due to α-decay (Raynaud 2015)

These mechanisms were not considered for the Benchmark calculations report, but were presented as an additional study in the SEDS 2020 presentation. It was shown that in the specific Benchmark conditions, the above effects are covered by the standard conservative CSAS design calculations.

Specific models / Own development

The Benchmark calculations were performed using standard CARO-E for the irradiation part (no specific models or own developments).

The storage part was calculated by CSAS R&D (see above) which can be considered own development but using the standard CSAS models for inner pressure calculation and cladding creep.

Specific boundary conditions / Assumptions

The GRS specifications were respected with three exceptions:

- Instead of Zy-4 cladding material, Zy-4 based Duplex cladding with a thin outer liner but otherwise identical mechanical properties was used.
- The CARO-E calculated axial dependent oxide thickness that was kept for the CSAS R&D storage calculations and not reset to the GRS proposed value.
- The storage simulation begins with the begin of wet storage (t2), i.e. the temperature decrease (t0) and pressure decrease (t1) were omitted.

No further assumptions were done.

A.4 GRS results

Benchmark for thermo-mechanical fuel rod behaviour

GRS Results Description

Felix Boldt, Mark Péridis, Maik Stuke

August 2020

Code system description

GRS contributes to this benchmark with a combined approach of two codes. The base irradiation was simulated with the TRANSURANUS (TU) code, performed by TÜV-NORD. Due to detailed base burnup calculation and operational corrosion models the TRANURANUS code was used for this purpose. The wet storage calculation, drying procedure and dry storage conditions were simulated with the GRS fuel rod code TESPA-ROD Version 20.3.1.

The TESPA-ROD code analyses the thermo-mechanical load on the fuel rod cladding for operation and accident scenarios as well as long-term storage transients. The TESPA-ROD code represents the fuel rod behaviour in a 1½ dimensional spatial resolution. It provides the transient radial temperature distribution in a cross-sectional area of a fuel rod while the axial temperature distribution is approximated from an axial power factor. Characteristic fuel volumes like fuel rod plena or gap volume are described in distinguished volumes. Fission gas communication among these volumes is assumed.

Geometrical Model

Recently TESPA-ROD was extended with a multiple axial zone Model. The fuel rod's active fuel column is axially divided in 10 equidistant zones. This deviation of the 32 axial zones proposed in the specifications leads to a averaging between the corresponding axial levels, especially for the input data generated by the TU calculations of the operational behaviour.

Input description

TESPA-ROD considers basic geometrical input given in the benchmark specifications /BOL 19a/. Further it uses the decay heat prediction by OREST and during dry storage the coolant temperature prediction by COBRA-SFS directly, averaged on 10 axial zones. Other input data is taken from TU calculations. Best stability for TESPA-ROD calculations are achieved for operational temperatures as initial conditions. First parameter set is calculated by TESPA-ROD according to the pellet and cladding geometry, burnup, corrosion state, coolant conditions. The TESPA-ROD simulation starts at the end of the stretch-out operation (EOL) given by the TU calculation. Deviations between the simplified TESPA-ROD estimate and the TU result lead to adjustments in following parameters:

- Local burnup
- Corrosion thickness
- Pellet cladding gap size
- Cladding hydrogen content

The local burnup was adapted from TU for the different axial zones, adjusted due to the axial averaging effect on 10 axial zones.

TU showed smaller values for the pellet diameter. The TESPA-ROD model uses a fuel densification and swelling model which is directly linked to the burnup. Further a radial pellet relocation model increases the pellet diameter during the first power ramps and reduces the pellet-cladding gap. In comparison to TESPA-ROD with its rigid pellet model, TU uses a viscoplastic pellet model, allowing deformations of the pellet due to outer effects such as the cladding or gas pressure. As solution a reduction was imposed on the TESPA-ROD fuel outer radius (RFO) and cladding inner radius (RCI) to meet the TU

swelling which eventually leads to a pellet-cladding gap closure and a forced tensile strain on the cladding, which leads to an increase in hoop stress. Large cladding stresses are observed during drying processes and dry storage.

References

/BOL 19a/ Boldt, F., Stuke, M.: Benchmark for thermo-mechanical fuel rod behaviour during dry storage, Specifications, Version 3. Hrsg.: Gesellschaft für Anlagen- und Reaktorsicherheit (GRS) gGmbH, Dezember 2019.

/BOL 19b/ Boldt, F.: Implementation of Hydrogen Solid Solubility Data and Precipitation Threshold Stresses in the Fuel Rod Code TESPA-ROD. Nuclear Engineering and Radiation Science, DOI 10.1115/1.4042118, 2019.

/KAU 18/ Kaufholz, P., Stuke, M., Boldt, F., Péridis, M.: Influence of kinetic effects on terminal solid solubility of hydrogen in zirconium alloys. Journal of Nuclear Materials, Bd. 510, S. 277–281, DOI 10.1016/j.jnucmat.2018.08.011, 2018.

/SON 18/ Sonnenburg, H.-G.: TESPA-ROD Code Prediction of the Fuel Rod Behaviour During Long-term Storage, AMNT 2018. atw International Journal for Nuclear Power, Nr. 63 Issue 6/7, S. 374–377, 2018.

/WIS 14/ Wiss, T., Hiernaut, J.-P., Roudil, D., Colle, J.-Y., Maugeri, E., Talip, Z., Janssen, A., Rondinella, V., Konings, R. J.M., Matzke, H.-J., Weber, W. J.: Evolution of spent nuclear fuel in dry storage conditions for millennia and beyond. Journal of Nuclear Materials, Bd. 451, Nr. 1-3, S. 198–206, DOI 10.1016/j.jnucmat.2014.03.055, 2014.

A.5 PSI Results

Paul Scherrer Institut
5232 Villigen PSI
Switzerland

+41 56 310 21 11
www.psi.ch

Piotr Konarski
NES
OHSA/C06

direct +41 56 310 26 79
piotr.konarski@psi.ch

To: F. Boldt (GRS)

Cc: C. Cozzo
H. Ferroukhi
G. Khvostov

Villigen PSI, 03 May 2022

Your Ref:
Our Ref: SB-RND-ACT-009-19.003 V.1
Class:

PSI's contribution to the benchmark for dry storage

Dear Mr Boldt,

Responding to your request, a short memorandum explaining how PSI participated in the benchmark for dry storage has been prepared and attached to this letter. It gives an overview of the fuel code, main models and specific boundary conditions used for the benchmark calculations.

Best regards,

Piotr Konarski

1 CODE SYSTEM USED IN THE BENCHMARK

The fuel performance tool used in this work is Falcon V1.4. It is a 2D finite element code co-developed by Electric Power Research Institute (EPRI) and PSI. Falcon is able to model both BWR and PWR rod designs. Its modeling capabilities cover a wide range of fuel and cladding materials, and accident tolerant fuels are also part of a continuous development. Falcon can be applied to simulate both steady state and transient scenarios which allows to model LOCA and RIA accidents. Fuel performance simulations can be carried out in two different geometries: the axisymmetric r-z plane and the radial-azimuthal cross-section r-θ. The first one can be applied to study the entire fuel rod and the second one can be used if a detailed analysis of a certain part of the rod in required. In this work, the r-z plane geometry is used to account for the different conditions over the full rod length and to allow using a broader set of models. Also the conditions were provided for an axisymmetric problem.

2 SPECIFIC MODELS USED IN THE BENCHMARK

In general, Falcon has more than one model to describe each physical phenomenon. The available models have been tested and the ones giving the most reasonable results have been chosen for this work. The list of main models used in this work is given in Table 1.

Table 1: Main models used in the simulations.

Phenomenon	Model used
Fission gas release	Forsberg/Massih
Cladding annealing	MATPRO
Radial power distribution	TUBRNP
Cladding waterside corrosion	EPRI/SLI
Cladding creep	Limbäck/Andersson
Gap conductance	Ross and Stoute

3 OWN DEVELOPMENTS

A standard version of the code has been used. No developments related to dry storage have been made.

4 SPECIFIC BOUNDARY CONDITIONS/ASSUMPTION USED FOR THE CALCULATION

As boundary conditions, GRS has provided the coolant parameters to simulate the base irradiation and the cladding outer surface temperature to model the wet storage, drying and dry storage. PSI decided to carry out a single simulation taking into account both base irradiation and storage. A single simulation requires the same boundary conditions during the entire life cycle. In order to use the fixed clad outer surface temperature boundary condition it is necessary to first simulate the base irradiation using the coolant enthalpy rise model. One of the outputs

from this simulation is the cladding outer surface temperature. The obtained temperature can be combined with the one provided by GRS for the wet storage, drying and dry storage and used to perform one simulation taking into account every stage of the fuel rod life cycle.

Another assumption worth mentioning is that the power transients at the beginning and at the end of each reactor cycle last 3 hours.

4.1 Input parameters

The input parameters related to M5 were not used in this work since this cladding material is not available in Falcon. In addition, certain parameters describing the fuel pellet geometry could not be used. Namely, the pellet length, the chamfer depth and width and the dishing depth and radius. Falcon accounts for chamfers and dishes but by taking into account their volumes and not geometrical dimensions.

4.2 Assumptions and boundary conditions

The active part of the simulated fuel rod is divided into 31 axial sections as requested by the benchmark organisers. Radially, the rod is represented by 11 concentric rings. 5 of them represent the fuel material, 1 is used to model the gap and 5 to model the cladding. The top and bottom plugs and plenums are also modelled. The full mesh used in this work is shown in Figure 1.

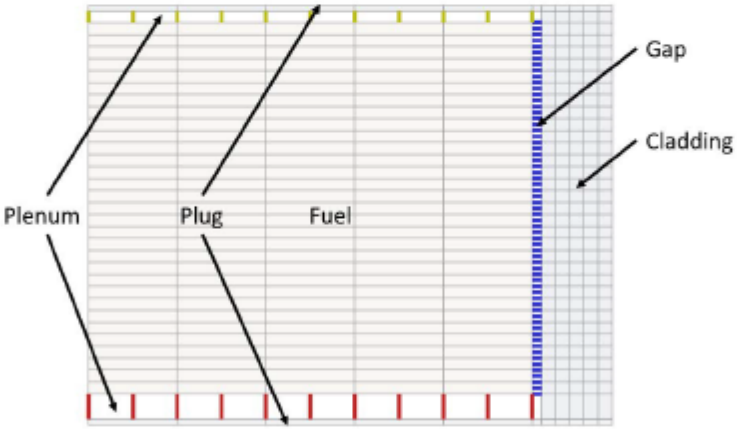

Figure 1: Mesh used in the simulations.

4.3 Output parameters

Some output parameters could not be calculated in Falcon directly, and some others could not be calculated at all. The first parameter that was calculated indirectly in post-processing is the total hoop strain of the cladding (ECTH). The organisers requested the engineering strain and

Falcon calculates the Lagrange strain. The engineering strain was obtained from the cladding inner radius (RCI). The second parameter calculated indirectly is the total amount of hydrogen in axial node (HTOT). This output parameter was calculated from the cladding oxide layer thickness, the hydrogen pickup ratio suggested by GRS for Zircaloy-4 0.15 and from the Pilling-Bedworth ratio for ZrO_2 1.56.

The first parameter that cannot be calculated by Falcon is the total plastic strain of the cladding (ECP). It is not possible to extract the plastic component of the strain in Falcon. The last three parameters that were not provided in this work are related to the hydrogen behavior. These are HDIS, HRAD and HCIR.

A.6 TUEV results

TÜV NORD EnSys GmbH & Co. KG

TÜV NORD contribution to the GRS project

Long-term behavior of temporarily stored fuel elements with significantly longer interim storage

Reference: order number 734001 / RS1552 / UA-3411

Executive Summary – December 2021

TÜV NORD EnSys GmbH Co. KG, hereafter called TNE, contributed as a subcontractor the GRS Project 'Long-term behavior of temporarily stored fuel elements with significantly longer interim storage'. Main tasks within this contributions was the setup of a benchmark specification for comparative calculation of the thermo-mechanical fuel rod behavior during dry storage including the fuel rod design parameters, the in pile power history and the wet pool storage boundary conditions. This specification including the parameters and the described procedure were tested by primary calculations and verification of the results. These results were provided to the participants of the benchmark for orientation and for use if the codes were not able to calculate the in pile and wet storage stages.

Further, these basic calculations were included in to the code benchmark of for thermo-mechanical fuel rod behavior during dry storage. TNE uses the release V1M1J18 of the fuel rod performance code TRANSURANUS /1/. TNE only calculated the in pile and the wet storage stages of the entire life of the specified fuel rod. The drying and storage stages are not calculated within this benchmark by TNE since the preliminary implementation of the hydride reorientation model was not sufficient to be verified in an acceptable manner.

The hydrogen pick up into the cladding material during the in pile life of the fuel is not a standard implementation in our version of the TRANSURANUS fuel rod performance code (TU-code). TNE implemented a hydrogen pick up correlation coupled to the oxidation kinetics of the outer cladding. In water – metal reaction during the in pile file of the fuel rod hydrogen is produced. A part of this hydrogen is solved in the metal phase of the cladding. This part is called the pickup fraction. More information is given in /2/ and /3/. The waterside corrosion models implemented in the TU-code cover a set of different cladding materials. For our calculations according the benchmark specification /4/ standard correlations for Zircaloy 4 cladding material were used. A description of these calculations and the results are resented in /5/.

/1/ P. Van Uffelen, Cs. Győri, A .Schubert, J. van de Laar, Z. Hozer, G. Spykman,
Extending the application range of a fuel performance code from normal operating to design basis accident conditions
Journal of Nuclear Materials, 383 (2008), 137 – 143

/2/ Anand M. Garde, William H. Slagle and David Mitchell
Westinghouse Electric Company, LLC
Hydrogen Pick-Up Fraction for ZIRLO™ Cladding Corrosion and Resulting Impact on the Cladding Integrity,
Paper 2136, Proceedings of Top Fuel 2009, Paris, France

/3/ Adrien Couet, Arthur T. Motta, Robert J. Comstock,
Hydrogen pickup measurements in zirconium alloys: Relation to oxidation kinetics,
Journal of Nuclear Materials 451 (2014) 1-13

/4/ GRS Gesellschaft für Anlagen- und Reaktorsicherheit (GRS) gGmbH
Benchmark for thermo-mechanical fuel rod behaviour during dry storage
Specifications Version: 3, December 2019

/5/ TÜV NORD GmbH & Co. KG
Langzeitverhalten zwischengelagerter Brennelemente bei deutlich längerer Zwischenlagerung
Zusammenfassender Bericht über die Mitarbeit der TÜV NORD EnSys GmbH & Co. KG in dem vom BMWi geförderten Projekt RS 1552 „Langzeitverhalten zwischengelagerter Brennelemente bei deutlich längerer Zwischenlagerung“
Referenz: Auftragsnummer 734001 / RS1552 / UA-3411
Stand 13.02.2020

A.7 UJV Rez results

July 2020

Dry Storage Benchmark Code Description

General Information

Vítězslav Matocha

Jan Klouzal

Martin Dostál

1. Code

Code name: **TRANSURANUS**

Code version: v1m3j12

Code type: 1 ½-D

2. Specific models

Categorization of modelling of relative movement of pellets and cladding in axial direction in fuel-clad contact conditions (stick, friction or frictionless):

- Friction forces are calculated with friction coefficients 0.1

Nodalization:

- 32 axial segments, 100 (fuel) and 10 (cladding) nodes in radial direction

Fuel relocation model:

- Modified FRAPCON-3 model of fuel relocation according to Lanning [2], reverse relocation is not considered, (ireloc = 8)
- **Based on internal validation relocation model is reduced by the coefficient 0.75**

Fuel creep model:

- **Fuel creep model implemented by UJV. Irradiation induced creep according to IFA-701 [7]**

Cladding creep model:

- Default cladding creep model for Zircaloy according to Lassmann and Moreno [1] – Zr-4 cladding FR
- **Cladding creep model for E110 according to Rogozyanov [9] implemented by UJV – M5 cladding FR**

Cladding instantaneous plasticity model:

- Default yield stress for LWR according to Lassmann and Moreno [1] – Zr-4 cladding FR
- **Default yield stress for E110 cladding, added irradiation hardening by UJV – M5 cladding FR**

Fuel thermal expansion coefficient correlation:

- Default correlation of fuel thermal expansion coefficient according to Leibowitz [3] and Chawla [4] with a correction for the influence of stoichiometry according Gibby [5]

Cladding thermal expansion coefficient correlation:

- Default cladding thermal expansion coefficient correlation according to Lassmann and Moreno [1]

Fuel Young's modulus correlation:

- Default fuel Young's modulus correlation according Lassmann and Moreno [1]

Fuel Poisson's ratio correlation:

- Default LWR fuel Poisson's ratio correlation according to Lassmann and Moreno [1]

Cladding Young's modulus correlation:

- Default correlation of cladding Young's modulus according to Lassmann and Moreno [1] – Zr-4 cladding FR
- Default correlation of cladding Young's modulus for E110 cladding – M5 cladding FR

Cladding Poisson's ratio correlation:

- Default correlation of cladding Poisson's ratio according to Lassmann and Moreno [1] – Zr-4 cladding FR
- Default correlation of cladding Poisson's ratio for E110 cladding – M5 cladding FR

Fuel swelling correlation:

- Default fuel swelling correlation developed by Lassmann from the original MATPRO swelling model

Fuel thermal conductivity:

- Default $(U\text{-}Gd)O_2$ correlation fitted to data from ITU

Other information:

- Standard version of mechanical analysis is used. The fuel is treated by a visco-elastic approximation, the cladding is treated by an explicit method; cracking is not treated.
- Number of cracks in the fuel is set to $n = 2$. This parameter influences modulus of elasticity of the fuel. It multiplies modulus of elasticity by a factor k ($k = (2/3)^n$). It is free parameter without any direct physical substantiation.

- Default URGAS algorithm for single gas atom diffusion in a spherical grain with the diffusion coefficients of Matzke (thermal) and constant athermal diffusion coefficient.

3. Own developments/changes in models

All own developments and changes in models are highlighted in the previous chapter.

4. Specific boundary conditions/assumption used for the calculation

The dry storage benchmark calculation was based on a standard TRANSURANUS input file as is used in a calculation for Czech NPPs. Naturally necessary adjustments for this calculated task were done according to a specification but without any special tuning. With a few exceptions default models available in the code were generally used. Basic settings and a model selection are described in the previous chapter. Models for M5 cladding are completely missing in the UJV code version so fuel rods with this cladding were modeled as E110 cladding.

The calculation was logically divided into two parts - base irradiation and dry storage. The calculation of base irradiation started with nominal parameters of fuel rods and coolant according to a specification. Inlet coolant temperature was prescribed. The dry storage phase was modelled as LOCA which allows to make required changes in coolant and mainly cladding outer surface temperature was prescribed. The calculation was done without restart.

Standard parameters as temperature, dimensional changes, cladding hoop stress and gas pressure were predicted. Only Xe and Kr production and release were calculated. Models for a total amount of hydrogen, an amount of dissolved hydrogen, a share of radial hydrides and a share of circumferential hydrides are currently absent in our routinely used version of the TRANSURANUS code.

5. References

[1] K. Lassmann, A. Moreno: *The Light-Water-Reactor Version of the URANUS Integral Fuel-Rod Code*. Atomkernenergie, Bd. 30, 1977.

[2] D. D. Lanning, C. E. Beyer, C. L. Painter: *FRAPCON-3: Monitoring to Fuel Rod Material Properties and Performance Models for High Burn-up Applications.* Pacific Northwest, PNNL-11513, NUREG/CR-6534 Vol. 1, 1997.

[3] L. Leibowitz: *Properties for LMFBR safety analysis*. Argonne National Laboratory. ANL-CEN-RSD-76-1,1976.

[4] T. C. Chawla: *Thermophysical properties of mixed oxide fuel and stainless-steel type 316 for use in transition phase analysis*. Null. Eng. Design, 1981.

[5] R. L. Gibby: *Thermal expansion of mixed oxide fuel*. HEDL-TME-3, 1974.

[6] K. J. Geelhood, W. G. Luscher, C. E. Beyer: *PNNL Stress/Strain Correlation for Zircaloy*. Pacific Northwest, PNNL-17700, July 2008.

[7] R. Szőke, T. Tverberg: *Update on in-pile results from the fuel creep test in IFA-701*. OECD HRP, HWR-1092, 2014.

[8] F. J. Erbacher et al.: *Burst Criterion of Zircaloy Fuel Claddings in a Loss-of-Coolant Accident*. Zirconium in the Nuclear Industry, 5th Symposium, ASTM STP 754, p. 271-283 (1982).

[9] A.Ya. Rogozyanov, G.P. Kobylyansky, A.A. Nuzhdov: *Behaviour and Mechanisms of Irradiatio-Thermal Creep of Cladding Tubes Made of Zirconium Alloys*. Journal of ASTM Int., Vol 5 No 2, 2008.

Gesellschaft für Anlagen- und Reaktorsicherheit (GRS) gGmbH

Schwertnergasse 1
50667 Köln
Telefon +49 221 2068-0
Telefax +49 221 2068-888

Boltzmannstraße 14
85748 Garching b. München
Telefon +49 89 32004-0
Telefax +49 89 32004-300

Kurfürstendamm 200
10719 Berlin
Telefon +49 30 88589-0
Telefax +49 30 88589-111

Theodor-Heuss-Straße 4
38122 Braunschweig
Telefon +49 531 8012-0
Telefax +49 531 8012-200

www.grs.de

ISBN 978-3-949088-62-9